STUDIES ON THE FLOW STRESS OF METALS AND ALLOYS

Hiromu Suzuki, et al

Institute of Industrial Science
The University of Tokyo
Azabu, Tokyo

March 1968

REPORT OF THE INSTITUTE OF INDUSTRIAL SCIENCE
THE UNIVERSITY OF TOKYO

VOL. 18, NO. 3 (SERIAL NO. 117) MARCH, 1968

東 京 大 学

産 技 術 研 究 所 報 告

第 18 巻 第 3 号

(通 巻 第 117 号)

UDC 539.374 : 539.388.2
621.7.011

STUDIES ON THE FLOW STRESS OF METALS AND ALLOYS

BY

HIROMU SUZUKI, *Professor*
SHIN HASHIZUME, *Research Associate*
YUTAKA YABUKI, *Research Associate*
YUKINORI ICHIHARA, *Assistant*
SATOSHI NAKAJIMA, *Assistant*
AND
KEIJI KENMOCHI, *Research Student*

昭 和 43 年 3 月

THE Institute of Industrial Science, University of Tokyo was established on May 31, 1949 in order to contribute to cultural progress in Japan through promotion of industrial science.

Up to March 1962, it has been located in Chiba City, and in April 1962, it was moved to the present location in Azabu, Tokyo.

Since its foundation, the Institute has taken a major part in the advancement of knowledge and techniques in various fields of industrial science through extensive research works on basic technical problems encountered in engineering and industry as well as production research of new scientific achievements in the laboratories.

The Institute is also participating actively in education and training of young scientists and engineers as an integral part of the Graduate School of University of Tokyo.

The Institute consists of the following five departments;

Department of Applied Physics and Applied Mechanics——Applied Mathematics, Applied Optics, Acoustic Engineering, Vacuum Techniques, Applied X-rays, Physics of Fluid, Strength of Materials, and Applied Elasticity, Dynamical Strength of Materials.

Department of Mechanical Engineering and Naval Architecture——Mechanical Dynamics, Mechanism, Heat Transfer, Heat Power Engineering, Fluid Mechanics, Chemical Machineries, Theory of Machining and Machine Tools, Metal Forming Engineering, Precision Technology, Welding Engineering, Automatic Control, Strength and Dynamics of Ships.

Department of Electrical Engineering and Electronics——Theory of Electric Circuits, Electric Machines and Apparatus, Electric Power Engineering, Electric Control, Electoron Tube Engineering, Communication Equipment Engineering, Space Electronic Engineering, Applied Electronics, Electric Computer Engineering, Information Processing Engineering.

Department of Industrial Chemistry and Metallurgy——Industrial Inorganic Chemistry, Industrial Organic Chemistry, Chemistry of Aromatics and their related Compounds, Chemistry of Natural High Polymers, Applied Electrochemistry and Photochemistry, Technical Analyses, Chemical Engineering, Ferrous Metallurgy, Non-Ferrous Metallurgy, Metals and Alloys, Metallurgical Technology, Radio Isotope Engineering.

Department of Building and Civil Engineering——Soil Engineering, Structural Engineering, Reinforced and Pre-Stressed Concrete Design, Highway and Traffic Engineering, Hydraulic Engineering, Surveying, Building Construction, Environment Control, Design of Building Elements, Earthquake Engineering, Function and Design of Architecture, History of Industrial Science and Technology.

UDC 539.374 : 539.388.2
621.7.011

STUDIES ON THE FLOW STRESS OF METALS AND ALLOYS

BY

HIROMU SUZUKI*

SHIN HASHIZUME** YUTAKA YABUKI***

YUKINORI ICHIHARA† SATOSHI NAKAJIMA†

AND

KEIJI KENMOCHI††

CONTENTS

* Professor of the University of Tokyo, Dr. of Eng.
** Researcher of the University of Tokyo, Dr. of Eng.
*** Researcher of the University of Tokyo.
† Assistant of the University of Tokyo.
†† Research Student of the University of Tokyo.

SYNOPSIS

The basic data on the flow stress of metals and alloys are of vital importance to the practical plastic working operation. While many measurements have been made at room temperature, there exist, apart from those on common steels, remarkably few number of thorough data for the hot working temperature range, because the flow stress there is influenced not only by strain and temperature but also by strain rate, and consequently the determination of the flow stress becomes prohibitively difficult.

For this reason, the authors have developed compression type of high temperature-high speed testing machines specially suited for flow stress measurement, i.e., a cam-plastometer and a drop-hammer type, and by overcoming several difficulties involved in this kind of experiment, measured the flow stress of widely used materials (twenty-one non-ferrous metals and alloys and forty-nine steels) in the hot working temperature range of each material and in the strain rate range 0.1–650 sec^{-1}.

The results of the experiments that had extended over the period between 1951 and 1966 have been presented in the form of data sheet, and a discussion on the behavior of the flow stress thus obtained has been given.

In Part 1, a description has been given of each of the testing machines, and several technical aspects of the experiment such as the methods for maintaining a constant strain rate and measuring load and strain in a high speed experiment, the effects of oxidation, dimensions, directionality, and temperature changes, of the specimen, the effect of friction at the contact surface, etc. have also been discussed.

In Part 2, the flow stress of non-ferrous metals and alloys in ordinary use, obtained in the strain rate range 0.1–650 sec^{-1} and up to the strain of 0.8, has been discussed. The temperature range explored is −75 to 650°C for aluminium, 200 to 500°C for duralumin, −75 to 300°C for zinc, 18 to 500°C for magnesium, and 18 to 900°C for titanium, copper and its alloys.

In general, the flow stress of these materials decreases with increasing temperature and increases with increasing strain rate. It has been ascertained that an Arrhenius type of equation holds between the flow stress and absolute temperature and that the flow stress is proportional to a power of strain rate. However, when plastic deformation is accompanied by precipitation, phase changes, recrystallization, etc., the flow stress changes in a complex manner with temperature, strain, and strain rate: the flow stress versus temperature curves for copper-tin and copper-zinc alloys exhibit a stress peak, and there exists a temperature region in which the flow stress increases with increasing temperature.

In Part 3, the flow stress of carbon, high strength, low alloy, and stainless steels; measured in the strain rate range 0.2–650 sec^{-1} and in the temperature range 800–1200°C, has been discussed. In particular, in the case of 0.15% carbon and 18% Cr–8% Ni stainless steels which were considered representative of the above steels, the temperature range has been extended to 0–1200°C.

Under normal conditions, the flow stress of these steels also obey an Arrhenius equation and a strain rate-power law. Likewise the flow stress is influenced by many other factors: the flow stress-temperature curve for a 0.15% carbon steel exhibits three stress peaks; one due to ageing between 200 and 400°C, one due to a phase change around 800°C, and the other of an unknown origin around 1000°C.

In Part 4, to facilitate application, all the experimental results have been summarized in the form of stress-strain curves with temperature and strain rate as parameters.

INTRODUCTION

The flow stress of metals and alloys is a vitally important factor controlling the working force during plastic deformation, and its knowledge is very useful in that

(1) compared with the conventional criterion based on mere experience, a reasonable working schedule can be set up, such as the determination of reduction per pass, working speed and temperature of, say, a rolling process, consequently enabling enhanced production and reduced cost.

(2) plastic deformation efficiency can be determined, and room for improvement will be located.

(3) damage to tools can be prevented by the knowledge of the necessary working force and the load limit the tools can withstand. In addition a prediction can be made on the degree of abrasion of tools.

(4) design and performance data of tools and various types of equipment can be obtained.

These account for only part of the benefits arising from the knowledge of the flow stress.

In general, the flow stress of metals and alloys depends not only on the properties of the materials themselves such as quality and thermal history, but also on the conditions under which deformation takes place, such as environment, stress distribution, strain rate, and temperature.

The flow stress at room temperature, especially at low strain rates of the order of $10^{-3}\,\mathrm{sec}^{-1}$, has been extensively studied for most metals and alloys. Except in a few cases such as lead in which recrystallization proceeds at room temperature, the influence of strain rate on the flow stress at low temperatures is so small that an extrapolation of low strain rate data can be made to high strain rates.

At high temperatures, however, the flow stress is influenced by a competition between two mutually opposing tendencies, i. e., work hardening due to deformation and softening due to recrystallization. Thus the behavior of the flow stress is dependent on a combination of strain rate and temperature, and it is impossible to isolate the effect of one from that of the other. Moreover, temperature-enhanced phenomena such as diffusion, precipitation, and phase changes all contribute to strain rate sensitivity in a complex manner and add various features to the behavior of the flow stress. Consequently the flow stress at high temperatures cannot be estimated from those measured for different materials and/or working conditions, but must be measured under the actual conditions of interest.

In order for the measured flow stress to serve as useful data for practical applications, it must satisfy the following requirements:

(1) it should be reported as a true flow stress. In this connection, one must distinguish between an apparent flow stress and a true flow stress. The former is an apparent flow stress which containes several other contributions such as frictions between the tools and the specimen, internal, losses due to stress other the true stresses under consideration, etc., while the latter is the uniaxial yielding stress, the kind treated in the theory of plasticity. In other words, an apparent flow stress applies only under a given condition and for a given process, where-as a true stress can be applied to the general mode of plastic working processes.

(2) strain rate should remain constant during the flow stress measurement. This condition

is not met in practice. To take an example from a rolling process again, the strain rate becomes maximal at the entrance to the roll or in its vicinity, begins to decrease along the roll bite, and finally becomes zero at the outlet. Similarly in drawing and forging processes, the strain rate changes at various stages of deformation.

In taking measurements, it would, therefore, be desirable to reproduce these variations in strain rate that are characteristic of each working method. However, the dependence of strain rate on the working method and condition is so complicated that it is impossible to cover all the cases of practical interest. For this reason, the common procedure of applying the experimental results to practice is to introduce an average strain rate for a given process and adopt the experimental flow stress measured a a strain rate equal to this average.

(3) the range of strain must be wide enough to cover the range which is encountered in the actual working process. With a few exceptional cases such as extrusion in which reduction per stroke is extremely large, the actual strain does not exceed 50%. Measurements should, therefore, be made at least to this limit.

(4) the strain rate and temperature of experiment should be systematically varied over the range of practical interest. If they differ appreciably from those existing under the actual operation, no realistic interpolation can be made of the data to the domain of actual working conditions.

Very few previous investigations satisfy all four of these requirements. To the author's knowledge, only five complete cases may be cited.

In 1955 Inoue[1-1] measured the flow stress of fifteen steels (from low carbon steels to stainless steels) in the temperature range 800–1200°C and in the strain rate range $1–10^2\,sec^{-1}$, using two types of tensile testing machine. The flow stress-strain curves were determined in which the maximum strain realized was 0.25, and a general relation between flow stress, strain rate, and temperature was established for the conditions of practical interest.

In 1954 Alder and Phillips[1-2] measured the flow stress of aluminium (temperature range: −190 to 550°C), copper (18 to 900°C), and 0.17% carbon steel (930 to 1200°C) in the strain rate range $1–40\,sec^{-1}$ and up to a strain of 0.5 using a cam-plastometer.

In 1957 measurements were taken by Cook[1-3] on twelve steels in the strain rate range $1–100\,sec^{-1}$ and in the temperature range 900–1200°C and up to a strain of 0.5.

In 1959–60 Arnold and Parker[1-4] determined the flow stress of aluminium and five aluminium alloys at temperatures between 300 to 550°C and at the strain rates 1, 10, 20 and $30\,sec^{-1}$ by means of a cam-plastometer.

In 1963–64 Bailey and Singer[1-5] carried out plane strain compression tests and obtained flow stress-strain curves for several non-ferrous metals and alloys, at various temperatures (Al: 22–600°C, Al–5.7% Zn alloy: 400–550°C, Al–4.2% Cu alloy: 300–500°C and Pb: 22–300°C), with strain rates being chosen from 0.4, 2, 9, 41, 101, 203 and $311\,sec^{-1}$.

In all of these measurements, interest was restricted to only a few kinds of materials, i.e., mainly steels, and many materials of industrial importance including non-ferrous metals and alloys have received very little attention.

Since practically all metals and alloys must undergo plastic deformation in one form or another before they become products, it is of scientific as well as industrial importance to collect basic data on the flow stress of widely used materials and clarify the influence of temperature and strain rate upon the flow stress.

In the present investigation the flow stress of commonly used materials including non-ferrous metals and high alloy steels has been carefully measured as a function of temperature

and strain rate, the purpose being to provide fundamental data that may be applied to the actual plastic working operation. Attempts have also been made to establish general relations between flow stress, strain rate and temperature. The experimental results that will be presented in this paper have been accumulated in our laboratory since 1951.

PART 1. EXPERIMENTAL APPARATUS AND METHOD

1·1 EXPERIMENTAL APPARATUS

1·1·1 Testing Machines

The data obtained will not be of much practical value unless the strain rates used in the measurement cover the range of those enconuntered in the actual working operation. Except in a few cases such as a high speed-high energy process, most practical strain rates are of the order of 1–500 sec^{-1}. Even during hot working, in which the influence of strain rate is large, the rates seldom exceed 100 sec^{-1}. Therefore, most measurements were made in the range of 1–100 sec^{-1} with the provision that this range could be extended to 0.1–650 sec^{-1} when a more extensive study of the influence of strain rate and temperature was required.

Widely used material testing machines allow strain rates of the order of 10^{-3}–10^{-1} sec^{-1}. These are too slow to meet the requirements set down for the present investigation, and consequently a special type of testing machine had to be constructed.

Among the conventional types of impact testing machine are Lueg's[1-6] drop hammer type, Charpy's or Izot's pendulum type, Nadai's[1-7] fly wheel type, pneumatic or oil pressure type, and explosive forming type. However, since no single type can produce the necessary range of strain rate alone, the strain rate range was divided into two parts: below 100 sec^{-1}, a cam-plastometer was used, and above 100 sec^{-1}, a drop hammer type of compression testing machine was used.

In the following, a description will be given of each of these two types of testing machine.

1·1·1·1 Cam-plastometer

This is a special type of compression testing machine designed by Orowan[1-8] in 1950, and is capable of maintaining a constant strain rate. The cam-plastometer used in the present experiment is similar to Orowan's except for a few modifications. Fig. 1·1 is a schematic diagram of this machine. The machine consists of the frame and driving parts. The former comprises a crosshead, a plunger, and a cam, and the latter a speed change gear, a clutch, and an electric motor.

By combining a cam having an included angle of 36° or 72° with a two-step speed changer, any strain rate in the range of 0.1–100 sec^{-1} can be produced.

The main features of this machine are as follows:

Maximum capacity	15 tons
Strain rate	0.1–100 sec^{-1}. Stepless speed change. Constant strain rate.
Maximum strain	0.8 in natural strain (0.5 in conventional strain)
Specimen	12 mm dia × 18 mm height and 8 × 12.

For high temperature measurements, the specimens were compressed in a sub-press which

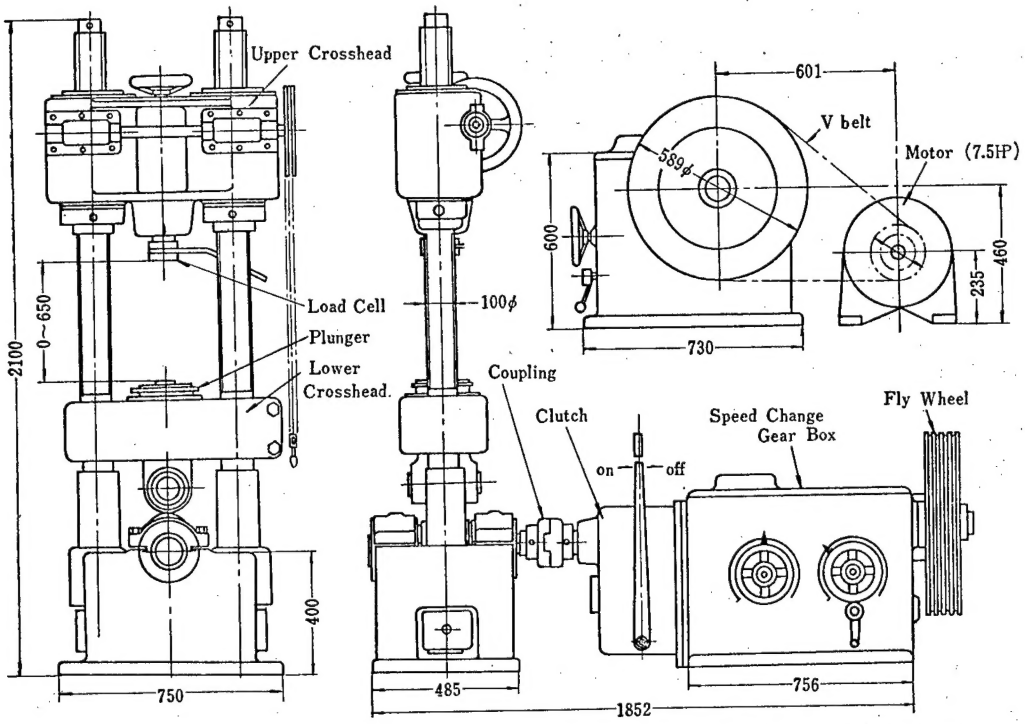

Fig. 1·1 Cam-plastometer for the Flow Stress Measurement. Strain Rate Range: 0.1~100 sec^{-1}.

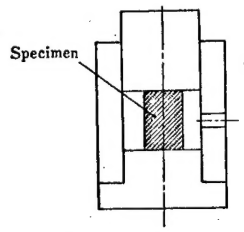

Fig. 1·2 Sub-press.

is made of heat-resistant alloys such as S-816, Inconel, and 25% Cr-20% Ni steel so as to minimize heat losses (Fig. 1·2).

1·1·1·2 Drop-Hammer Type of Impact Testing Machine

This machine is a compression type in which the energy for compression is generated by the free drop of a hammer. Fig. 1·3 is a schematic diagram of this machine. The main features are:

Height of the machine	9 m
Effective distance of drop	8 m
Hammer	25 and 50 kg
Anvil	3.5 tons
Specimen	12 mm dia × 18 mm height and 15 × 22.5

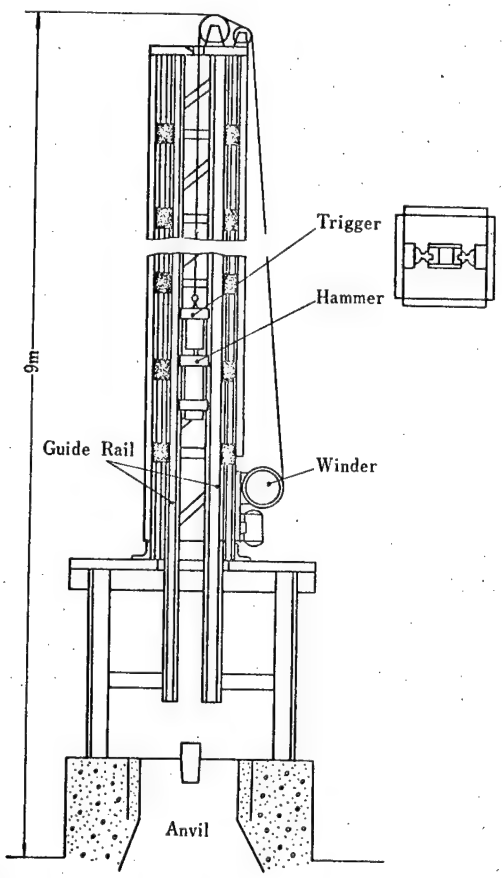

Fig. 1·3 Drop-Hammer Type of Testing Machine.
Weight of Hammer 25, 50 kg, Maximum
Strain rate 700 sec^{-1}.

1·1·1·3 Characteristics of the Testing Machines used

Among the many requirements for an ordinary type of testing machine, the most important for flow stress measurement is the constancy of strain rate. This point will be discussed for each of the machines used.

a. cam-plastometer

It is a device for producing a constant strain rate. For its proper performance, the compression stroke prescribed by the cam must be exactly followed. In this connection the following three defects need be eliminated.

1) The compression load can cause loosening of and elastic deformation in the components of the machine.

2) Insufficient flywheel energy gives rise to a variation in the angular speed of the cam at the compression stage.

3) At the initial moment of compression, the impact load springs the plunger and consequently the cam curve cannot be accurately followed for lack of contact between the cam and the plunger.

Fig. 1·4 is the measured interval change between the two compression plates as a function of the load that was applied to the plates by means of an oil jack. The displacement amounts to 0.084 mm for a 15 ton load, corresponding to 0.7% strain for the smaller specimen. Unless the test material is extremely hard, the contribution from 1) can safely be neglected. Moreover, though the compression plate interval in this case was taken to be as large as 360 mm, necessitating installation of the oil jack, this interval does not exceed 65 mm in actual flow stress measurements. Accordingly the elastic deformation is expected to be sufficiently small and not a serious problem.

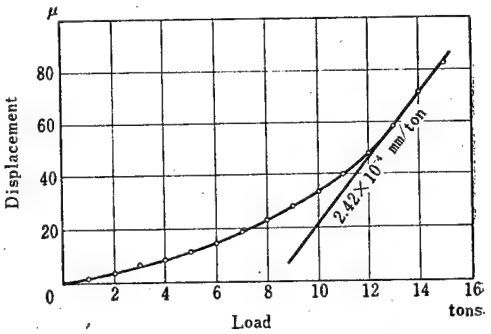

Fig. 1·4 Displacement Between the Compression Plates of the Cam-Plastometer, Maximum Displacement: 0.084 mm for a 15 tons Load.

For the estimation of the contributions form 2) and 3), compression tests were carried out in which specimen of aluminium, copper, and 5% Cr steel were strained at the strain rates of 0.13 and 100 sec^{-1}. The maximum load applied were 4, 13 and 25 tons for aluminium, copper, and 5% Cr steel, respectively. For the aluminium and copper specimens the strain rate remained constant: the 5% Cr steel specimen, on the other hand, exhibited an appreciable change in strain rate when the load exceeded 13 tons. Since the present experiment was designed for the maximum load of 10 tons and the maximum load of 25 tons used in the case of 5% Cr steel was well beyond the limit of the testing machine 15 tons, it was concluded that corrections for 2) and 3) were unnecessary.

b. drop hammer type of testing machine

With this type of testing machine it is a known fact that the strain rate does not stay constant during the whole stage of deformation. That is, the strain rate changes

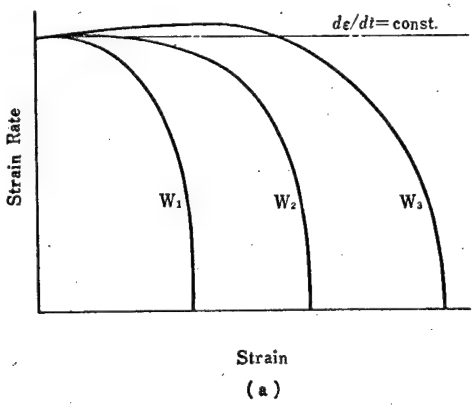

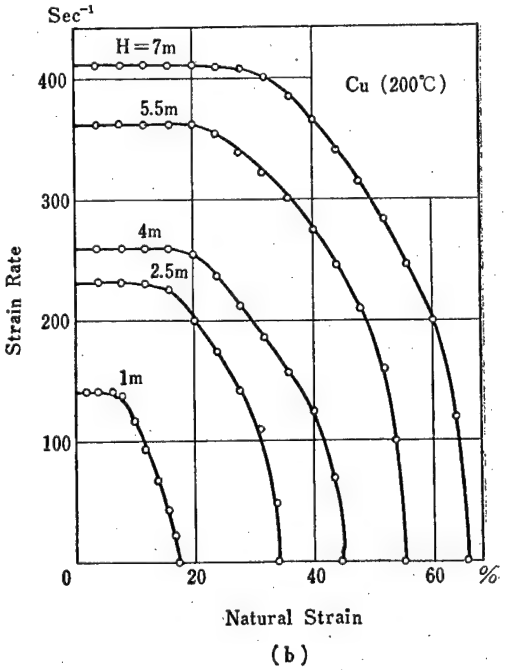

Fig. 1·5 (a), 1·5 (b) Strain Rate-Strain Relation. (a) with Weight of Hammer as a Parameter, (b) with Height of Fall as a Parameter.

from a maximum at the moment of impact to zero when deformation ceases.

It is possible, however, to produce a constant strain rate at least in some region of strain. Fig. 1·5 (a) shows how the strain rate changes with the weight of hammer, the distance of fall being constant. When the hammer weight is small (W_1), the strain rate begins to decrease in the early stages of deformation, and as the hammer weight increases (W_1 to W_2), the region of constant strain rate also increases. When the hammer weight exceeds a certain critical value (W_2), the strain rate goes through a maximum which is larger than the initial value, and no relatively constant strain rate region exists any longer. The critical values for the total strain and the strain region for constant strain rate were approximately 0.7 to 0.8 and 0 to 0.35 or 0.4, respectively.

Lueg et al also observed the existence of such a constant strain rate region and reported its magnitude to be 0–0.35 which is in good agreement with the present result.

1·1·2 Measuring Instruments

In determining the flow stress, three quantities must be continuously known: the applied load, the amount of deformation, and the time. The short time involved in the case of a high strain rate experiment demands the use of electronic or optical sensing instruments and not mechanical ones.

Fig. 1·6 shows the arrangement of the measuring instruments used in the present experiment. A capacitor strainmeter was used for the measuring of load. For the measurement of strain, a photo-electric tube was used with the drop hammer type of testing machine, and a capacitor strainmeter similar to the one for load measurement was used with the cam-plastometer. The time was measured by means of the intensity modulation of a cathode-ray tube.

All the above three quantities were DC amplified and fed into an oscilloscope and recorded by a 35 mm camera.

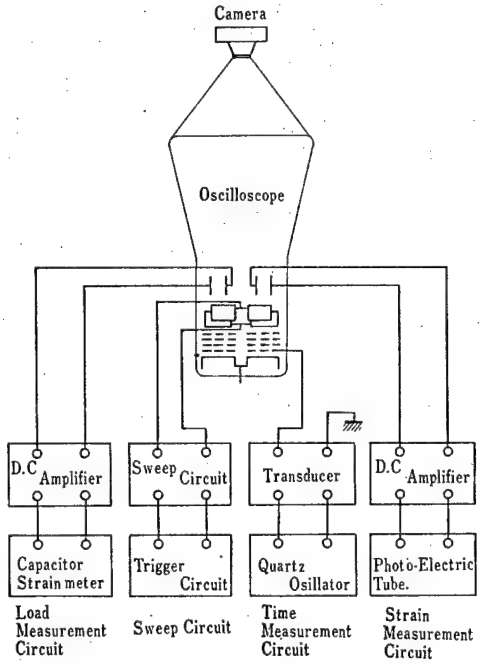

Fig. 1·6 Arrangement of the Measuring Instruments.

1·1·2·1 Load Measuring Instrument

As mentioned above, a capacitor strainmeter was used for this purpose. This has a high sensitivity and the error arising from the deformation at the sensing part can be practically eliminated by increasing the rigidity there.

Fig. 1·7 shows the load measuring instrument used in conjunction with the drop hammer type of testing machine. The detector forms part of the specimen holder and has two electrode plates mounted on the inside.

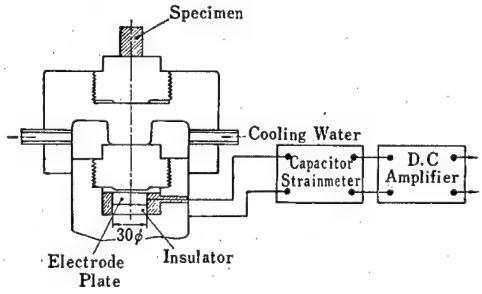

Fig. 1·7 Apparatus for Load Measurement. (Drop-Hammer)

Upon application of a force to the specimen, the decrease of the electrode separation results in a change in capacity, which is transmitted on a 3 Mc carrier and finally FM detected.

The greatest difficulty encountered during measurement is the vibration which shows up on the recorder and is primarily due to the mechanical vibration of the load measuring instrument. To avoid this the natural-frequency of the detector must be sufficiently high. Therefore, the part of the specimen holder that was likely to be the source of vibration was made rigid by an epoxy resin.

The electrode chamber was sealed to avoid any change of sensitivity due to oxidation of the electrodes.

The upper part of the specimen holder was water cooled to minimize thermal expansion at the electrode gap either due to ambient temperature changes or due to heat coming from the specimen.

The load measuring instrument of the cam-plastometer is shown in Fig. 1·8, the principle of which is the same as that for the drop hammer type of testing machine.

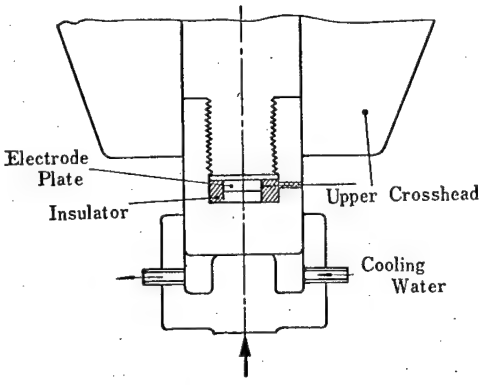

Fgi. 1·8 Apparatus for Load Measurement. (Cam-Plastometer)

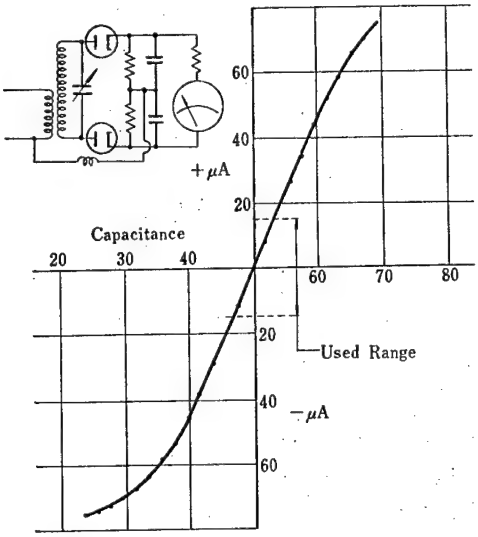

Fig. 1·9 Characteristic of the Capacitor Strainmeter.

Fig. 1·9 represents the characteristics of the capacitor strainmeter, i. e., the output current as a function of the capacitance of a standard placed at the position of the detector. In actual measurement of the flow stress the linear region between the capacitance change and the current was used.

The effect of ambient temperature changes on the sensitivity of the strainmeter was investigated in the temperature range of 5–30°C. There was a shift of zero point observed but no change in the sensitivity.

1·1·2·2 Strain Measuring Instrument

In the case of a drop hammer type of testing machine, strain was indirectly determined from the displacement of the hammer, assuming that the hammer was always in contact with

the specimen during the deformation stage. A schematic diagram is shown in Fig. 1·10, in which the light from a source lamp passes through a first lens to produce a parallel bundle, travels through a slit and a hammer slit, where it is subsequently collected by a second lens and finally enters a photo-electric tube. The displacement of the hammer gives rise to a change in the amount of light reaching the photo-electric tube.

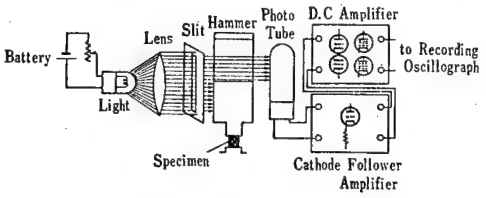

Fig. 1·10 Apparatus for Strain Measurement. (Drop-Hammer)

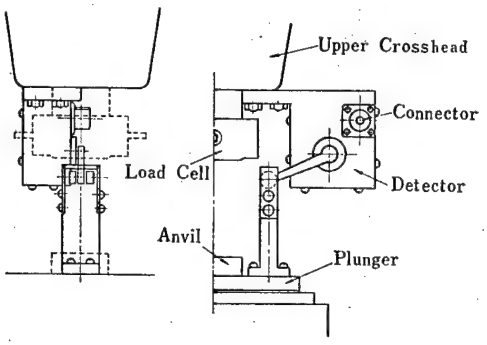

Fig. 1·11 Apparatus for Compression Strain Measurement.

In using a photo-electric tube, correction must be made for luminous intensity changes both before and after a measurement so as to eliminate the effect of long-term drift.

Because of these difficulties associated with the use of a photo-electric tube, a capacitor strainmeter was used for the case of a cam-plastometer experiment in which the strain rate is rather small. The detector part is shown in Fig. 1·11.

1·1·2·3 Time Signal

The intensity modulation of an oscilloscope was used as the time signal. A sine wave generated by a quartz oscillator was transformed to a square wave, and this was fed to the first grid of a cathode ray tube.

1–, 5–, and 10 kc quartz oscillators were used according to the magnitude of strain rate to be measured.

1·1·2·4 Recorder

Recording of the wave form on a 5″ cathod ray tube screen was made on 35 mm X-ray films. Examples are shown in Fig. 1·12 in which the compression load and displacement were fed into the Y_1 and Y_2 deflection plates.

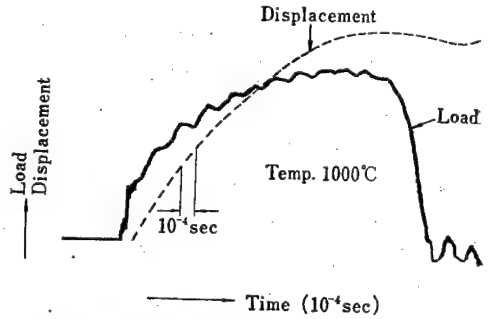

Fig. 1·12 Load & Displacement-Time Curve.
Testing Machine..... Drop-Hammer
Specimen ..... 0.12% C, Steel
Hammer Weight..... 25 kg
Height of Fall ..... 1 m
X Axis ..... Time
Y_1 Axis ..... Load
Y_2 Axis ..... Displacement

1·2 EXPERIMENTAL CONDITIONS

1·2·1 Heating of the Specimen and Temperature drops During Measurements

For the high temperature measurements, the specimens were heated in a furnace maintained at the test temperature for a given length of time. The holding time must be as short as possible to avoid oxidation but still long enough for there to be no temperature gradient

along the specimen. The optimum holding time was experimentally determined.

Allowance had to be made for the temperature drop that occurs when the specimen is removed from the furnace and placed on the anvil for a compression test.

1·2·1·1 Heating of the Specimen

As a rapid heating method, high frequency induction or self-heating by means of a large current was available. However, both of these methods make it difficult to determine the specimen temperature and structural changes within the specimen may occur.

As Bickwede[1-9] states "the growth of crystal nuclei is more dependent on the heating rate than on the holding time", different heating methods were liable to yield different results. It was, therefore, decided that the heating conditions should be similar to those actually encountered in practice which is to heat specimens in a furnace.

To determine the optimum holding time, the following experiment was carried out. As Fig. 1·13 shows, a specimen having a thermocouple at its center was inserted into a furnace maintained at a given temperature, and the temperature of the specimen was followed as a function of time. 18% Cr–8% Ni stainless steel was used as a specimen because it had the lowest heat conductivity among the materials used in the present experiments.

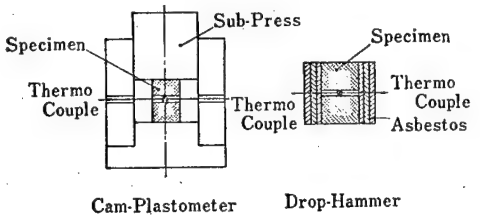

Fig. 1·13 Arrangement for Temperature Rise Measurement in the Furnace.

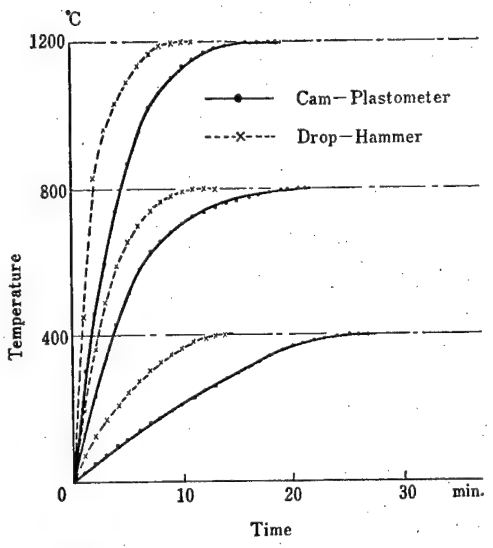

Fig. 1·14 Results for the Arrangement in Fig. 1·13.

The results are shown in Fig. 1·14. The specimen reaches the furnace temperature in 35 or 15 min depending on whether the specimen is held in a sub-press or not. From these results the corresponding times in actual flow stress measurements were taken to be 40 and 20 min, respectively.

For low temperature measurements, specimens were cooled in iced water (0℃) and in a mixture of dry ice and ethyl alcohol (−75℃).

The direct cooling allows a shorter immersion time, but since there is no possibility of oxidation and or structural changes at low temperatures, the same holding times as used in high temperature measurements were employed.

1·2·1·2 Temperature Drop

The decrease in the temperature of the specimen during measurements takes place in two stages:

(1) during the mounting of the specimen on the anvil,

(2) during compression.

Since the contribution from (2) was considered to be larger than that from (1), measurements were taken on (2) only.

The exprimental method and results are shown in Figs. 1·15 and 16. A thermo-couple was attached closely to the lower surface of the specimen where the temperature drop was expected to be the largest. With the use of a sub-press, and at the holding temperature 1200°C, the temperature drop was nil for the first 5 sec and 20 deg for the first 10 sec. The maximum time necessary for one run at the lowest strain rate is 7 sec after removing the specimen from the furnace, during which the maximum temperature drop is estimated to be 8 deg. At test temperatures below 1200°C, the temperature drop is expected smaller.

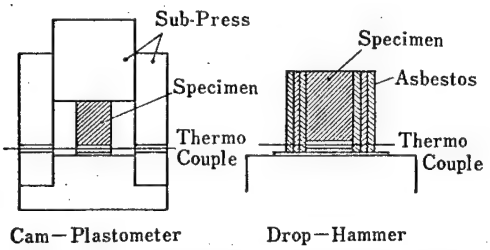

Fig. 1·15 Arrangement for Temperature Drop Measurement on the Anvil.

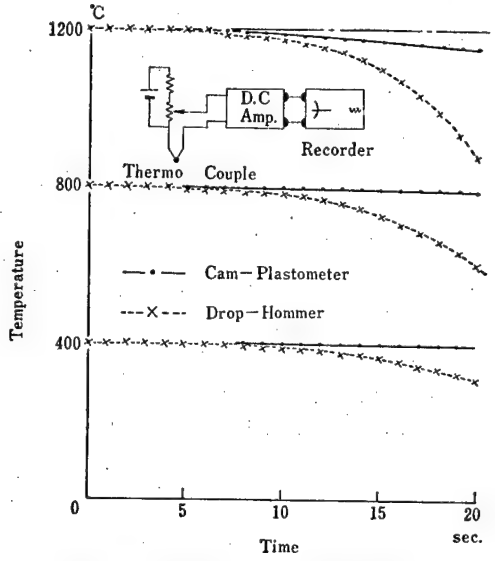

Fig. 1·16 Results for the Arrangement in Fig. 1·15.

In case of drop hammer measurements in which a sub-press could not be used, temperature drop was minimized by wrapping the specimen triply in asbestos and placing glass ribbons between the contact surface of the anvil and the specimen. Measurements under these conditions showed a larger temperature drop than for the cam-plastometer measurements. However, a shorter time of measurement 3 sec compensated for this, yielding a maximum of a 10 deg drop during one run.

1·2·1·3 Oxidation of the Specimen

Since no special care was taken to avoid oxidation during heating, there was the possibility of the specimen reducing the effective volume and altering its coefficient of friction at the contact surface.

According to the results of a preliminary experiment, zinc, aluminium, and stainless steel showed no appreciable sign of oxidation, while common steels and Cu-base alloys were easily oxidized. For a quantitative test, the latter two alloys were further heated at the maximum temperatures of 1200 and 800°C respectively, and the degree of oxidation was investigated.

For the purpose of lubrication, specimens for flow stress measurements were coated with glass powder which serves also as an oxidation inhibitor. To include this contribution, the above specimens were treated in the same way.

The results are shown in Table 1·1, in which the degree of oxidation is expressed by the weight of the scale removed by a sand paper from the surface of a specimen. It can be seen from this table that the specimens heated in a sub-press are oxidized very little even if they are not treated: if treated, there is practically no oxidation.

Table 1·1 Oxidation of the Specimen

Specimen	Temp.	Time	Treatment	before Heating	after Heating	Oxidation	Remark
99.9% Cu	800°C	40 min		18.183 gr	17.900 gr	0.283 gr	With a Sub-Press
			glass	18.046	18.025	0.021	
0.15% C-Steel	1200°C	40 min		15.928	15.792	0.136	With a Sub-Press
			glass	15.902	15.821	0.079	
0.15% C-Steel	1200°C	20 min		15.950	15.255	0.695	With Asbestos
			glass	15.924	15.892	0.032	

12φ×18h

1·2·2 Dimensions of the Specimen

The limited capacity of the cam-plastometer dictated the allowable specimen dimensions according to the strength of the material being tested. Even for the same material, a change of test temperature, mode of test, i.e., whether it is compressed by a cam-plastometer or by a drop hammer type of testing machine necessitated dimensional modifications.

All the specimens were similar in shape with a height to diameter ratio of 1.5. Although the law of similarity is expected to hold, allowances must be made for many sources of uncertainty such as grain size which is related with the pile-up of dislocations and segregation of solute atoms, differences in temperature drop, etc. which may be affected by specimen size.

The maximum and minimum dimensions used were 15 mm in diameter×22.5 mm in height and 8×12, respectively, the ratio of these two volumes being 6.5, for which the size effect is expected to be small. The specimens were prepared mainly by metallurgical processes and machined at the last stage. The effect of segregation is expected also to be small.

The effect of temperature drop has heen mentioned previously. As a double check, stress-strain curves were taken for two different sizes of killed low carbon steel, at 1000°C and at the strain rates of 3.5 sec^{-1} and 30 sec^{-1}. As Fig. 1·17 shows, both specimens yielded practically the same results.

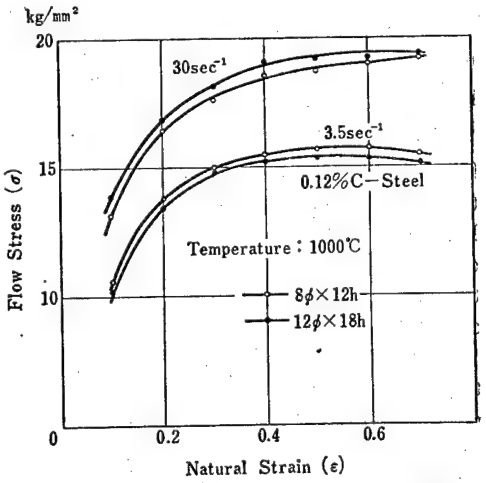

Fig. 1·17 Effect of the Dimensions of the Specimen on the Flow Stress.

1·2·3 Effect of Texture

Specimens taken from a rolled ingot often possess a preferred orientation, which can be detected by microscopic examination. Specimen were taken from three kinds of steels SS 41, FTW 60 and HIZ, each in the direction of rolling, width, and thickness, and subjected to tests at 800 to 1200°C, and at the strain rate of 0.3–10 sec^{-1}. Part of these results are shown

in Fig. 1·18 and are considered to be representative.

It can be seen there-from that the texture dependence is negligible, in agreement with the general assertion that hot working produces no texture. In view of the accuracy of experiment, it is difficult to attach any significance to the scatters of the data.

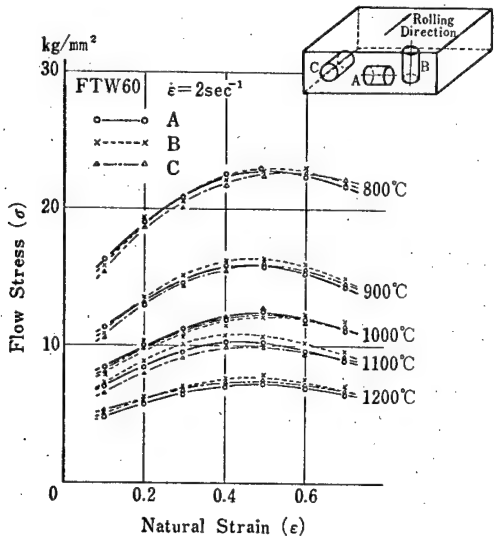

Fig. 1·18 Effect of Texture.

1·2·4 Friction at the Contact Surface

In compression tests, no accurate flow stress can be determined unless the problem of friction at the contact surfaces is properly dealt with. Much effort has been devoted to this solution, among which are Siebel's[1-10] circular conical compression test piece, Meyer and Nehl's[1-11] triple test piece, Siebel's and Schroeder-Webster's[1-12] correction formulas. In each of these cases the use of a special type of test piece or the knowledge of coefficients of friction at various temperatures and strain rates makes the determination of flow stress rather difficult.

In the present experiment care was taken to reduce the friction at the contact surfaces. The simplest and most effective method in use for reducing friction is due to Sims[1-13], as shown in Fig. 1·19 (a). According to Sims, the number of and the interval between grooves at the contact surface are important to the reduction of friction. However, on account of the trouble involved in making 0.02 mm deep grooves at a fixed interval at both ends of a specimen, specimens as shown in Fig. 1·19 (b) were adopted for the present experiments.

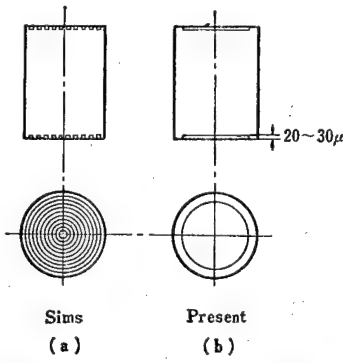

Fig. 1·19 (a), (b) Device for Reducing Friction. (a) Sims, (b)Present.

For a quantitative determination of the effect of friction on the true flow stress, aluminium specimen were statically compressed at room temperature, for five

different friction conditions. Fig. 1·20 shows that the apparent flow stress increases with increasing friction.

The degree of barreling also increases with increasing friction. For its quantitative description, it is convenient to introduce Ikejima's[1-14] barreling coefficient which is defined as

$$B=\Delta A/A_{\mathrm{th}},\quad \Delta A=A_{\max}-A_{\mathrm{th}} \tag{1}$$

where $A_{\max}$ is the maximum radial cross-section of a cylindrical specimen, and A_{th} is a theoretical cross-section for the corresponding strain with no barreling. Fig. 1·21 gives the relation between B and strain. The B for case (e) is very small and is of the order of 0.01 for a 70% compression. One can take this as an ideal case of no friction and define for each strain a stress-deviation $\Delta\sigma/\sigma_0$, where σ_0 is the stress of the ideal case and $\Delta\sigma$ is the difference between σ_0 and the stress of a non-ideal case for the corresponding strain. Fig. 1·22 gives the relation between $\Delta\sigma/\sigma_0$ and B for the conventional strain of 0.5. Conversely, given this relation for every strain, one can estimate the stress-deviation from an experimental B.

Throughout the present experiments, the barreling coefficient never exceeded 0.5 %. Errors in the measured flow stress, therefore, are estimated to be less than 0.3%.

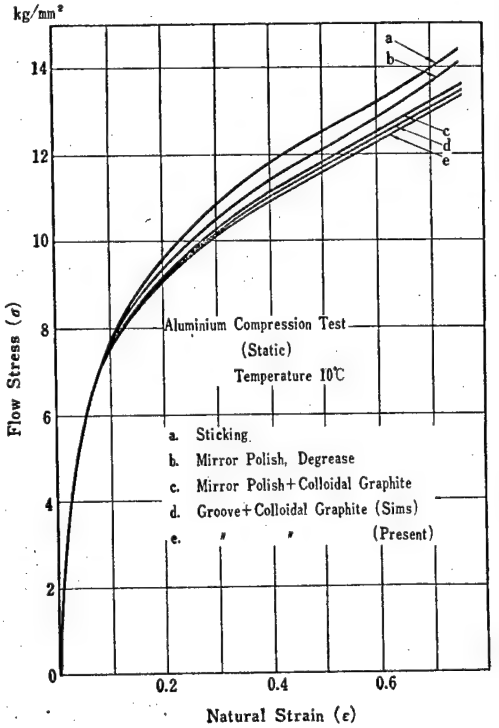

Fig. 1·20 Effect of Friction at the Contact Surface.

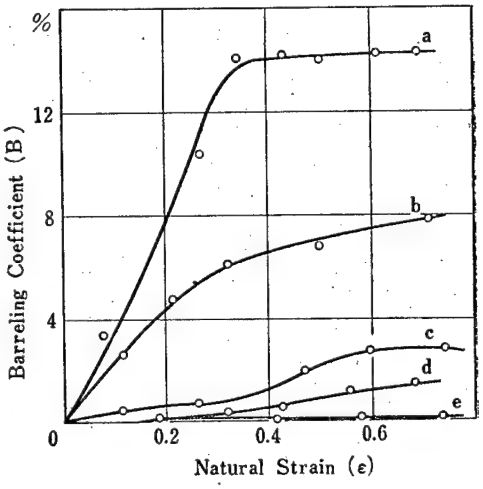

Fig. 1·21 Relation Between the Barreling Coefficient B and Strain ε.

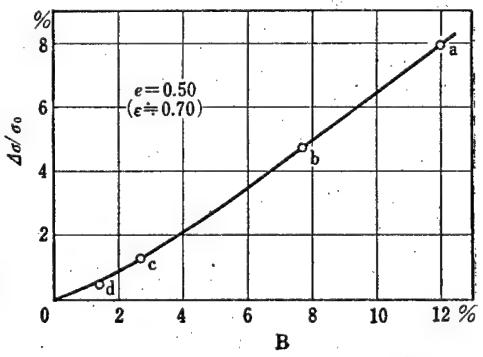

Fig. 1·22 Relation Between the Barreling Coefficient B and Compression Stress-Deviation.

1·3 OUTLINE OF EXPERIMENTS

1·3·1 Materials

The materials investigated were magnesium, titanium, 99.99% zinc and three commercial grade zinc, two different grades of aluminiums and duralumin, 99.99 and 99.9% copper and ten copper-base alloys, ten carbon steels, six high strength steels, eighteen low alloy steels, and fifteen stainless steels, i.e., seventy kinds altogether.

The prior histories and chemical compositions are listed in Tables 4·1 and 4·2.

1·3·2 Experimental Method

A cam-plastometer was used for strain rates below 100 sec^{-1} and a drop-hammer type of testing machine for strain rates above 100 sec^{-1}.

Below 600°C, the specimens were heated in a nichrome furnace and above 600°C in a siliconcarbide furnace. Temperature was automatically controlled to within 7 deg above 600°C and 3 deg below 600°C. Boiling water, iced water, and dry ice plus ethyl alcohol were used to obtain 100, 0, and −75°C respectively.

Zinc and duralumin specimens that were thermally treated were preserved in dry ice so as to suppress age-hardening. The maximum period of preservation did not exceed 60 hours, and efforts were made to take measurements as soon after thermal treatment. as possible. Static compression tests indicated no difference between the stress-strain curves obtained before and after preservation.

In the case of drop-hammer experiments, measurements were made on three quantities: time, load, and strain. In the case of cam-plastometer experiments, on the other hand, time was not directly measured but computed from the number of revolutions of the flywheel.

1·3·3 Lubricants

The lubricants used were colloidal graphite at temperatures below 600°C, lead glass between 600 and 800°C, and pyrex glass above 1000°C.

1·3·4 Determination of the Flow Stress

Measurements were made of time of deformation, load and strain. True stress was computed from measured loads, assuming that the specimens were uniformly deformed maintaining a cylindrical form and a constant volume.

In drop-hammer experiments, the range in which strain rate remains constant to the accuracy of 3% does not extend to more than 0.4 in terms of natural strain. For this reason strains over 0.4 were not measured.

The degree of barreling was small enough to regard the measured stress as the flow stress of the material, probably to an accuracy of 3%. This approximation was made in analyzing data.

Experiements were repeated at least three times for one condition, and the average values were used in the plotting of flow stress against strain.

BIBLIOGRAPHY

(1-1) K. Inoue: Tetu-to-Hagane, Vol. 41, 1955
(1-2) J.F. Alder, V.A. Phillips: J. Inst. Metals, Vol. 83, 1954
(1-3) P.M. Cook: Proc. Inst. Mech. Engr, 1957.
(1-4) R.R. Arnold, R.J. Parker: J. Inst. Metals. Vol. 88, 1959

(1-5) A. J. Bailey, A. R. E. Singer: J. Inst. Metals, Vol. 92, 1963.
(1-6) W. Lueg, G. Bürger, K. Fink: Archiv für Eisenhüttenwesen, 1955.
(-17) A. Nadai, M. Manjoine: Proc. ASTM, Vol. 40, 1940.
(1-8) E. Orowan: BISRA Report MW/F/22/50, 1950.
(1-9) D. J. Bickwede: "Flat Rolled Products: Rolling and Treatment", 1959.
(1-10) E. Siebel, A. Pomp: K-W Inst. für Eisenforsch, Vol. 8, 1926.
(1-11) H. Meyer, F. Nehl: Stahl u. Eisen, Vol. 45, 1925
(1-12) W. Schroeder, A. Webster: J. Appl., Mech., Vol. 16, 1945
(1-13) N. Loizon, R. B Sims: J. Mech. Physics. Solids, Vol. 1, 1953.
(1-14) Ikeshima: J. Japan Inst. Metals, Vol. 17, 1953.

PART 2. THE FLOW STRESS FOR NON-FERROUS METALS AND ALLOYS

In this Part, the experimental results concerning the flow stress of the non-ferrous metals and alloys will be discussed.

2·1 FLOW STRESS-STRAIN CURVES

The flow stress-strain curves of non-ferrous metals and alloys compressed at the strain rates of 0.13 to 650 sec^{-1} are given in Figs. 4·1 to 4·21. The temperature range explored is from −75 to 650°C for aluminium, 200 to 500°C for duralumin, −75 to 300°C for zinc, 18 to 500°C for magnesium, 400 to 900°C for titanium, and 18 to 900°C for copper and its alloys. The temperatures shown in the figures refer to those before compression, and no correction was made for temperature rise due to plastic deformation.

The experimental results concerning the face-centered-cubic metals (aluminium in Figs. 4·1 and 4·2, copper in Figs. 4·4 and 4·5) and the hexagonal-close-packed metals (zinc in Figs. 4·16 to 4·19, magnesium in Fig. 4·20, and titanium in Fig. 4·21) show that the stress required for a given plastic strain increases with increasing strain rate, and decreases with increasing temperature. Above room temperature, the flow stress changes in a very complex manner with strain, strain rate, and temperature. For instance, stress-strain curves do not remain similar upon changing strain rate; the curves obtained at and above 500°C and at the strain rates of 2.5 and 0.13 sec^{-1} show a stress maximum below 0.3 strain for tough pitch copper with a further plastic deformation following at a lower steady stress. These anomalous plastic behaviors may be characterized as follows:

1) The stress peak seems to occur above 0.5 T_m (T_m: melting point in °K), and the lowest critical temperature for the occurrence of such an anomaly decreases with increasing strain rate (Fig. 4·4).

2) The initial part of the stress-strain curve for non-ferrous metals does not rise rapidly but gradually, in contrast to the case with mild steel at room temperature.

3) The strain at the peak stress is by far larger than in the case of mild steel which shows a sharp yielding point at a small strain.

4) The magnitude of the maximum stress and its associated strain depends on the temperature and strain rate selected, and this strain decreases with increasing temperature and decreasing strain rate.

5) Work hardening occurs until the stress peak is reached, and then plastic deformation proceeds at a lower stress.

6) In some alloys the first peak is followed by a second smaller peak.

7) No heterogeneous deformation such as Lüder's bands has been observed.

In magnesium and zinc, the stress-strain curves shown in Figs. 4·16 and 4·20 are quite different from those for the other metals and alloys investigated in that the flow stress falls down rapidly as the strain goes beyond 0.2 or 0.3.

In Cu–Zn and Cu–Sn alloys the effect of temperature and strain rate on the deformation behavior is quite complicated. The flow stress of these alloys sometimes increases with increasing temperature. Further, the peak stress for Cu–Sn alloys increases with increasing concentration of the alloying element. The same tendency was also observed to a lesser degree in Cu–Zn alloys.

2·2 TEMPERATURE DEPENDENCE OF THE FLOW STRESS

Metallurgically speaking, the plastic flow stress at high temperatures and low strain rates is governed by such processes as recovery, recrystallization, grain growth and so on. The experimentally established form for the temperature dependence of flow stress

$$\sigma = A\,exp(B/T) \qquad (1)$$

where A and B are constants not necessarily independent of temperature, may then be accounted for by the fact that the above processes are rate processes obeying and Arrhenius type of equation.

The stress-strain curves of commercial-purity aluminium, copper, magnesium, zinc, and titanium have been obtained by using a cam-plastometer. The effect of temperature on the flow stress of these metals is shown in Fig. 2·1 in which anomalies are observed at 175–200°C with zinc, 200–250°C with aluminium, 400–500°C with copper, 200–300°C with magnesium, and 600–700°C with titanium, all somewhere around 0.5 T_m. There is a temperature independent region around 0.5 T_m, above which temperature as well as strain rates affects the flow stress strongly.

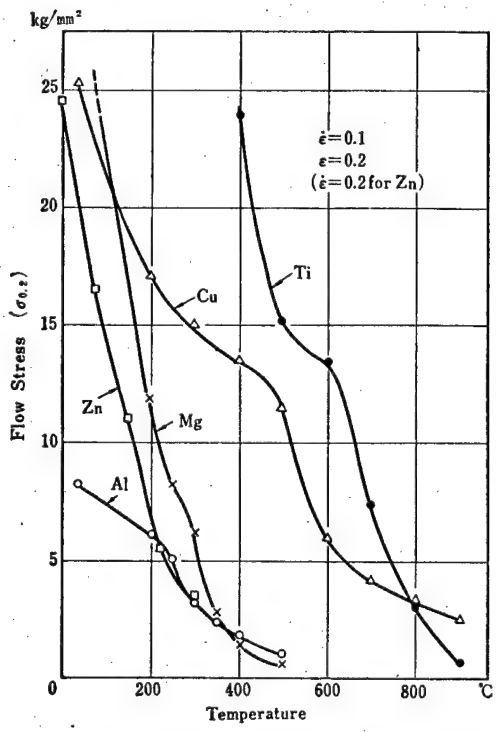

Fig. 2·1 Temperature Dependence of the Flow Stress of Commercial-Purity Metals.

In Fig. 2·2 is shown the difference in flow stress between annealed and as-drawn tough pitch copper specimens. This difference disappears above 400 to 500°C, in accord with the view that the high temperature flow is related to some diffusion-controlled processes.

Fig. 2·3 is the $\log\sigma - 1/T_k$ curves for tough pitch copper. Of interest to note is the appearance of two kinks in the curves: one around 0.5 T_m and the other below 0.5 T_m. The fact that the kink at 0.5 T_m corresponds to that in Fig. 2·1 points to the onset of a diffusion-controlled mechanism, since this is where the rate of diffusion begins to become appreciable.

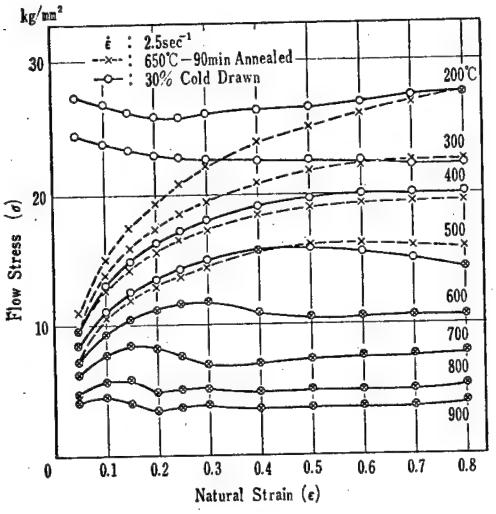

Fig. 2·2 Difference in Flow Stress Between Annealed and Cold Worked Specimens of Tough Pitch Copper. Compressed at the Strain Rate of 2.5 sec^{-1}.

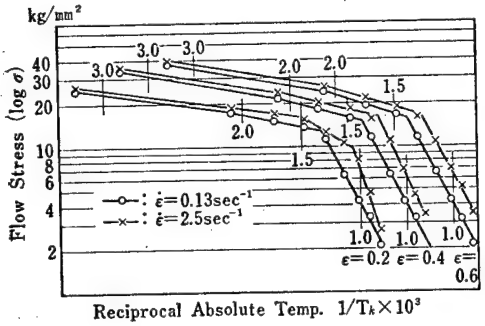

Fig. 2·3 Arrhenius Plot of the Flow Stress of Tough Pitch Copper.

It is generally known that the flow mechanism undergoes a change at about 0.25, 0.5, and 0.8 T_m. In copper, aluminium, and titanium, however, the second kink occurs at 0.36, 0.6, and 0.55 T_m, respectively. Whether or not these kinks indeed correspond to a change of the flow mechanism remains to be ascertained.

The test temperatures for the Cu-Zn alloys are given in the phase diagram of Fig. 2·4. A microstructural examination revealed that the alloys containing up to 35 wt% Zn are α-phase, and those of 40 wt% Zn are $(\alpha+\beta')$-phase. Fig. 2·5 shows the temperature de-

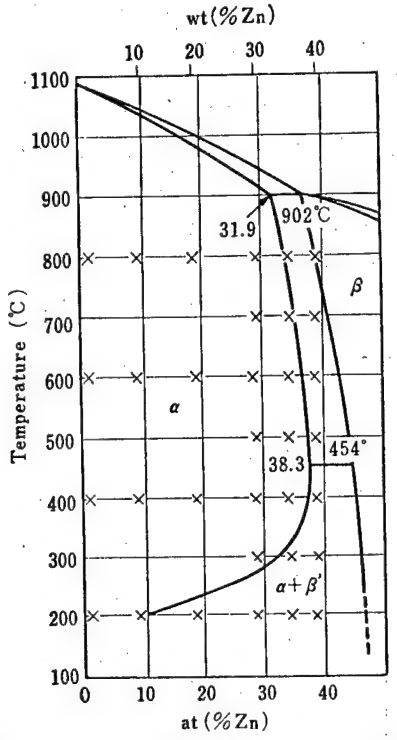

Fig. 2·4 Phase Diagram of the Cu-Zn System. Crosses denote the Positions at which Measurements were Made.

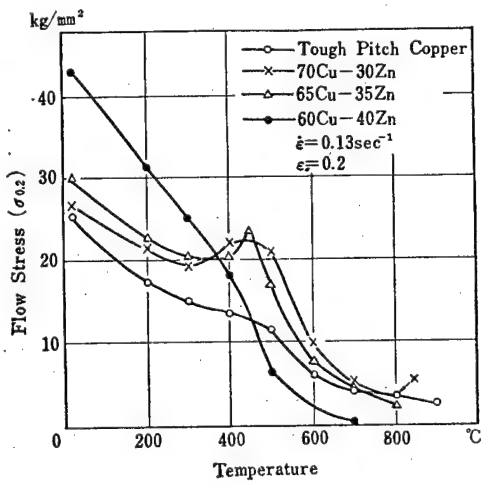

Fig. 2·5 Temperature Dependence of the Compression Stress of Copper and Copper-Zinc Alloys at $\varepsilon=0.2$. Strain Rate: 0.13 sec^{-1}.

pendence of the flow stress for three zinc alloys and tough pitch copper. The curves for 70% Cu–30% Zn and 65% Cu–35% Zn alloys are different from the previously obtained curves in that they exhibit a reverse temperature dependence of the flow stress a little below $0.5T_m$. In particular, Fig. 2·6 shows this temperature dependence for the 65% Cu–35% Zn alloy with strain rate as a parameter. The temperature at which the stress peak appears increases with increasing strain rate.

Ardley and Cottrell[2-1] have observed that the critical resolved shear stress of β-brass reverses it temperature dependence in the neighborhood of 200°C, and attributed it to the formation of a superstructure.

From the appearance of superlattice lines in X-ray analysis, α-brass is also known to undergo an order-disorder transition. If the reverse temperature dependence of the flow stress shown in Fig. 2·6 were really due to the formation of a superstructure or precipitation, a specimen quenched from above the transition temperature (300 to 500°C) would yield a lower flow stress than a slowly cooled specimen. As Fig. 2·7 shows, however, heat treatments from 600°C had no effect on the flow stress of 65% Cu–35% Zn brass when measured at room temperature, which refutes the above possibility.

Cu–Sn alloys also exhibit a reverse temperature dependence around $0.5T_m$. Fig. 2·8 shows the temperature dependence of the flow

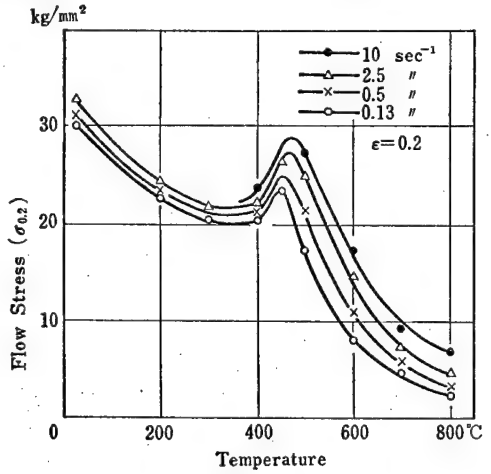

Fig. 2·6 Temperature Dependence of the Compression Stress of 65% Cu-35% Zn Alloys at $\varepsilon=0.2$.

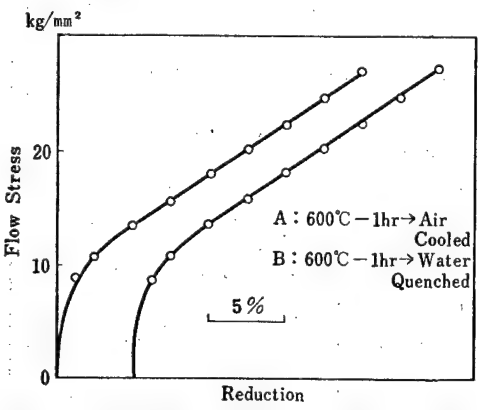

Fig. 2·7 Stress-Strain Curves of a 65% Cu-35% Zn Alloy at Room Temperature. Curve A, Slowly Cooled Specimen; B, Rapidly Cooled one from 600°C. Conventional Strain Rate in this Case in 1.4×10^{-3} sec^{-1}.

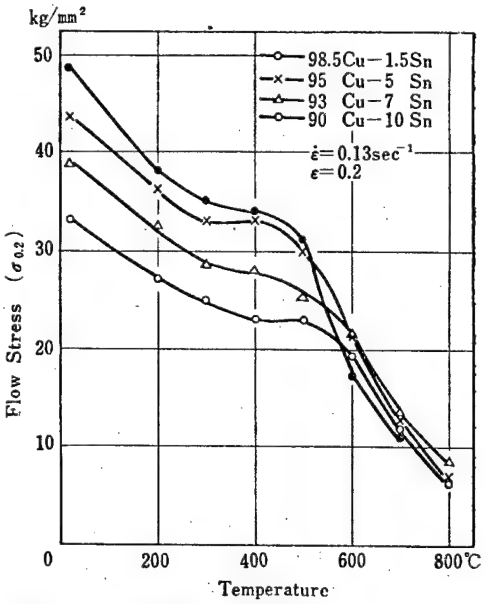

Fig. 2·8 Temperature Dependence of the Compression Stress of Cu-Sn Alloys at $\varepsilon=0.2$.

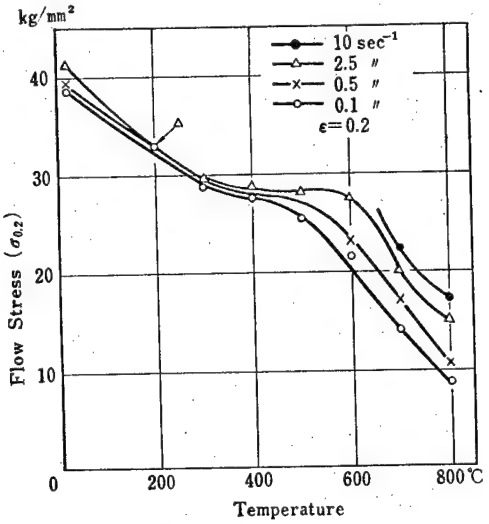

Fig. 2·9 Temperature Dependence of the Compression Stress of 93%Cu-7% Sn Alloys at $\varepsilon=0.2$.

stress at a strain rate of $0.13\,\mathrm{sec}^{-1}$ and at 0.2 strain. In particular, Fig. 2·9 refers to the details of that of the 93% Cu–7% Sn alloys.

A microscopic examination revealed that the 60% Cu–40% Zn alloys were $(\alpha+\beta')$-phase below 454°C and $(\alpha+\beta)$-phase above 454°C. With increasing temperature above 500°C, the β-phase increases its content at the expense of the α-phase, and becomes softer than tough pitch copper and α-brass. No reverse temperature dependence of the flow stress has been found in this case.

If these anomalous plastic behaviors are really due to the viscous motion of dislocations, one may expect to observe similar phenomena in every substitutional solid solution.

2·3 STRAIN RATE DEPENDENCE OF THE FLOW STRESS

It is generally asserted that the flow stress of metals and alloys is more susceptible to strain rate above recrystallization temperature than below. The experimentally established relation between the flow stress σ and the strain rate $\dot{\varepsilon}$ takes the form

$$\sigma=\sigma_0\dot{\varepsilon}^m \qquad (2)$$

where σ_0 is a proportionality constant. Campbell[2-2] and Hahn[2-3] derived Eq. (2) by relating the macroscopic strain rate with the motion of dislocations. The effect of temperature manifests itself in the exponent "m".

As Fig. 2·10 shows, Eq. (2) is valid at least in the case of aluminium. However, for some metals and alloys in which the flow stress-strain curve exhibits a stress peak, Eq. (2) does not hold in general but for particular

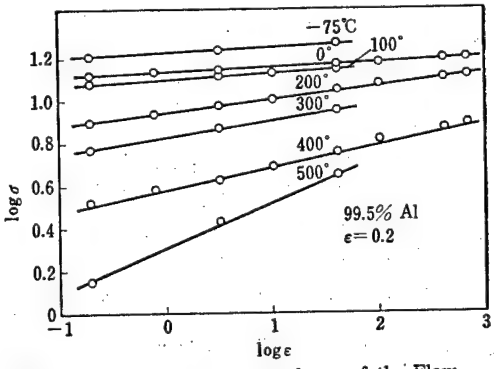

Fig. 2·10 Strain Rate Dependence of the Flow Stress of 99.5% Al at $\varepsilon=0.2$.

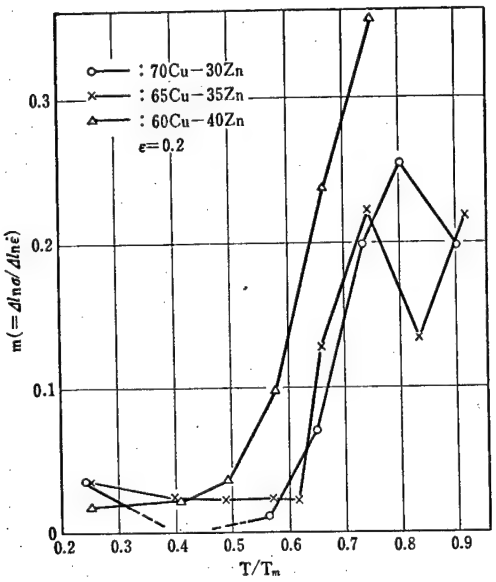

Fig. 2·14 "m"-Reduced Temperature Relation for Cu-Zn Alloys.

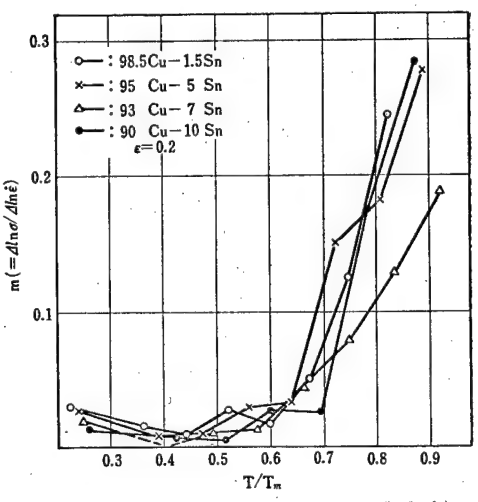

Fig. 2·15 "m"-Reduced Temperature Relation for Cu-Sn Alloys.

2·4 THE FLOW CHARACTERISTICS OF SPECIFIC MATERIALS

The flow stress of α-brass increases with increasing zinc concentration up to 10 wt%. When the concentration exceeds 20 wt%, the stress-strain curve reveals a new feature: at temperatures below $0.5\,T_m$, the flow stress is little affected by strain rate with work hardening occurring over a wide range of strain, and above $0.5\,T_m$, the initial work hardening of short duration is followed by a steady flow which is extremely sensitive to strain rate; with further increase of temperature the stress-strain curve begins to exhibit a stress peak, though not so clearly as in the case of tough pitch copper.

60% Cu–40% Zn alloys which contain not only the α-phase but also β or β'-phase show a different flow characteristic. Work hardening almost ceases above 300°C and the flow stress becomes influenced by strain rate instead. Above 500°C the flow beyond 0.05 strain proceeds at a constant stress. At 800°C the flow stress becomes so small that the applied load in low strain rate experiments cannot be read off from the film of the oscilloscope.

Fig. 2·16 shows the grain size and the zinc concentration dependence of the flow stress of Cu–Zn alloys which were compressed at $2.5\,sec^{-1}$ and at room temperature. The

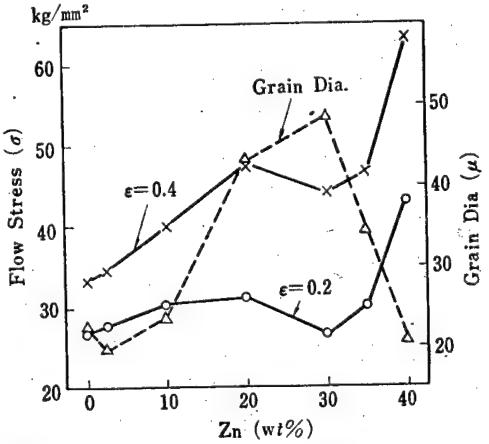

Fig. 2·16 Zinc Concentration Dependence of the Grain Size and the Flow Stress of Cu-Zn Alloys at Room Temperature.

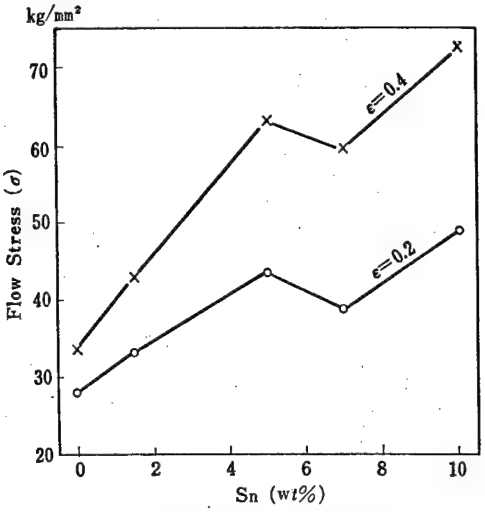

Fig. 2·17 Tin Concentration Dependence of the Flow Stress of Cu-Sn Alloys.

flow stress increases with increasing zinc concentration up to 20 wt% beyond which the flow stress begins to decrease down to a minimum at 30 wt% Zn. The flow stress of Cu-Sn alloys also becomes minimal at 6 to 8 wt% Sn (Fig. 2·17).

2·5 SUMMARY

From the analysis of the stress-strain curves of non-ferrous metals and alloys, the followings have been demonstrated:

1) The stress-strain curve exhibits a stress peak as temperature exceeds $0.5\,T_m$.

2) The temperature dependence of flow stress may be described by an Arrhenius type of equation, provided that the flow mechanism remains unchanged in the temperature range under consideration.

3) The magnitude of the peak stress of Cu-Zn and Cu-Sn alloys that appears in the vicinity of $0.5\,T_m$ increases with temperature, and the temperature of the stress peak shifts to the high temperature side upon increasing strain rate.

4) Eq. (2) is valid unless an anomalous plastic behavior sets in.

5) Contrary to the general impression, the strain rate sensitivity "m" of flow stress does not increase in a simple manner with temperature but tends to slacken or take a minimum around $0.5\,T_m$, sometimes taking a constant value when temperature reaches 0.7 and $0.8\,T_m$.

BIBLIOGRAPHY

(2-1) G. W. Ardley, A. H. Cottrell: Proc. Roy. Soc., A 219, 1953.
(2-2) J. D. Campbell: Acta. Met., Vol. 1, 1953
(2-3) G. T. Hahn: Ibd., Vol. 10, 1962.
(2-4) D. McLean: Mechanical Proporties of Metals, 1962.

PART 3. THE FLOW STRESS FOR STEELS

In this part, the experimental results concerning the flow stess of steels will be discussed.

3·1 FLOW STRESS-STRAIN CURVES

The flow stress natural strain curves for carbon, alloyed, and stainless steels are given in Figs. 4·22 to 4·70. The 0.15% C and 18% Cr-8% Ni steels were investigated in the temperature range 0–1200°C and in the strain rate range 0.8–650 sec^{-1}, where-as other steels were tested in the ranges where the actual hot working is usually performed, i. e., 800–1200°C and 0.8–100 sec^{-1}.

In general, the flow stress at a given strain increases with increasing strain rate and

decreases with increasing temperature. At high temperatures and at low strain rates, hardening occurs in the initial stages of deformation, followed by softening due to recrystallization as deformation proceeds. The flow stress thus goes through a maximum.

With the 0.15% C steel deformed in the temperature range 200–600°C and other steels tested at 800°C, no such maximum in the stress-strain curve was observed nor was there any definite strain rate dependence. On the other hand, the flow stress-strain curve exhibited an anomaly which is probably related with blue shortness or phase changes, as will be discussed later.

The low alloy steels of Figs. 4·38 to 4·53 which have only a limited use were included for their gradual variation in composition in order to see the effect of alloying elements.

3·2 TEMPERATURE DEPENDENCE OF THE FLOW STRESS

Figs. 3·1 and 3·2 show the temperature dependence of the flow stress for 0.15% C and 18% Cr–8% Ni steels, respectively. The strain selected is 0.2 and the strain rates studied were 0.2, 3.5, and 30 sec^{-1}.

In the case of the 18% Cr–8% Ni steel, the flow stress does not decrease uniformly with increasing temperature but shows an abrupt drop in the vicinity of 600–800°C. The occurrence of this anomaly at 0.5 T_m (T_m: melting point in °K) together with similar observations also

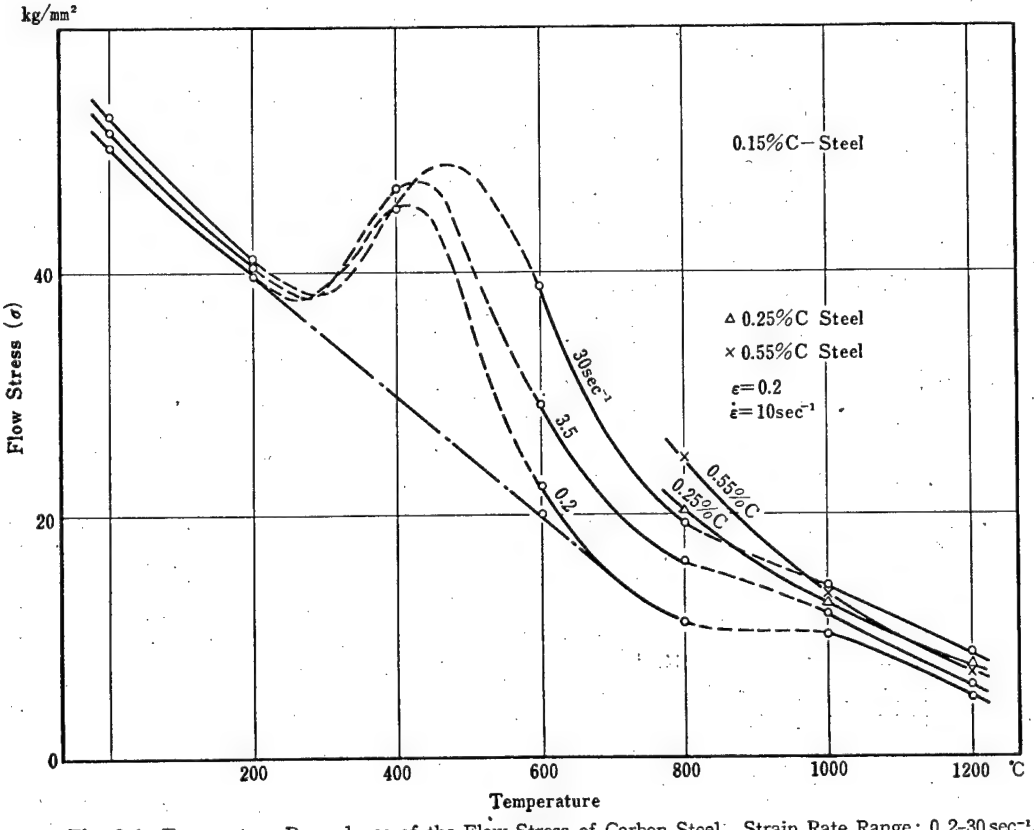

Fig. 3·1 Temperature Dependence of the Flow Stress of Carbon Steel. Strain Rate Range: 0.2–30 sec^{-1}.

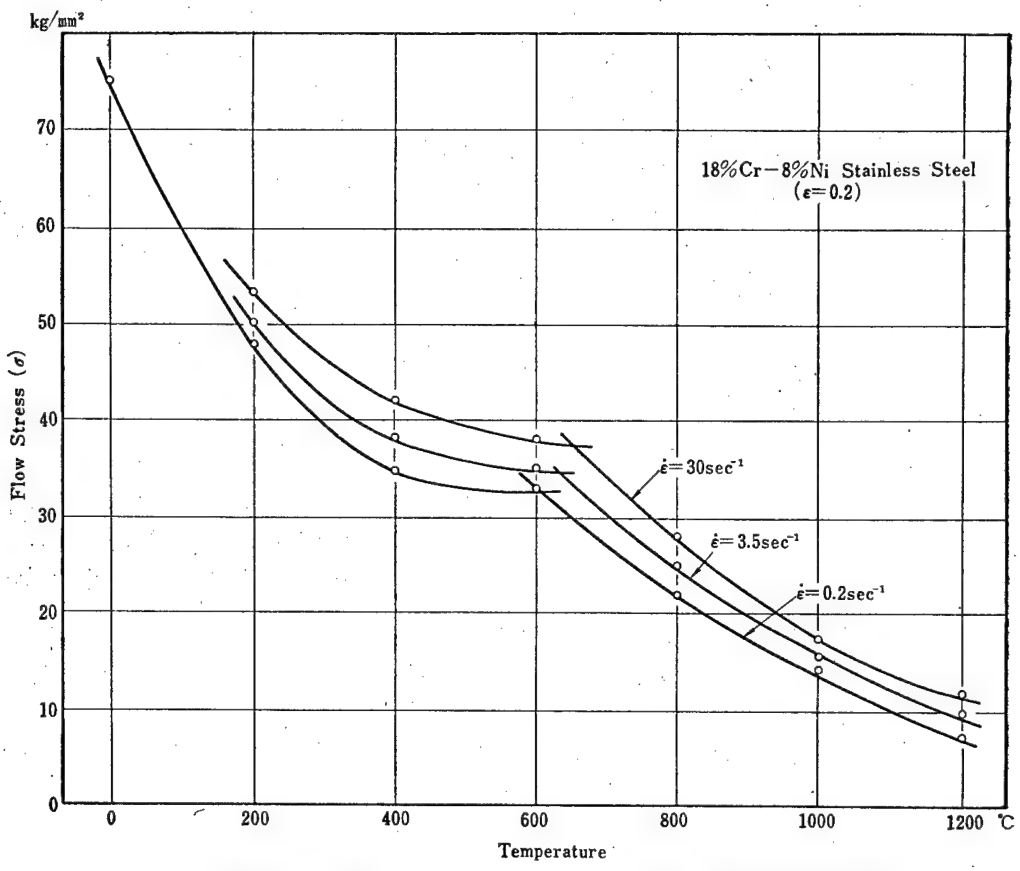

Fig. 3·2 Temperature Dependence of the Flow Stress of 18% Cr-8%Ni Stainless-Steel.

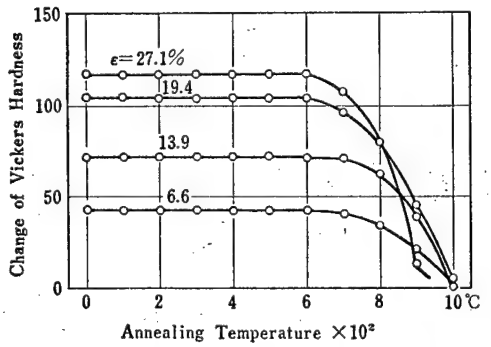

Fig. 3·3 Hardness Increase of Deformed 18% Cr-8% Ni Stainless Steel Over that of Fully Annealed One.

in non-ferrous metals indicates the beginning of recrystallization or grain growth during deformation. To corroborate this view, 18% Cr-8% Ni steel specimens prestrained in tension by 6-28% were annealed between 100 and 1000°C for 15 min and then water quenched. Fig. 3·3 shows the hardness increase over that of an unstrained specimen. The hardness begins to decrease around 600°C at high strains or around 700°C at low strains. The similarity of temperature dependence between hardness and flow stress supports the above interpretation.

In the case of 0.15% C steel, there was observed a peak in the flow stress around 200-600°C. Owing to the wide interval of temperature for the data, the exact location of the peak is difficult to specify. With increasing

temperature there exists a second peak the exact position of which is also unkown for the same reason. Fig. 3·4 is the flow stress-temperature curve of killed low carbon steel. The smaller temperature intervals (100 deg) for these data reveal the peaks more clearly than in Fig. 3·1. Finally a third peak exists around 900–1000°C.

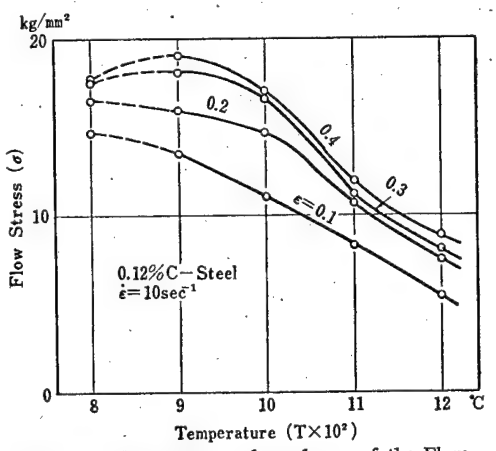

Fig. 3·4 Temperature dependence of the Flow Stress of 0.12% C-Steel.
Strain (ε)=0.1–0.4,
Strain rate ($\dot{\varepsilon}$)=10 sec^{-1}.

The existence of the first peak has been recognized by many researchers. For low strain rate and high temperature tensile tests this peak is characterised by the occurrence of a violent oscillation in the stresss-train curve taken around 200–300°C and a simultaneous rise in flow stress, with varying degree of intensity depending on the carbon content. It has been observed by Nadai and Manjoine that this peak is displaced to the high temperature side upon increasing strain rate. They have also observed that the temperature at which this peak occurs is 240°C at 10^{-4} sec^{-1}, 340°C at 0.5 sec^{-1}, and 560°C at 600 sec^{-1}.

The probable cause of this phenomenon is the ageing effect called blue shortness in which diffusion plays an important role. The strain rate and temperature dependence of the peak stress may then be accounted for by the kinetic behavior of a rate process. The peak position in the present experiment was estimated to be between 400 and 500°C, in agreement with the observation by Nadai and Manjoine[3-1].

The second peak was observed only in low carbon, low alloy, and 13% Cr steels among the materials investigated. As can be seen from the phase diagram, steels containing less than 0.8% carbon change from α-phase to ($\alpha+\gamma$)-phase around 720°C. The difference in carbon content between the two phases is expected to give rise to a change in the magnitude and temperature-strain rate dependence of the flow stress. This second anomaly at 800°C may then be explained as due to a phase change. Were it not for this phase change, the flow stress curve would extend smoothly beyond the transition point into the two regions, as shown by the dotted lines in Fig. 3·5.

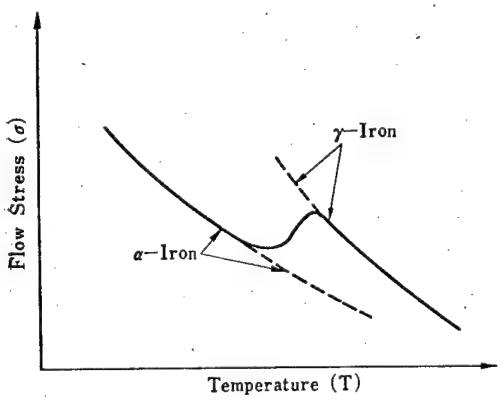

Fig. 3·5 Flow Stress-Temperature Curves of the α-& γ-Iron.

Above 800°C the flow stress in the α-region should monotonously decrease with increasing temperature. However, as is seen in the killed low carbon steel of Fig. 3·4 and less clearly in the 0.15% C steel of Fig. 3·1, this is not the case and the flow stress in the region seems to be accompanied by work hardening around 900–1000°C.

The steels that exhibited such an anomaly were, beside the above two examples, 1% Cr-0.5% Mo steel and 5% Cr-0.5% Mo steel, both with a carbon content of less than

0.15%. Similar observations were made in 0.17% C steel by Alder and Phillips[3-2] and in 0.15% C steel but not in 0.56% C steel by Cook[3-3].

It has been reported by Inoue[3-4] that in his high strain rate tensile experiments four steels underwent brittle fracture but they all yielded the same flow stress in this temperature range. In Zoteel's[3-5] high strain rate tensile tests of Armco steel, however, there is a clear indication of the flow stress increasing with temperature around 1000°C.

No decisive conclusion has been drawn yet as to the nature of this third anomaly, but it is prevalent to attribute it to the precipitation of Al_2O_3 or AlN.

Except for these anomalies, the temperature dependence of the flow stress of steels as well as non-ferrous metals and alloys can be described by an Arrhenius type of equation. Of the two steels that were investigated over a wide range of temperature, the flow stress of the 0.15% C steel does not obey an Arrhenius equation because of the existence of anomalies: the flow stress of the 18% Cr–8% Ni steel, on the other hand, lies on a curve composed of three segments of straight lines when plotted as a function of reciprocal temperature (Fig. 3·6). The position of the second kink in the curve agrees with that of the kink of Fig. 3·2 which was interpreted as due to recrystallization.

The appearance of the second peak around 200°C can be considered either due to some mechanism related with work hardening or due to the hardening effect caused by chromium carbide which is seen in a low strain rate tensile test of stainless steel carried out around 200–600°C[3-6]. The present experiment could not decide between the two.

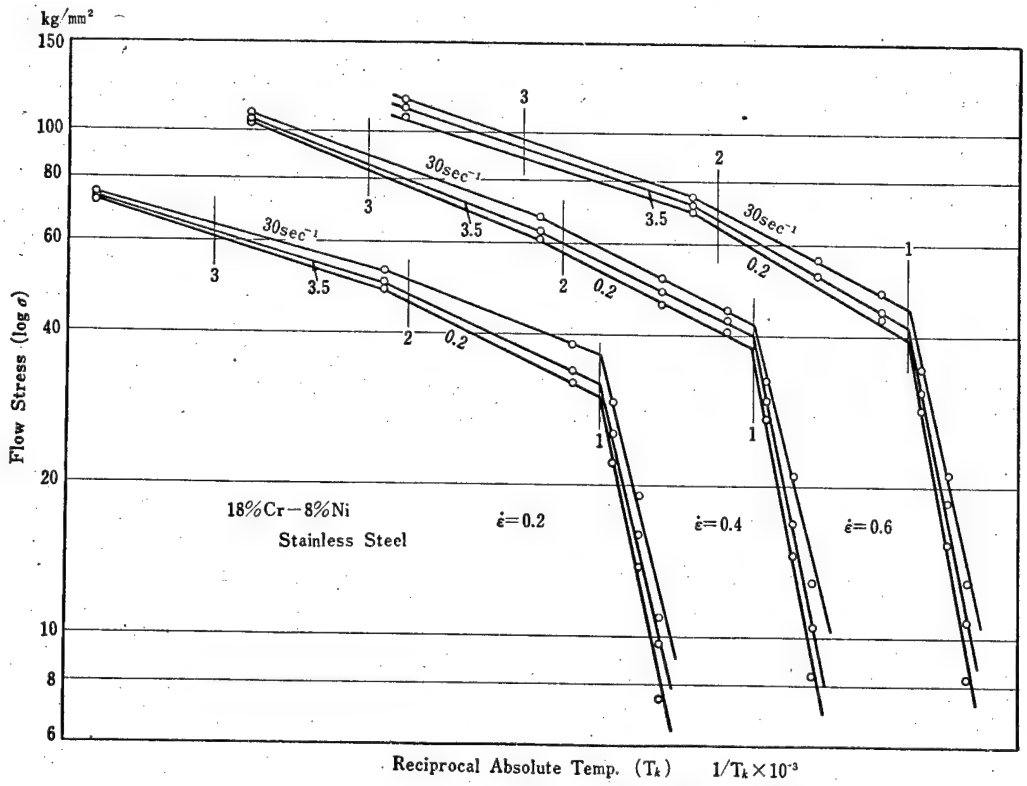

Fig. 3·6 Arrhenius Plot of the Flow Stress of 18% Cr-8% Ni Stainless Steel.

3·3 STRAIN RATE DEPENDENCE OF THE FLOW STRESS

As has been mentioned in the sections concerning the non-ferrous metals and alloys, the following relation holds between flow stress and strain rate:

$$\sigma = \sigma_0 \cdot \dot{\varepsilon}^m$$

Figs. 3·7 and 3·8 refer to the experimental results of 0.15% C steel and 18% Cr–8% Ni steel, respectively, each analyzed according to the above equation. Except for the 0.15% C steel at 400°C where blue shortness sets in, a linear relationship holds between $\log \sigma$ and $\log \dot{\varepsilon}$.

Fig. 3·9 shows the values of the exponent "m" which denotes the sensitivity of the flow

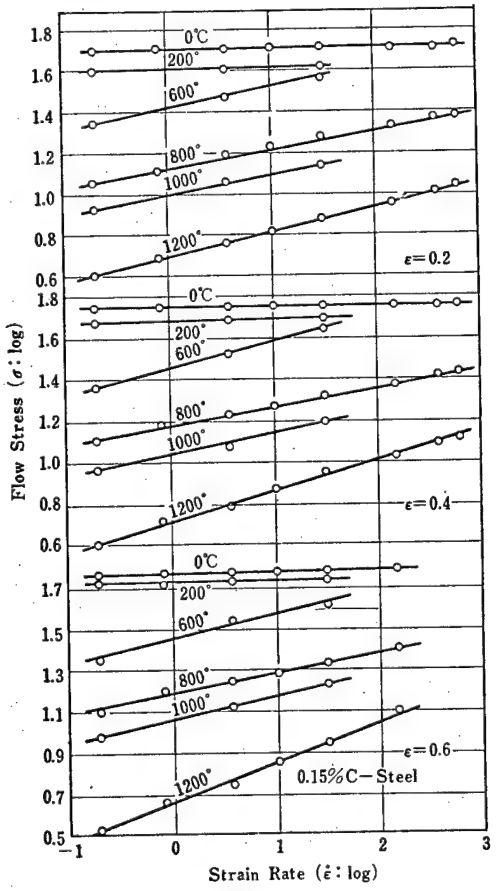

Fig. 3·7 Strain Rate Dependence of the Flow-Stress of 0.15% C-Steel.

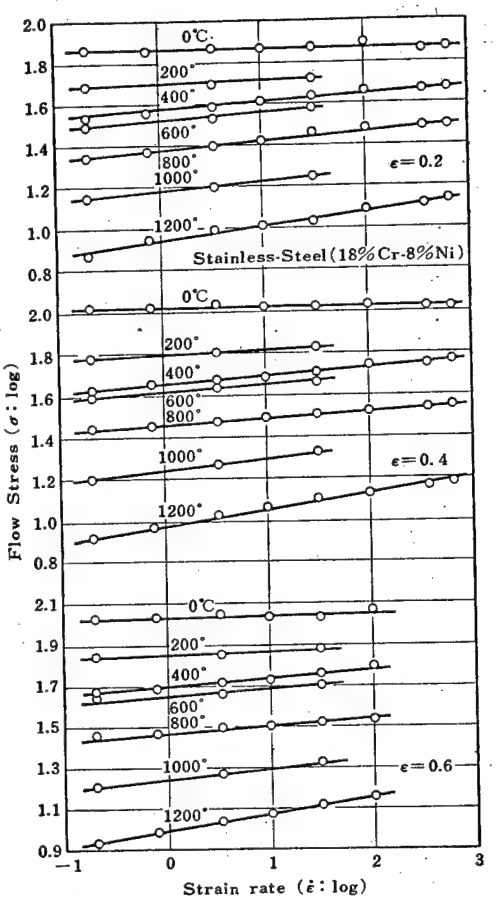

Fig. 3·8 Strain-Rate Dependence of the Flow Stress of 18% Cr-8% Ni Stainless Steel.

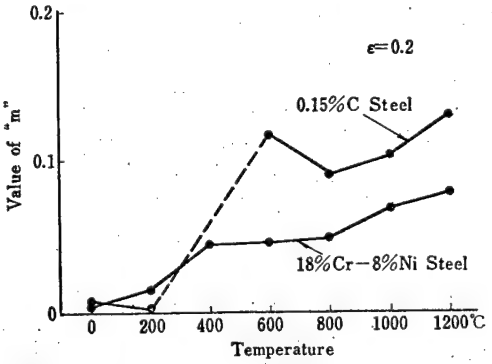

Fig. 3·9 "m" Value vs Temperature Curves for 0.15% C Steel and 18% Cr-8% Ni Stainless Steel.

stress to strain rate. "m" tends to increase with increasing temperature. In 0.15% C steel, however, "m" takes an unusually large value at 600°C. The existence of this anomaly has been recognized by other researchers.

3·4 THE FLOW CHARACTERISTICS OF SPECIFIC MATERIALS

3·4·1 Carbon Steels

The flow stress-strain curves at 0.2 strain and at a strain rate of 10 sec^{-1} are shown in Fig. 3·10 in which some of the results due to Inoue[3-1], Alder[3-2], and Cook[3-3] are included.

Up to 800°C, the flow stress tends to increase with increasing carbon content: at 1200°C, on the other hand, the flow stress takes on a constant value independent of carbon concentration. This is an established fact. For instance, the data due to Inoue and Cook indicate that the high temperature flow stress is practically independent of carbon concentration up to 1%.

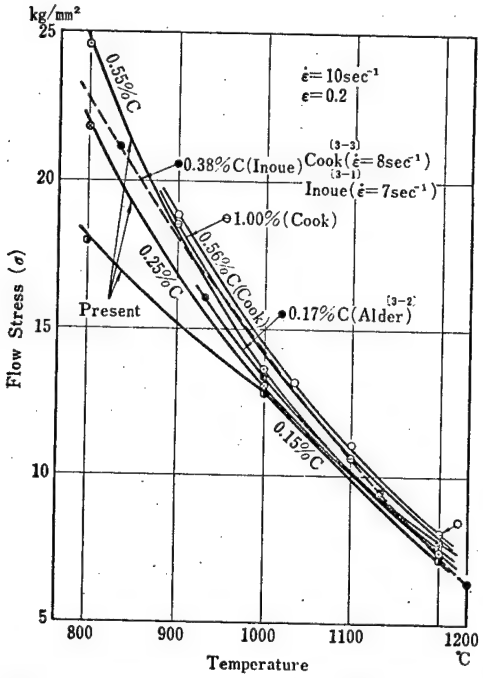

Fig. 3·10 Comparison of the Flow Stress of Carbon Steels Measured by Various Investigators. (Cook, Alder, Inoue and Present)

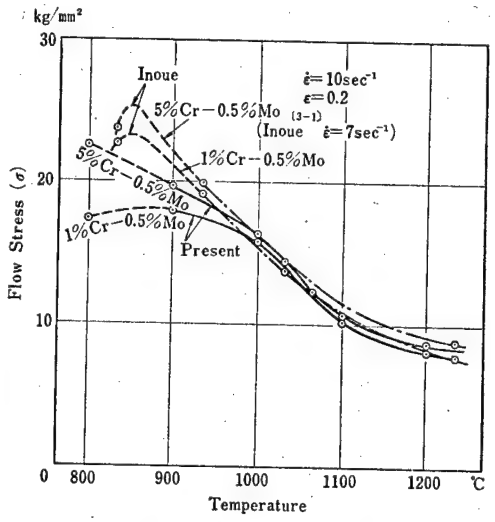

Fig. 3·11 Comparison of the Flow Stress of Low Alloy Steels Measured by Various Investigators. (Inoue and present)

3·4·2 Low Alloy Steels

Fig. 3·11 is the flow stress-strain curves of 1% Cr–0.5% Mo and 5% Cr–0.5% Mo steels together with Inoue's results.

There is to be seen a small but detectable concentration dependence: 5% Cr steel has a larger flow stress than 1% Cr steel. This is also true of Inoue's results.

Inoue's curves deviate from the present ones around 900°C where an anomaly related with some hardening effect is usually observed. The present experiments were unable to account for this difference.

It is generally known that the tensile strength of most chromium steels at room temperature decreases with increasing chromium concentration up to 6%.[3-7] Creep tests at 600°C as well as tensile tests up to 700°C confirm this.[3-8]

In the present experiment, however, the opposite tendency has been observed, probably owing to the high temperatures and the high strain rates used. As a matter of fact, Charpy impact tests yielded larger impact values for 5% Cr steel than for 2% Cr steel in the temperature range up to 700°C.[3-9] Nevertheless, the difference in flow stress between 1% and 5% Cr steels, especially at high temperatures, is not so large as to be important in practical applications.

The other low alloy steels of limited use have been investigated mainly to see the effect of alloying elements. Fig. 3·12 is the flow stress-strain curves of low alloys steels 1, 2, 3, 8, 9, and 10 at the strain rate 10 sec^{-1} and at the temperatures 1000 and 1200°C. The compositions are shown in Table 3·1 in which blanks denote the upper preceding values. In particular, the effects of manganese, chromium, copper, and nickel are shown in Table 3·2.

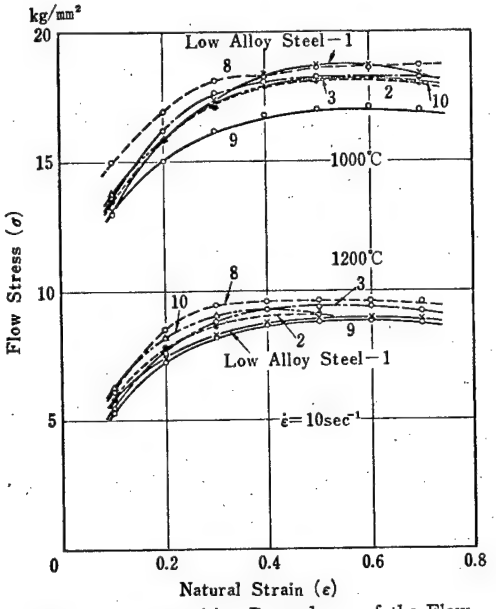

Fig. 3·12 Composition Dependence of the Flow Stress of Low Alloy Steels.

Table 3·1 Compositions of the Low Alloy Steels in Fig. 3·12.

Com. / No.	Mn	Cu	Ni	Cr
1	0.44	0.12	1.19	3.42
2	0.97			
3				4.21
8			3.17	
9		1.07		
10	2.18			

Table 3·2 Effects of Alloying Elements on the Flow Stress of Low Alloy Steels.

	1000°C	1200°C	Content %
C	Raises Flow Stress Slightly	Does not Alter	0.15 ⟶ 0.55
Mn	Does not Alter	Effective Within 0.5 Strain	0.44 ⟶ 2.18
Cu	Lowers	Alters Little	0.12 ⟶ 1.07
Cr	Raises	Alters Little	1 ⟶ 5
Ni	Effective Within 0.4 Strain	Raises	1.19 ⟶ 3.17

3·4·3 Stainless Steels

Fig. 3·13 is the flow stress-strain curves of 13% Cr, 13% Cr–0.5% Mo, 17% Cr, 18% Cr–8% Ni, 18% Cr–8% Ni–2% Mo steels at 0.4 strain and at a strain rate of 10 sec^{-1}.

The addition of molybdenum tends to suppress the decreasing tendency of the flow stress at high temperatures and is effective in increasing the flow stress in this region.

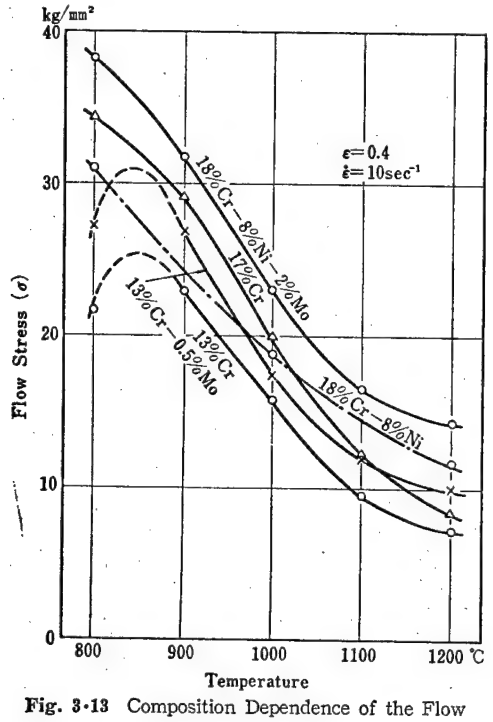

Fig. 3·13 Composition Dependence of the Flow Stress of Stainless Steels.

A large difference is seen between the flow stresses for the 13% Cr and the 17% Cr steels. As has been said of low alloy steels, the addition of chromium also tends to increase the flow stress at high temperatures and at high strain rates.

SUMMARY

A proper understanding of the flow stress of metals and alloys is a primary prerequisite to the determination of the mode of plastic working and the proper design of working tools. The fact that the flow stress depends not only on the properties of the material but also on the degree of deformation, deformation speed and temperature has made the measurements of flow stress difficult and restricted them to only a few kinds of materials. To narrow this gap, the authors have conducted investigations into forty-nine kinds of widely used steels and twenty-one kinds of non-ferrous metals and alloys. In this paper the results that have been obtained during the period between 1951 and 1966 have been presented. Although the first object of providing basic information concerning the flow stress which may be useful in practical appli-

cations has been achieved, the second object of relating the flow stress with strain, strain rate, and temperature has been confined to the proposal of empirical formulas.

The flow stress of metals and alloys at high temperatures is a complicated phenomenon in which two opposing tendencies, i. e., work hardening and recovery or recrystallization, compete simultaneously. It is hoped that the present experiment will contribute to the clarification of these phenomena and to the search for the equation governing their behavior with more accuracy and generality.

BIBLIOGRAPHY

(3-1) A. Nadai, M. Manjoine: J. Appl. Mech., June, 1941.
(3-2) J. F. Alder, V. A. Phillips: J. Inst. Metals, Vol. 83, 1954.
(3-3) P. M. Cook: Inst. Mech. Engr., 1957.
(3-4) K. Inoue: NIHON TOKUSHUKOKAN REPORT, January, 1955.
(3-5) B. C. Zoteel: Stal, 20-6, 1960.
(3-6) T. Maeda: Tetu-to-Hagane, 1950.
(3-7) C. A. Edwards: "The structure and Properties of Mild Steel", ASM, 1953.
(3-8) W. E. Bardgetl: "High-Temperature Steels", London, 1957.
(3-9) F. H. Clark: "Metals at High Temperature", Reinhold Pub. Co., 1950.

PART 4. DATA SHEET IN THE FORM

Table 4·1 List of Data Sheets.

Fig. No.	Test Materials	Treatment	Strain Rate Range	Temperature Range
4- 1	Aluminium	Cold Drawn→Annealed	0.2～650 sec^{-1}	−75～ 500°C
2	〃	Extruded→Cold Drawn→Annealed	0.1～ 10 〃	18～ 500〃
3	Duralumin	Cold Drawn→Annealed	0.2～100 〃	200～ 500〃
Fig. No.	Test Materials	Treatment	Strain Rate Range	Temperature Range
4- 4	99.9% Copper	Hot Rolled→Cold Drawn →Annealed	0.1～ 2.5sec^{-1}	18～ 900°C
5	99.99% Copper	〃	0.1～ 10 sec^{-1}	18～ 800°C
6	98% Cu-2% Zn Brass	Extruded→Cold Drawn→Annealed	〃	〃
7	90% Cu-10% Zn Brass	〃	〃	〃
8	80% Cu-20% Zn Brass	〃	〃	〃
9	70% Cu-30% Zn Brass	〃	〃	〃
10	65% Cu-35% Zn Brass	〃	〃	〃
11	60% Cu-40% Zn Brass	〃	〃	〃
12	98.5% Cu-1.5% Sn Bronze	〃	〃	〃
13	95% Cu-5% Sn Bronze	〃	〃	〃
14	93% Cu-7% Sn Bronze	〃	〃	〃
15	90% Cu-10% Sn Bronze	〃	〃	〃
Fig. No.	Test Materials	Treatment	Strain Rate Range	Temperature Range
4-16	Pure Zinc	Hot Rolled	0.2～650 sec^{-1}	−75～ 300°C
17	Zinc-1	〃	0.8～100 sec^{-1}	0～ 300°C
18	Zinc-2	〃	〃	〃
19	Zinc-3	〃	〃	〃
Fig. No.	Test Materials	Treatment	Strain Rate Range	Temperature Range
4-20	Magnesium	Extruded→Cold Drawn→Annealed	0.1～ 10 sec^{-1}	18～ 500°C
Fig. No.	Test Materials	Treatment	Strain Rate Range	Temperature Range
4-21	Titanium	Hot Rolled→Annealed	0.1～ 10 sec^{-1}	18～ 900°C
Fig. No.	Test Materials	Treatment	Strain Rate Range	Temperature Range
4-22	0.08% C Steel	Hot Rolled→Annealed	0.3～ 10 sec^{-1}	800～1200°C
23	0.12% C 〃	Forged→Annealed	0.8～100 〃	〃
24	0.15% C 〃	Hot Rolled→Annealed	0.3～ 10 〃	〃
25	0.15% C 〃	Forged→Annealed	0.2～650 〃	0～1200°C
26	0.2% C 〃	Hot Rolled→Annealed	0.3～ 10 〃	800～1200°C
27	0.25% C 〃	Forged→Annealed	3.5～ 30 〃	〃
28	0.27% C 〃	Hot Rolled→Annealed	0.3～ 10 〃	〃
29	0.45% C 〃	Hot Rolled→Annealed	0.3～ 10 〃	〃
30	0.55% C 〃	Forged→Annealed	3.5～ 30 〃	〃
31	0.95% C 〃	Hot Rolled→Annealed	0.3～ 10 〃	〃

OF FLOW STRESS-STRAIN CURVES

Chemical Composition (%)

Al	Cu	Si	Fe	Mn	Mg
99.5	0.1	0.15	0.5	0.01	0.01
Bal.	0.016	0.07	0.24		
94.95	3.5	0.1	0.5	0.5	0.45

Chemical Composition (%)

Cu	Fe	Pb	Sn	Zn	P	Ni	S	As	Sb	Bi	O_2
99.95	0.0057	0.0028				0.0038	0.001	0.0004	0.0016	0.00014	0.003
99.99	0.0017	0.0002				0.0014	0.001	0.0002	0.0006	0.00005	
98.47	0.018	0.0044	0.0032	Bal.							
90.06	0.033	0.0044	0.0032	Bal.							
79.21	0.023	0.004	0.0035	Bal.							
69.92	0.034	0.016	0.0088	Bal.							
65.05	0.017	0.0025	0.0072	Bal.							
60.16	0.025	0.013	0.0042	Bal.							
98.4	0.0112	0.0152	1.5		0.062						
94.5	0.0167	0.017	5.35		0.135						
92.78	0.0171	0.0173	7.03		0.138						
90.2	0.0183	0.0191	10.0		0.166						

Chemical Composition (%)

Pb	Cd	Fe	Cu	Sn	Al	Mg	Zn
0.002	0.0001	0.0007	0.0004	<0.0001			Bal.
0.286	0.068	0.0071	0.0011	0.0016			Bal.
0.287	0.072	0.0011	0.0018	0.0022			Bal.
0.0071	0.0007	0.0006	0.0012	0.0003	0.0096	0.0059	Bal.

Chemical Composition (%)

Mg	Al	Zn	Mn	Si	Cu	Ni
Bal.	0.01	0.003	0.008	0.004	0.003	0.0008

Chemical Composition (%)

Ti	Fe	N	H
Bal.	0.03	0.0084	0.0025

Chemical Composition (%)

C	Si	Mn	P	S	Cu	Cr	Ni
0.087	0.003	0.34	0.025	0.02			
0.12	0.2	0.5	0.01	0.03	0.1	0.08	
0.147	0.27	0.48	0.014	0.03	0.275	0.07	0.099
0.15	Tr.	0.4	0.01	0.016			
0.19	0.04	0.86	0.022	0.029			
0.25	0.08	0.45	0.012	0.025			
0.269	0.28	0.53	0.01	0.012			
0.43	0.26	0.74	0.022	0.016			
0.55	0.24	0.73	0.014	0.016			
0.96	0.087	0.91	0.033	0.029			

Table 4·2 List of Data Sheets.

Fig. No.	Test Materials	Treatment	Strain Rate Range	Temperature Range
4-32	High Strength Steel-I	Hot Rolled → Annealed	0.3～ 10 sec^{-1}	800～1200°C
33	〃 -II	〃	〃	〃
34	〃 -III	〃	〃	〃
35	〃 -IV	〃	〃	〃
36	〃 -V	〃	〃	〃
37	〃 -VI	〃	〃	〃
Fig. No.	Test Materials	Treatment	Strain Rate Range	Temperature Range
4-38	Low Alloy Steel-1	Forged → Annealed	3.5～ 30 sec^{-1}	800～1200°C
39	〃 -2	〃	〃	〃
40	〃 -3	〃	〃	〃
41	〃 -4	〃	〃	〃
42	〃 -5	〃	〃	〃
43	〃 -6	〃	〃	〃
44	〃 -7	〃	〃	1000 and 1200°C
45	〃 -8	〃	〃	800～1200°C
46	〃 -9	〃	〃	〃
Fig. No.	Test Materials	Treatment	Strain Rate Range	Temperature Range
4-47	Low Alloy Steel-10	Forged → Annealed	3.5～ 30 sec^{-1}	800～1200°C
48	〃 -11	〃	〃	〃
49	〃 -12	〃	〃	〃
50	〃 -13	〃	〃	〃
51	〃 -14	〃	〃	〃
51	〃 -15	〃	〃	〃
53	〃 -16	〃	〃	〃
54	1% Cr-0.5% Mo Low Alloy Steel	〃	0.8～100 sec^{-1}	〃
55	5%Cr-0.5 % Mo Low Alloy Steel	〃	〃	〃
Fig. No.	Test Materials	Treatment	Strain Rate Range	Temperature Range
4-56	12% Cr-12% Ni Stainless Steel	Hot Rolled → Annealed	0.8～100 sec^{-1}	800～1200°C
57	12% Cr-15% Ni 〃	〃	〃	〃
58	13% Cr 〃	〃	〃	〃
59	13% Cr-Mo 〃	〃	0.2～100 sec^{-1}	〃
60	17% Cr 〃	〃	0.8～100 sec^{-1}	〃
61	17% Cr-5% Ni-5% Mo-Ti 〃	〃	〃	〃
62	17% Cr-7% Ni-Mo 〃	〃	〃	〃
63	17% Cr-12% Ni-2% Mo 〃	Hot Drawn → Annealed	197 ～527 sec^{-1}	0～1200°C
64	17% Cr-13% Ni-2% Mo 〃	〃	〃	〃
65	17% Cr-14% Ni-Ti-W 〃	Hot Rolled → Annealed	0.8～100 sec^{-1}	800～1200°C
66 (a), (b)	18% Cr-8% Ni 〃	〃	0.2～650 sec^{-1}	0～1200°C
67	18% Cr-8% Ni 〃	〃	197 ～527 sec^{-1}	〃
68	18% Cr-12% Ni-Mo 〃	〃	0.8～100 sec^{-1}	800～1200°C
69	22% Cr-13% Ni 〃	Hot Drawn → Annealed	197 ～527 sec^{-1}	0～1200°C
70	25% Cr-20% Ni 〃	〃	〃	〃

Chemical Composition (%)

C	Si	Mn	P	S	Cu	Cr	Ni	Mo	V	B	
0.1	0.42	0.42	0.08	0.009	0.3	0.74	0.37				
0.16	0.26	1.22	0.01	0.005					0.064		
0.179	0.37	1.07	0.011	0.006		0.49	0.41	0.40		0.003	
0.12	0.26	0.78	0.015	0.009	0.34	0.51	0.87	0.44	0.062	0.003	
0.15	0.33	1.3	0.017	0.014							Nb: 0.066
0.164	0.39	1.14	0.004	0.005	0.12	0.8	1.05		0.84	0.0036	Sn: 0.017 Ti: 0.003

Chemical Composition (%)

C	Si	Mn	P	S	Cu	Cr	Ni				
0.32	0.39	0.44	0.018	0.019	0.12	3.42	1.19				
0.34	0.38	0.97	0.016	0.019	0.12	3.44	1.24				
0.3	0.36	0.54	0.014	0.02	0.12	4.21	1.23				
0.36	0.42	1.03	0.019	0.019	0.11	4.32	1.22				
0.3	0.41	1.02	0.016	0.017	0.13	4.27	3.18				
0.31	0.41	0.62	0.02	0.017	0.13	3.18	3.12				
0.32	0.47	1.15	0.027	0.019	0.13	3.16	3.12				
0.32	0.43	0.57	0.02	0.022	0.13	3.29	3.17				
0.28	0.41	0.55	0.019	0.018	1.07	3.46	1.24				

Chemical Composition (%)

C	Si	Mn	P	S	Cu	Cr	Ni	Mo	Co	Zn	
0.34	0.48	2.18	0.025	0.016	0.13	3.42	1.24				
0.33	0.47	2.29	0.022	0.018	0.13	4.44	1.27				
0.14	0.41	0.78	0.014	0.021	0.13	3.04	1.13				
0.14	0.36	0.80	0.014	0.022	0.13	4.00	1.13				
0.15	0.36	1.61	0.016	0.019	0.11	3.09	1.22				
0.18	0.36	1.68	0.017	0.02	0.12	4.36	1.22				
0.18	0.7	0.53	0.017	0.019	0.96	1.59	0.59	0.34	1.07	0.18	
0.15	0.1-0.35	0.3-0.6	0.03	0.03		0.8-1.2		0.45-0.65			
≦0.15	≦0.5	0.3-0.6	<0.03	<0.03		4-6		0.45-0.65			

Chemical Composition (%)

C	Si	Mn	P	S	Cu	Cr	Ni	Mo			
0.12	0.95	1.34	0.024	0.005		12.79	12.34				
0.021	0.62	1.23	0.016	0.009		11.85	15.06				
0.16	0.37	0.44	0.024	0.007		12.62					
0.12	0.12	0.29	0.014	0.016		12.11	0.5	0.45			
0.08	0.45	0.43	0.031	0.005		17.38	0.31				
0.05	0.45	0.68	0.021	0.014		16.47	4.71	4.25	Ti=0.20		
0.08	0.93	1.1	0.009	0.014		16.99	6.96	0.31	Al=0.93	N=0.02	Se=0.063
0.06	0.52	1.4	0.035	0.005		17.25	12.23	2.17			
0.035	0.60	1.12	0.029	0.006	2.06	16.99	12.59	2.13			
0.14	0.36	0.70	0.015	0.017		16.60	13.45		W=2.7	Ti=1.07	
0.08	0.49	1.06	0.037	0.005		18.37	9.16				
0.07	0.71	1.07	0.03	0.005		18.34	9.56				
0.07	0.67	1.34	0.03	0.01		17.29	12.04	2.26			
0.13	0.42	1.3	0.023	0.008		22.3	12.99				
0.12	1.26	1.56	0.01	0.009		25.49	21.28				

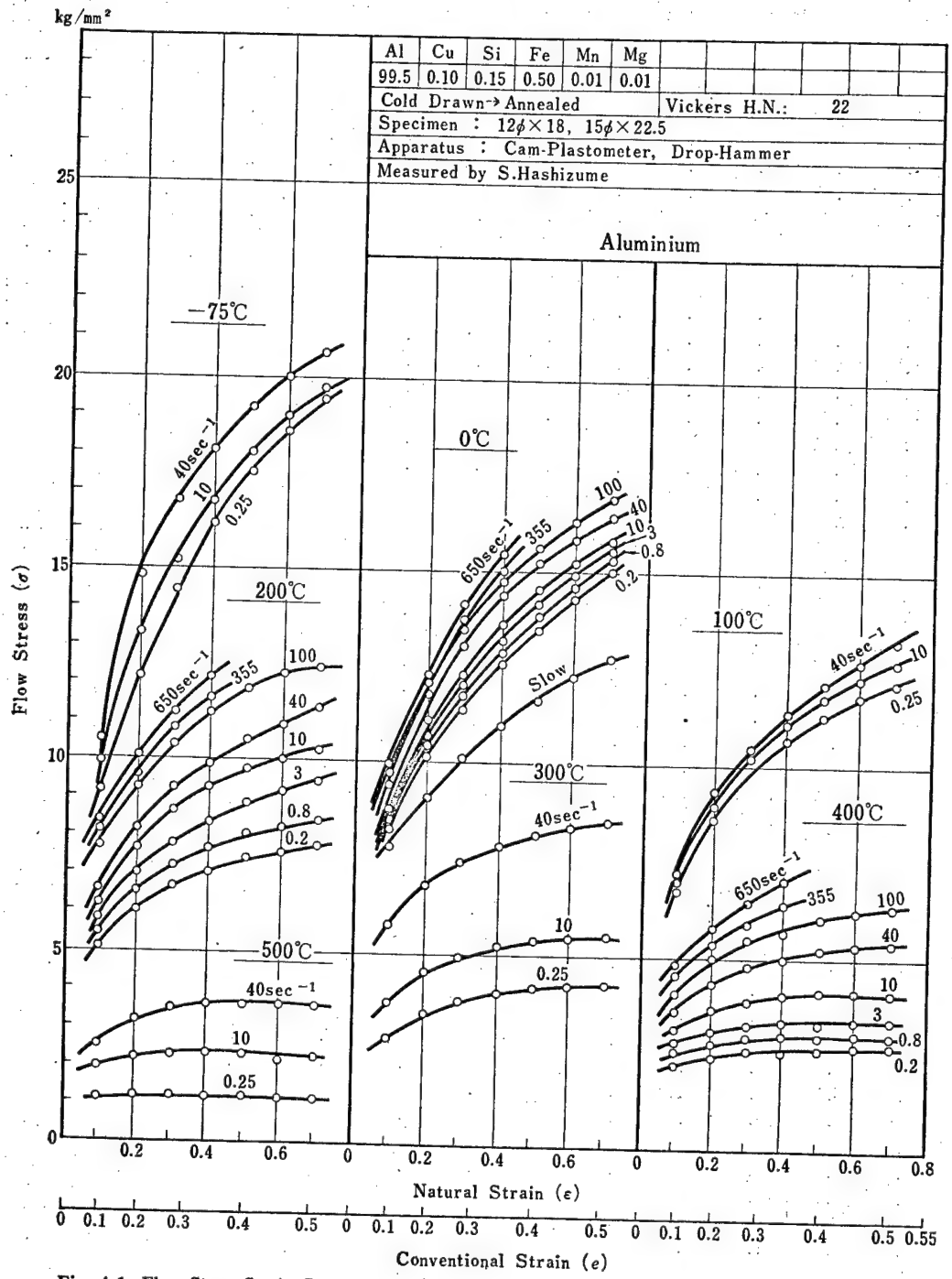

Fig. 4·1 Flow Stress-Strain Curves of Aluminium. Temperature Range: −75°~500°C, Strain Rate Range: 0.2~650 sec⁻¹.

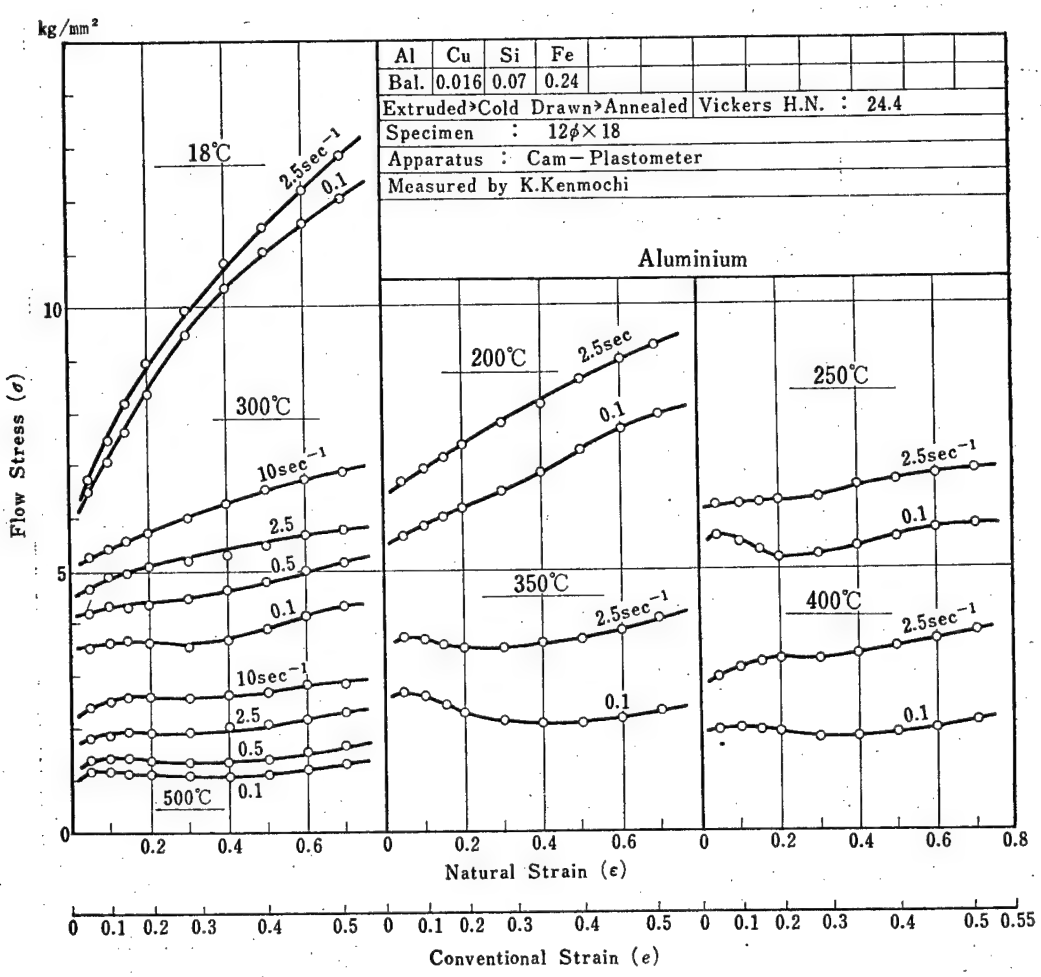

Fig. 4·2 Flow Stress-Strain Curves of Aluminium. Temperature Range: 18~500℃, Strain Rate Range: 0.1~10 sec⁻¹.

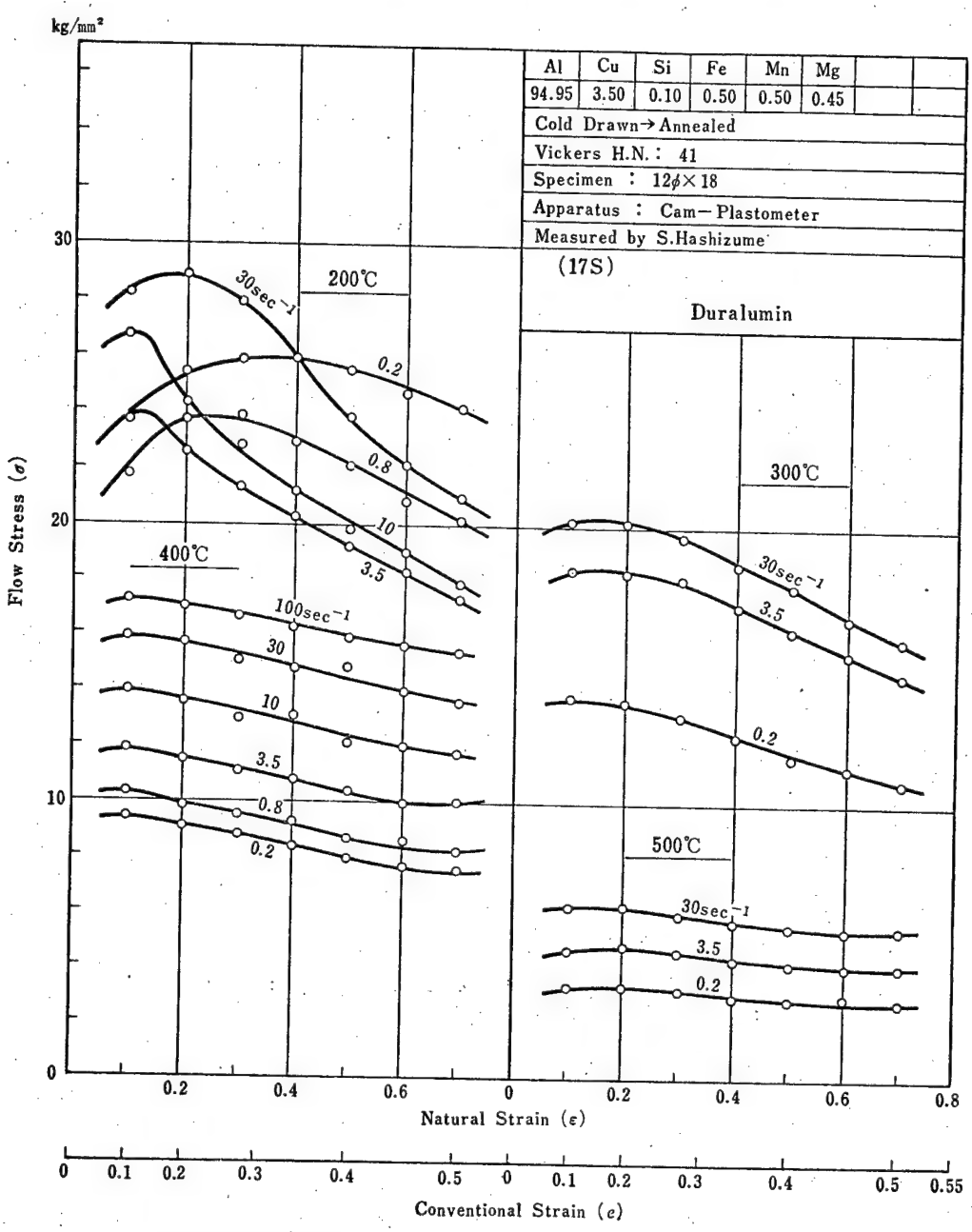

Fig. 4·3 Flow Stress-Strain Curves of Duralumin. Temperature Range: 200~500°C, Strain Rate Range: 0.2~100 sec^{-1}.

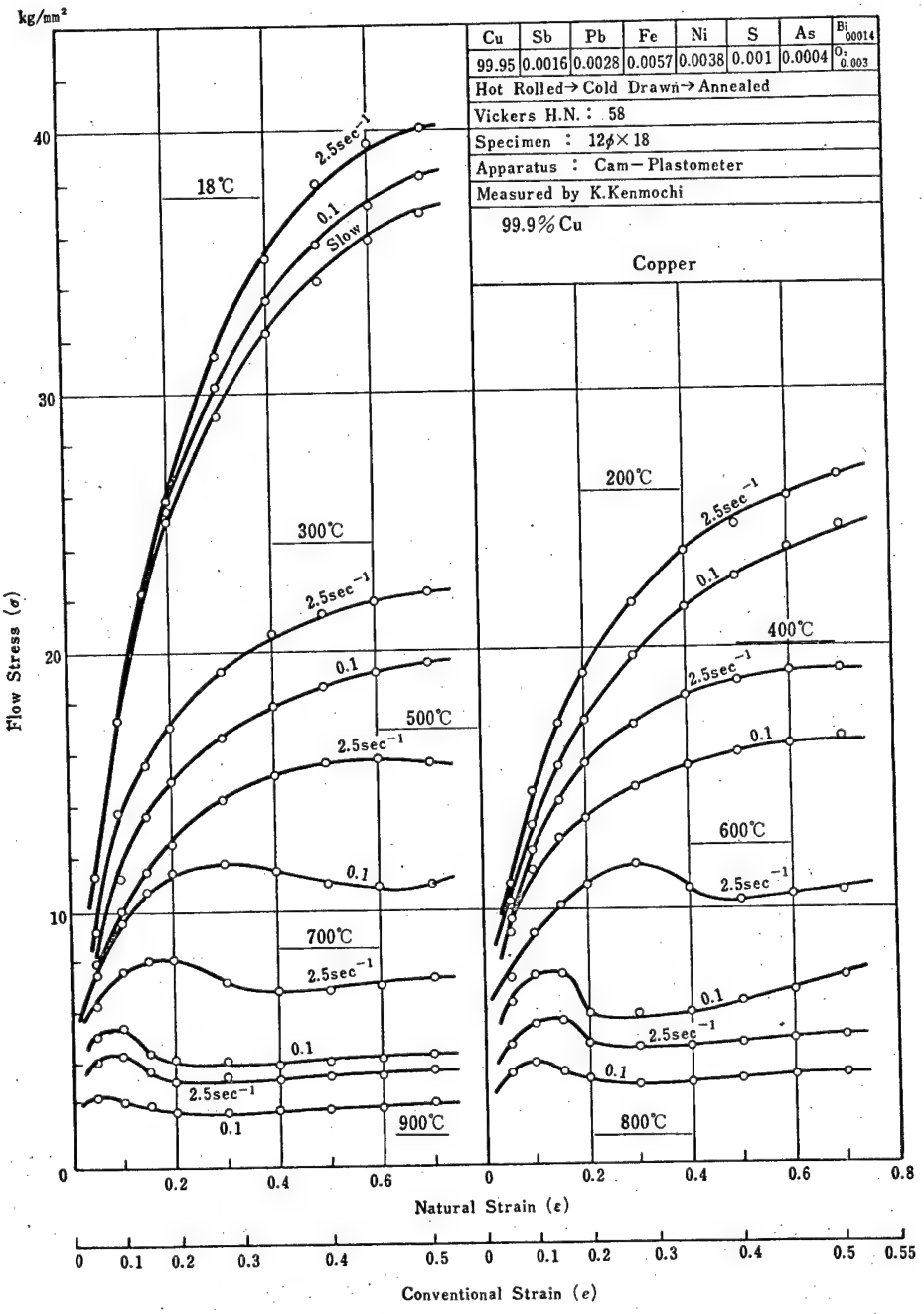

Fig. 4·4 Flow Stress-Strain Curves of 99.9% Cu-Copper. Temperature Range: 18~900°C, Strain Rate Range: 0.1~2.5 sec^{-1}.

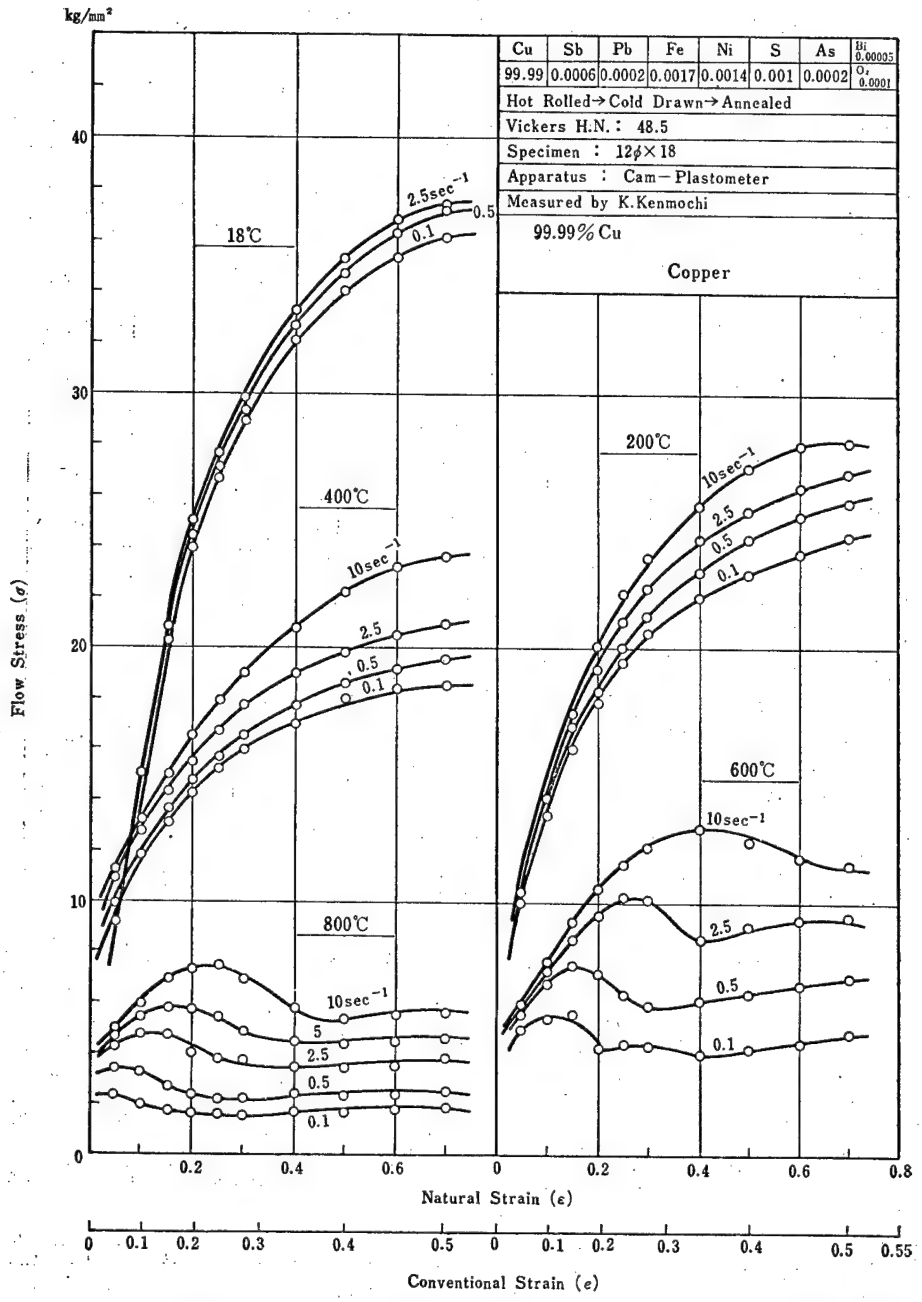

Fig. 4·5 Flow Stress-Strain Curves of 99.99% Cu-Copper. Temperature Range: 18~800°C, Strain Rate Range: 0.1~10 sec^{-1}.

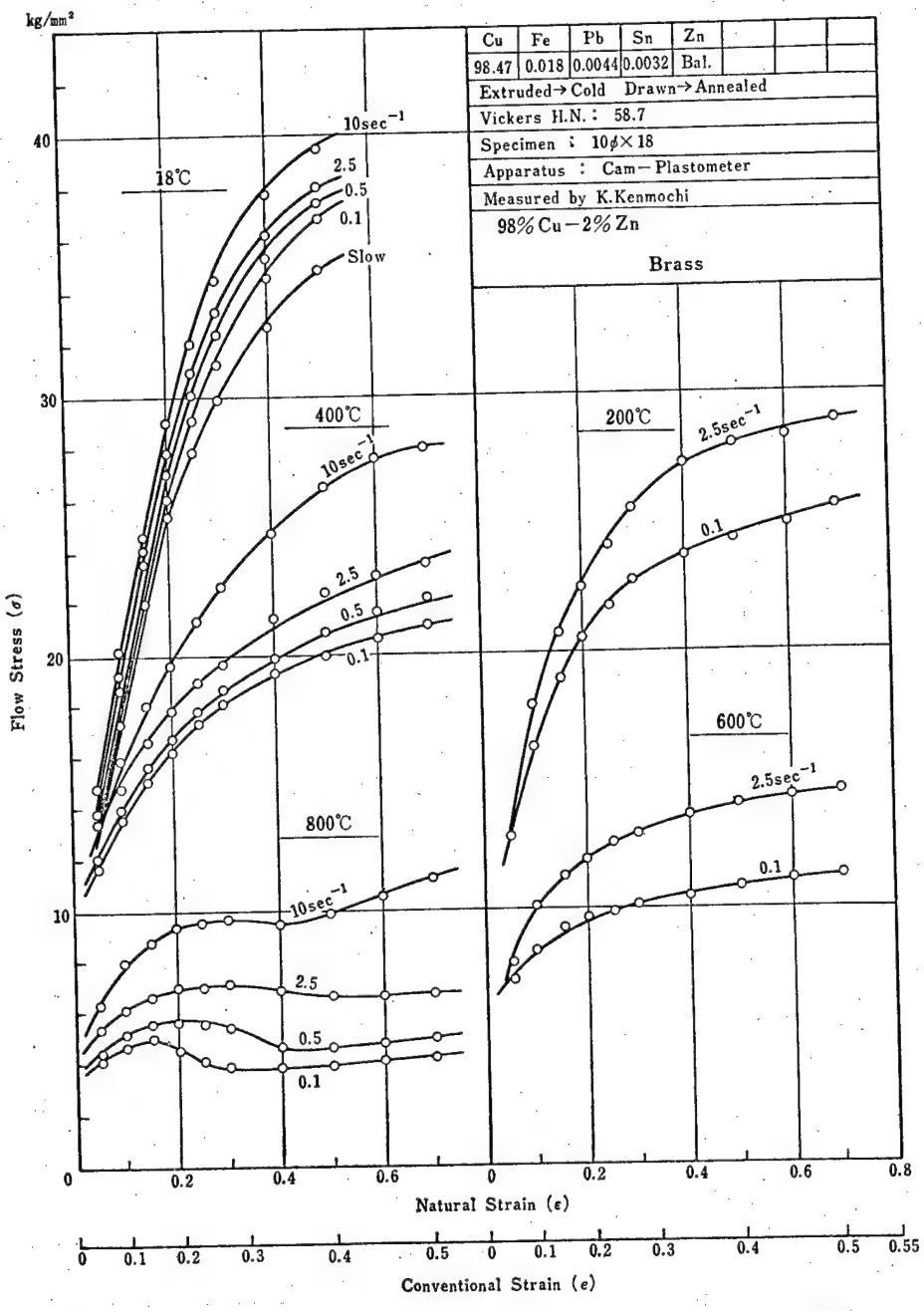

Fig. 4·6 Flow Stress-Strain Curves of 98% Cu-2% Zn Brass. Temperature Range: 18~800°C, Strain Rate Range: 0.1~10 sec^{-1}.

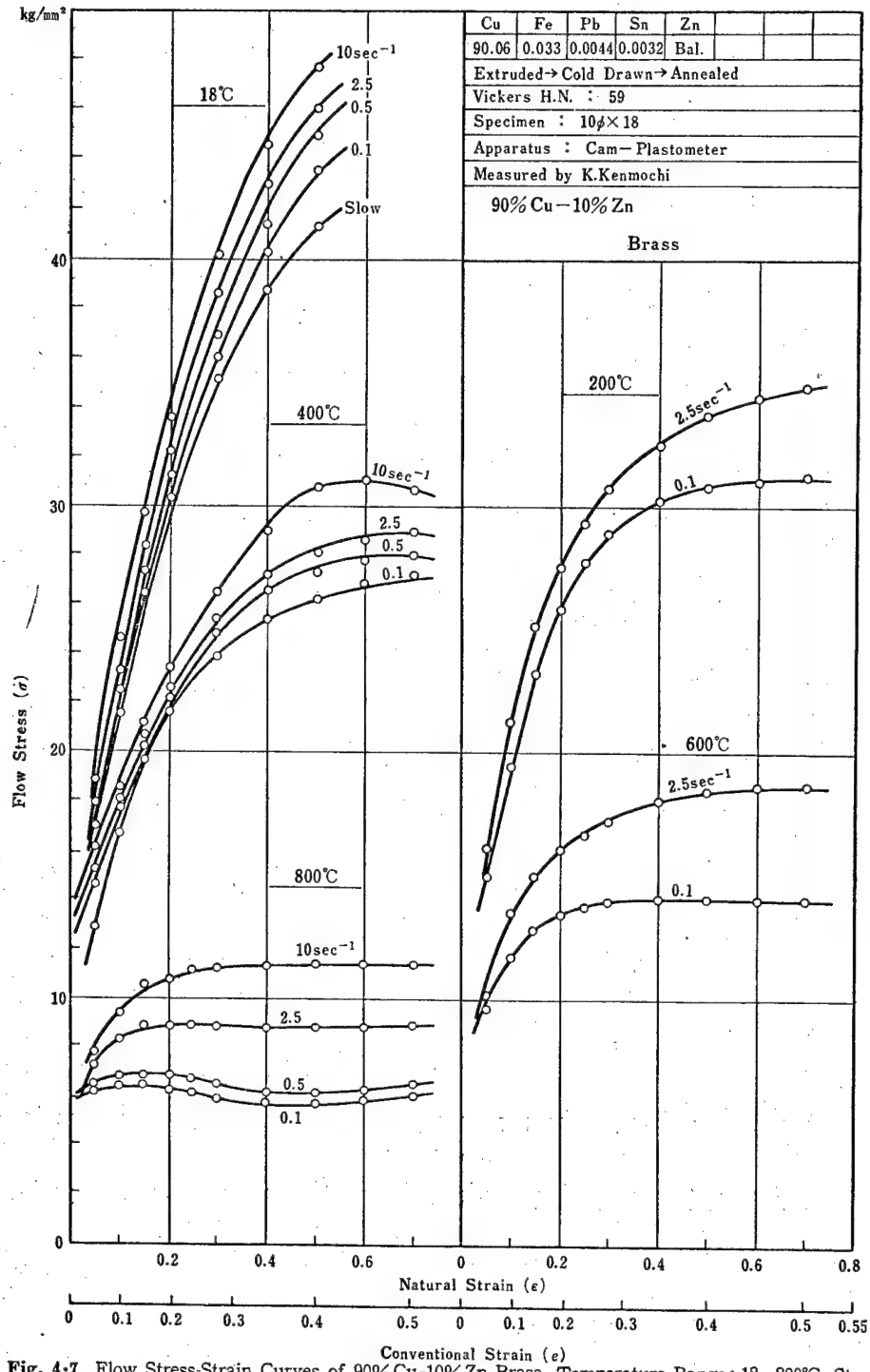

Fig. 4·7 Flow Stress-Strain Curves of 90% Cu-10% Zn Brass. Temperature Range: 18~800°C, Strain Rate Range: 0.1~10 sec⁻¹.

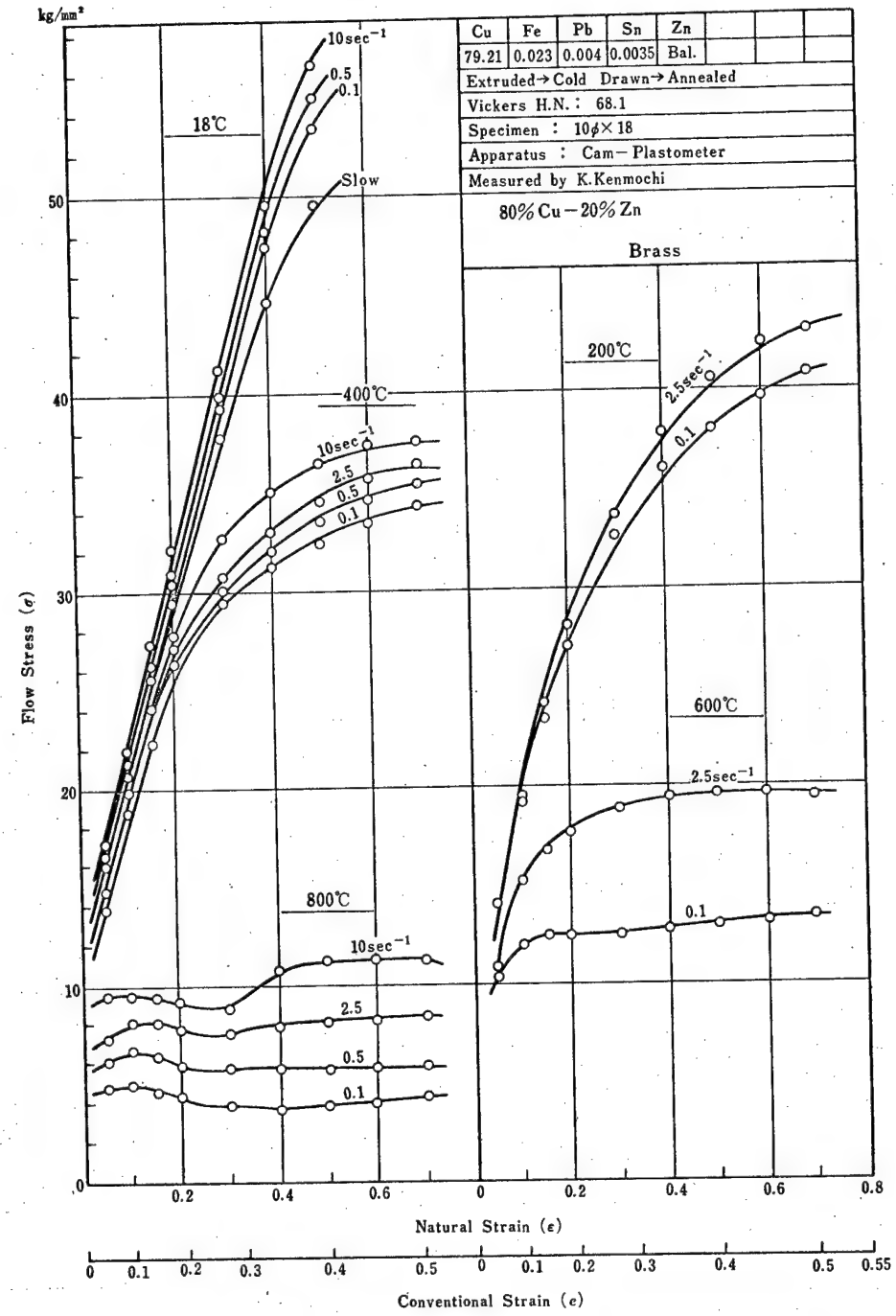

Fig. 4·8 Flow Stress-Strain Curves of 80% Cu-20% Zn Brass. Temperature Range: 18~800℃, Strain Rate Range: 0.1~10 sec^{-1}.

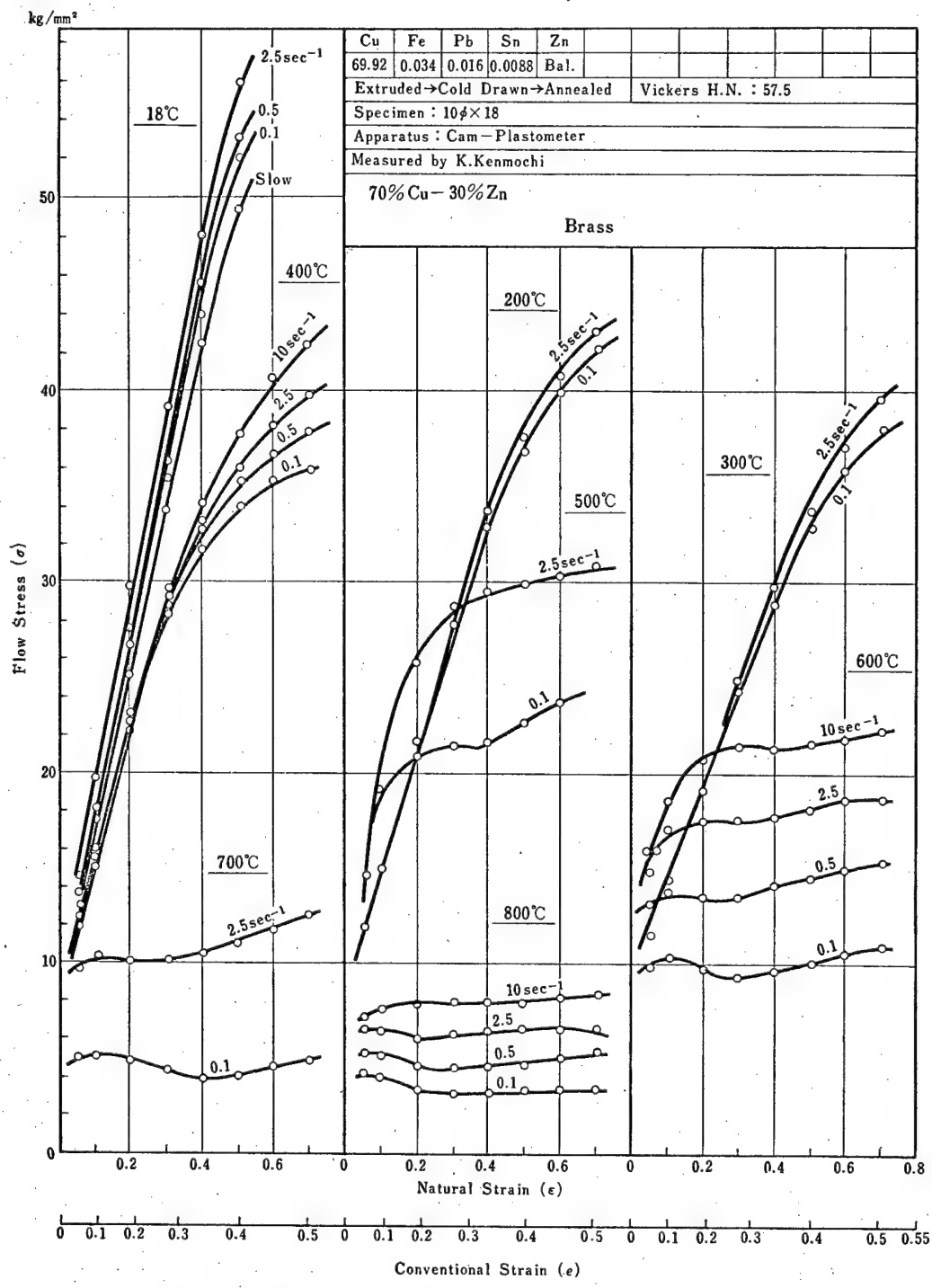

Fig. 4·9 Flow Stress-Strain Curves of 70% Cu-30% Zn Brass. Temperature Range: 18~800°C, Strain Rate Range: 0.1~10 sec⁻¹.

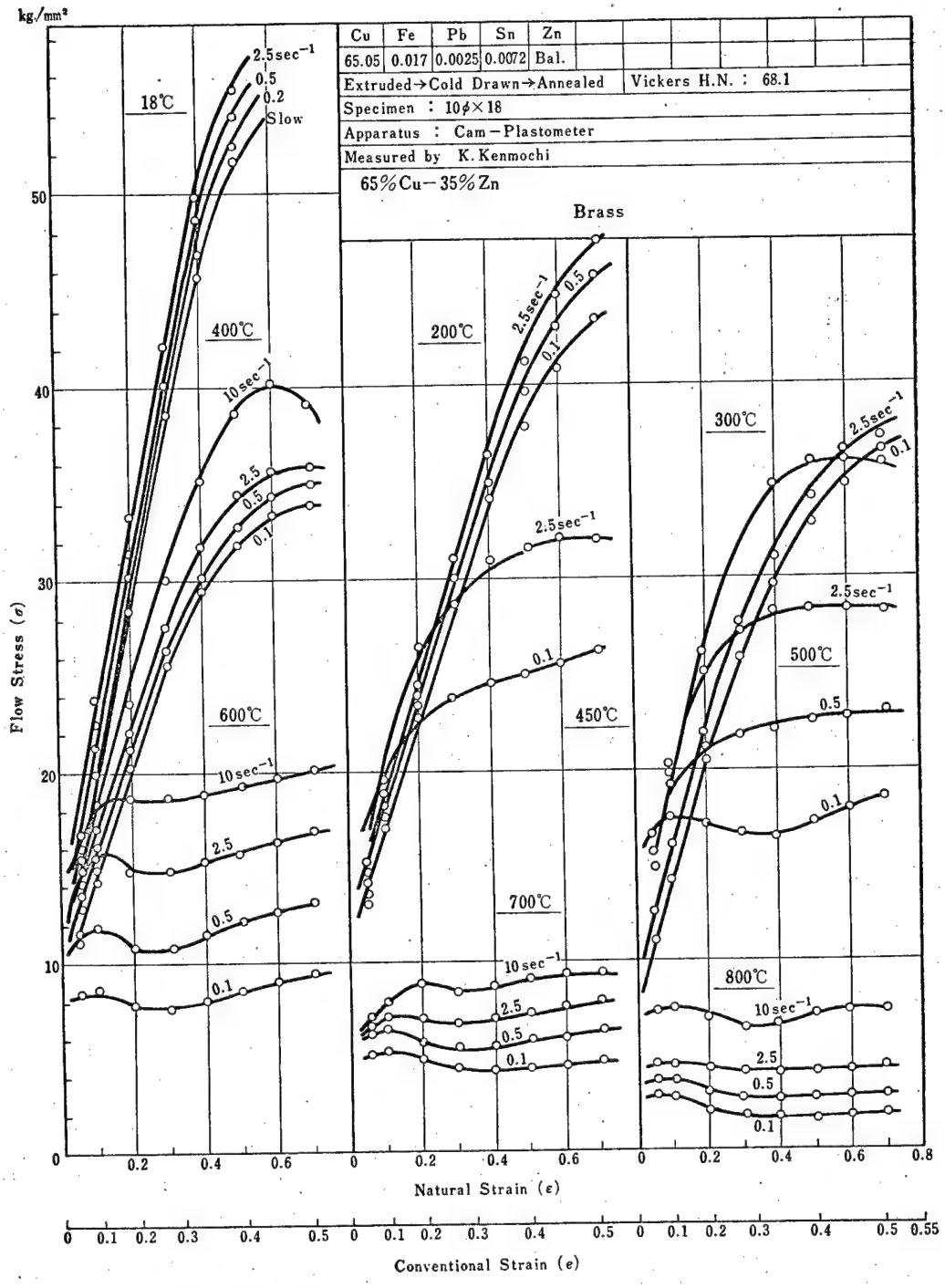

Fig. 4·10 Flow Stress-Strain Curves of 65% Cu-35% Zn Brass. Temperature Range: 18~800°C, Strain Rate Range: 0.1~10 sec^{-1}.

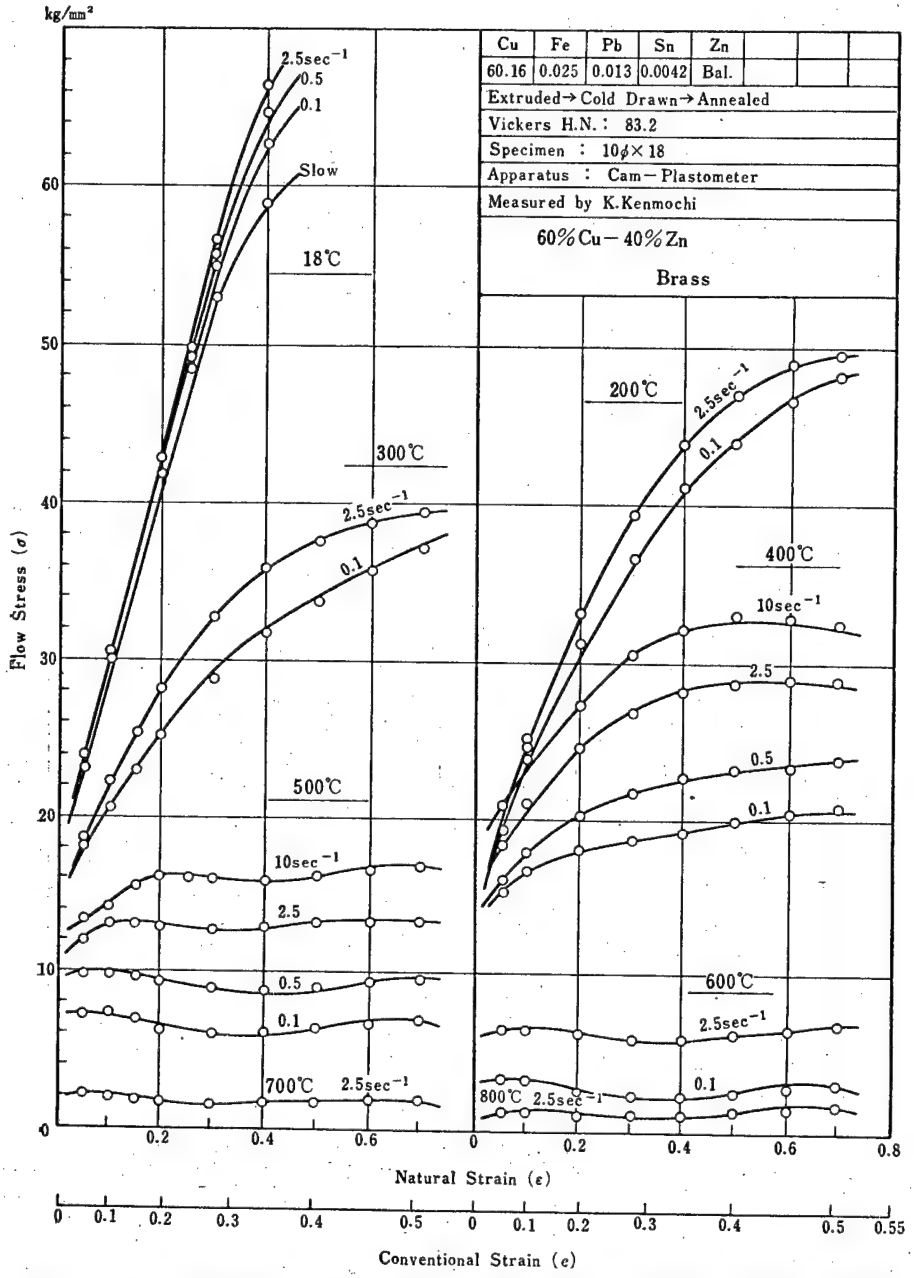

Fig. 4·11 Flow Stress-Strain Curves of 60% Cu-40% Zn Brass. Temperature Range: 18~800°C, Strain Rate Range: 0.1~10 sec^{-1}.

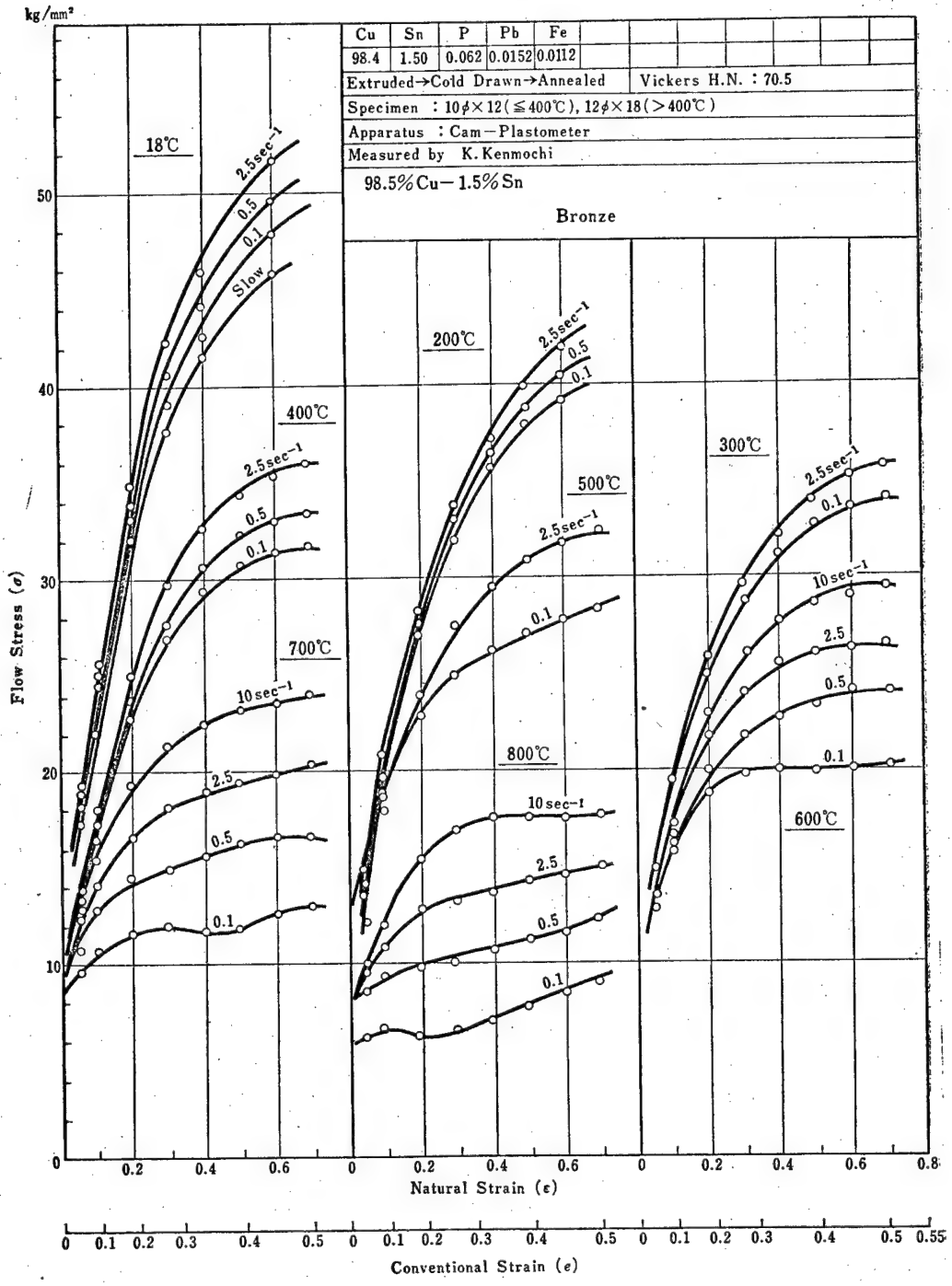

Fig. 4·12 Flow Stress-Strain Curves of 98.5% Cu-1.5% Sn Bronze. Temperature Range: 18~800°C, Strain Rate Range: 0.1~10 sec^{-1}.

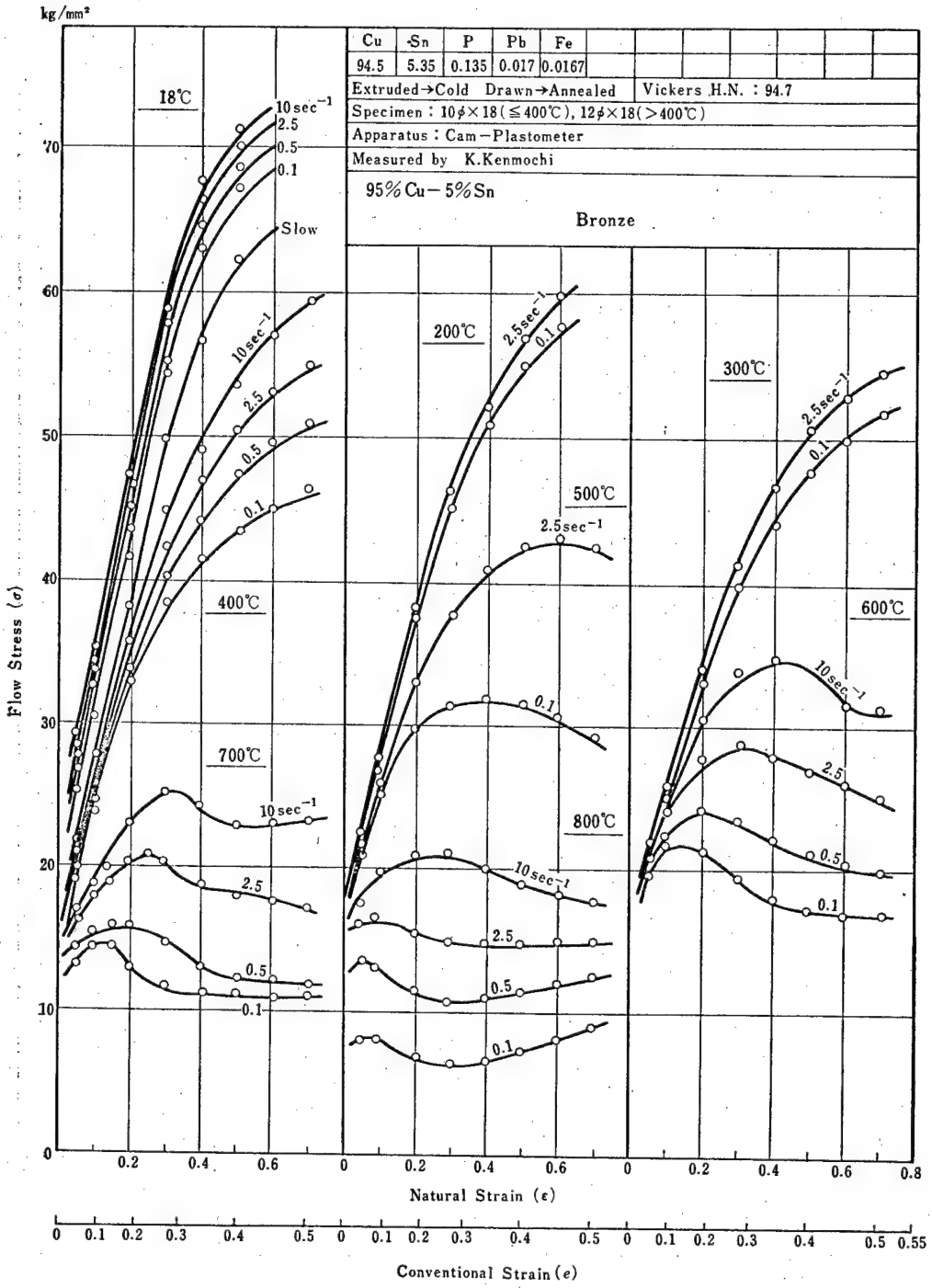

Fig. 4·13 Flow Stress-Strain Curves of 95% Cu-5% Sn Bronze. Temperature Range: 18～800℃, Strain Rate Range: 0.1～10 sec⁻¹.

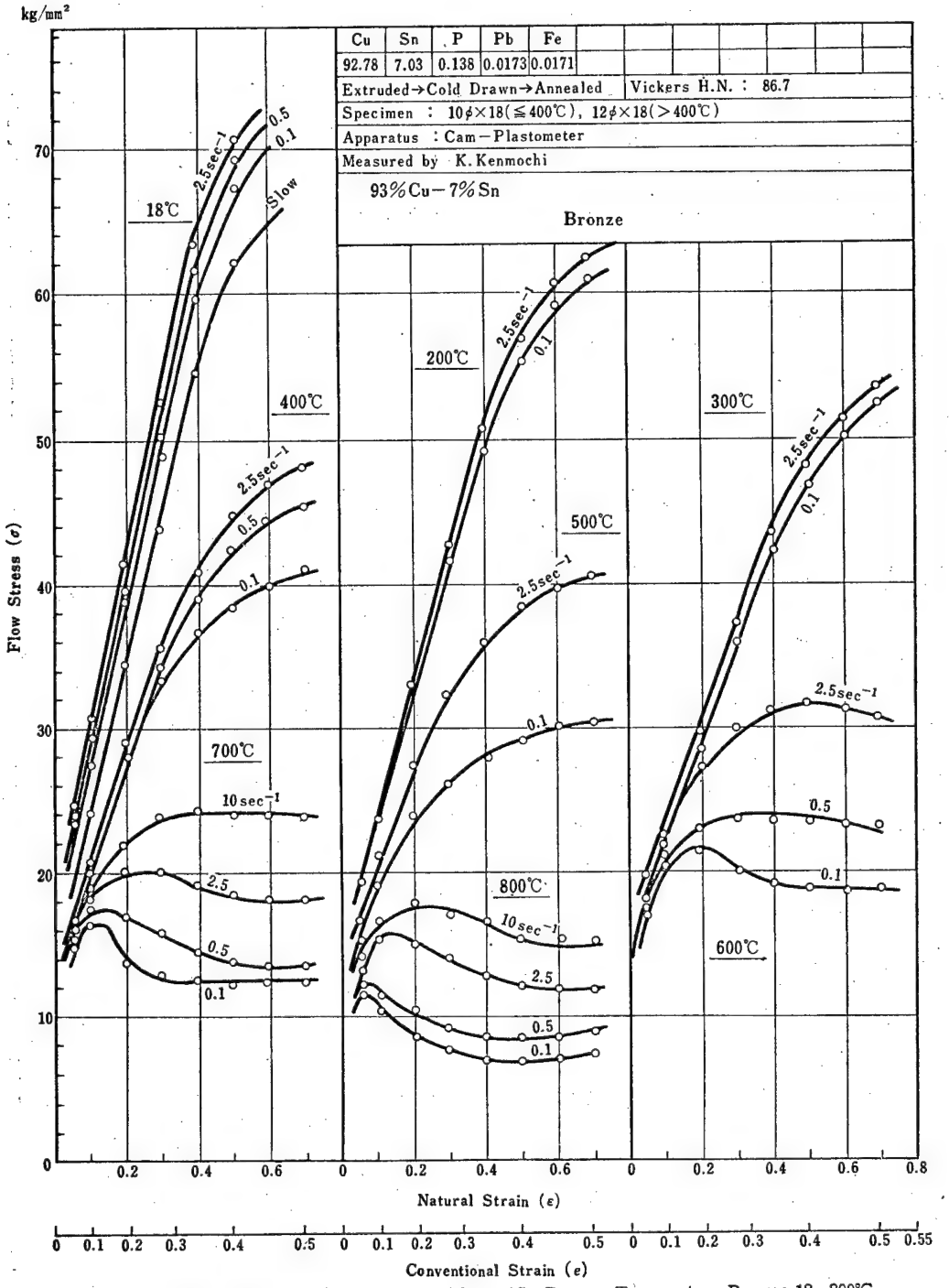

Fig. 4·14 Flow Stress-Strain Curves of 93% Cu-7% Sn Bronze. Temperature Range: 18~800°C, Strain Rate Range: 0.1~10 sec^{-1}.

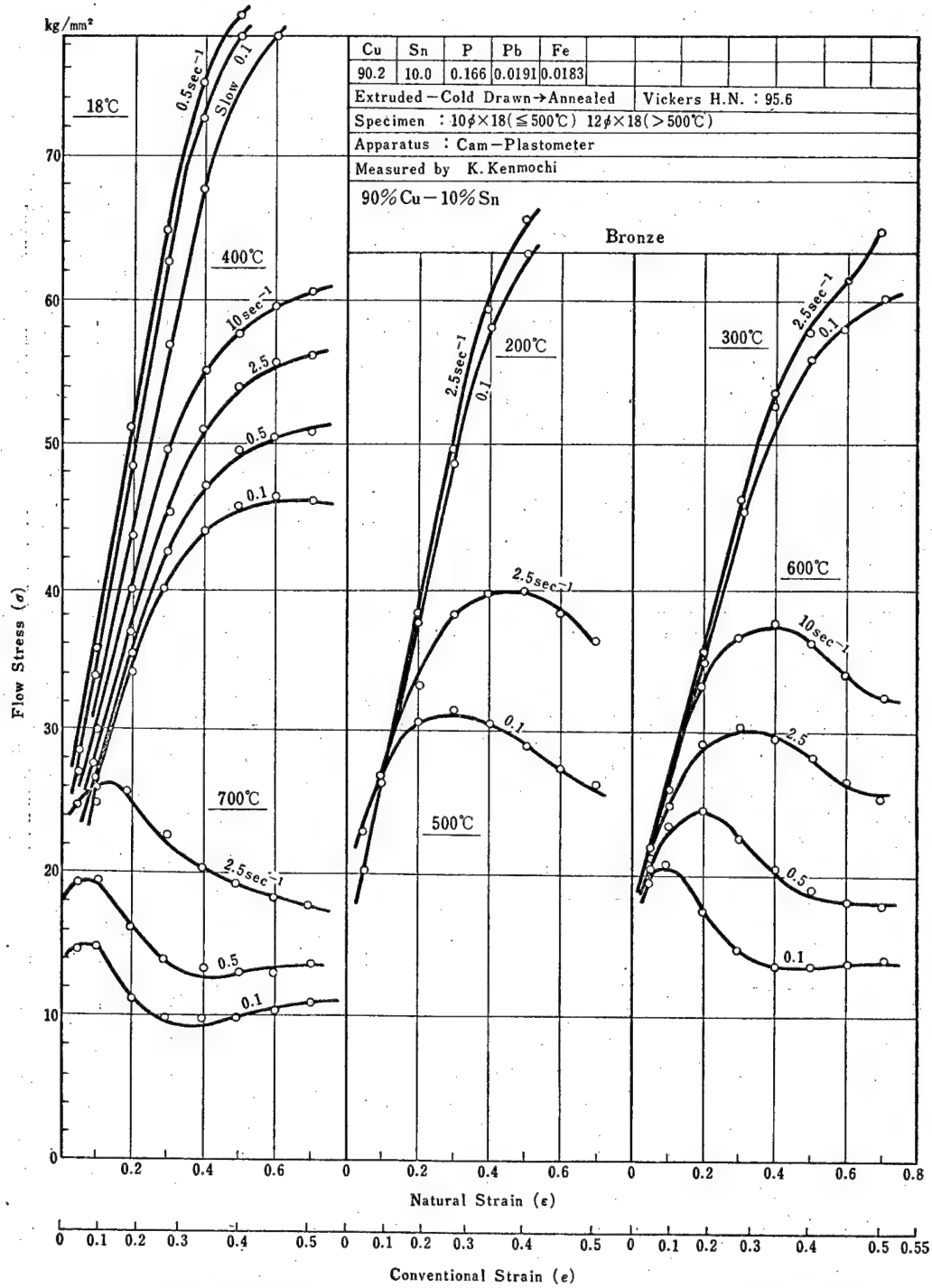

Fig. 4·15 Flow Stress-Strain Curves of 90% Cu-10% Sn Bronze. Temperature Range: 18~700°C, Strain Rate Range: 0.1~10 sec^{-1}.

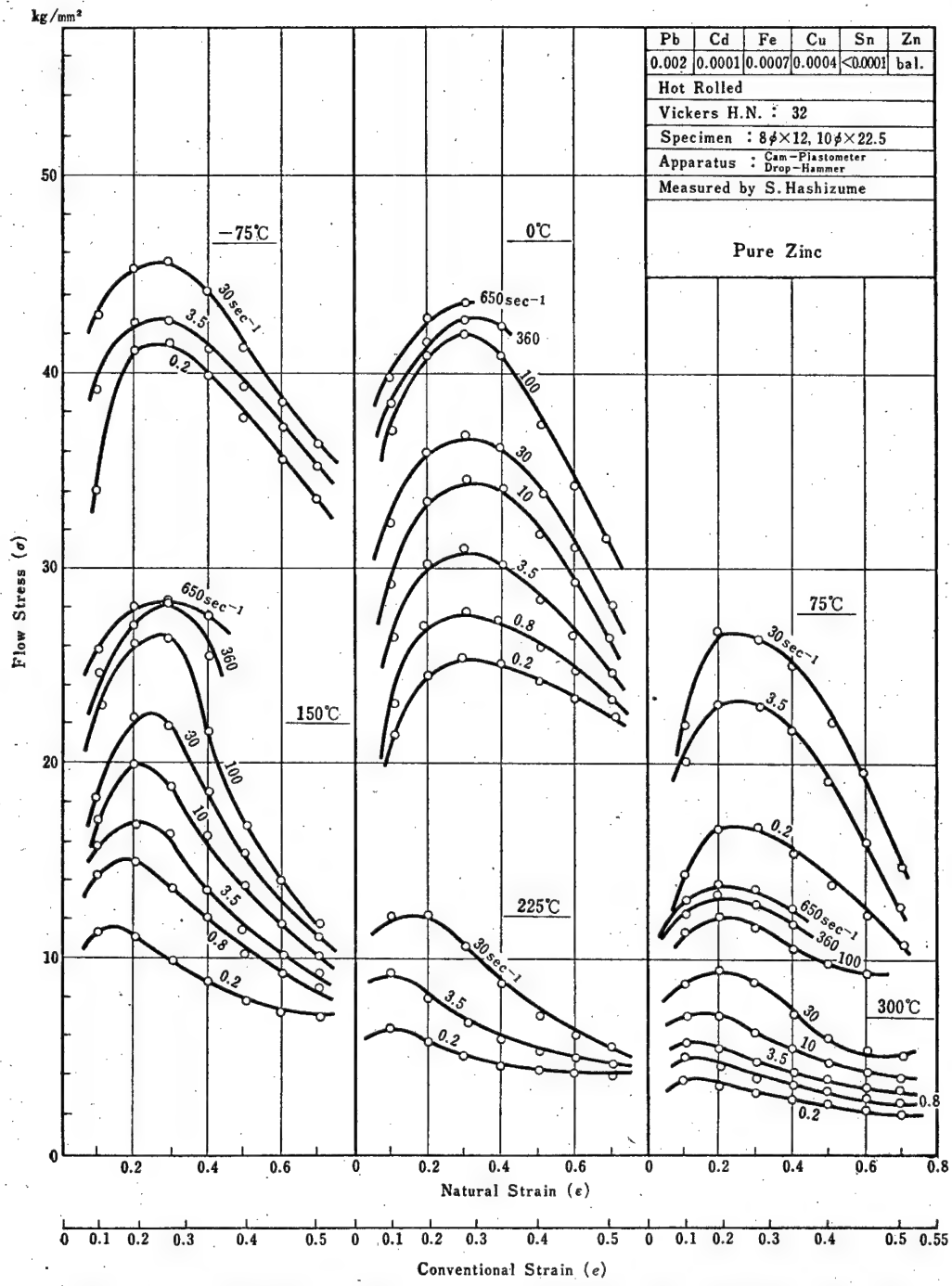

Fig. 4·16 Flow Stress-Strain Curves of Pure Zinc. Temperature Range: −75~300°C, Strain Rate Range: 0.2~650 sec^{-1}.

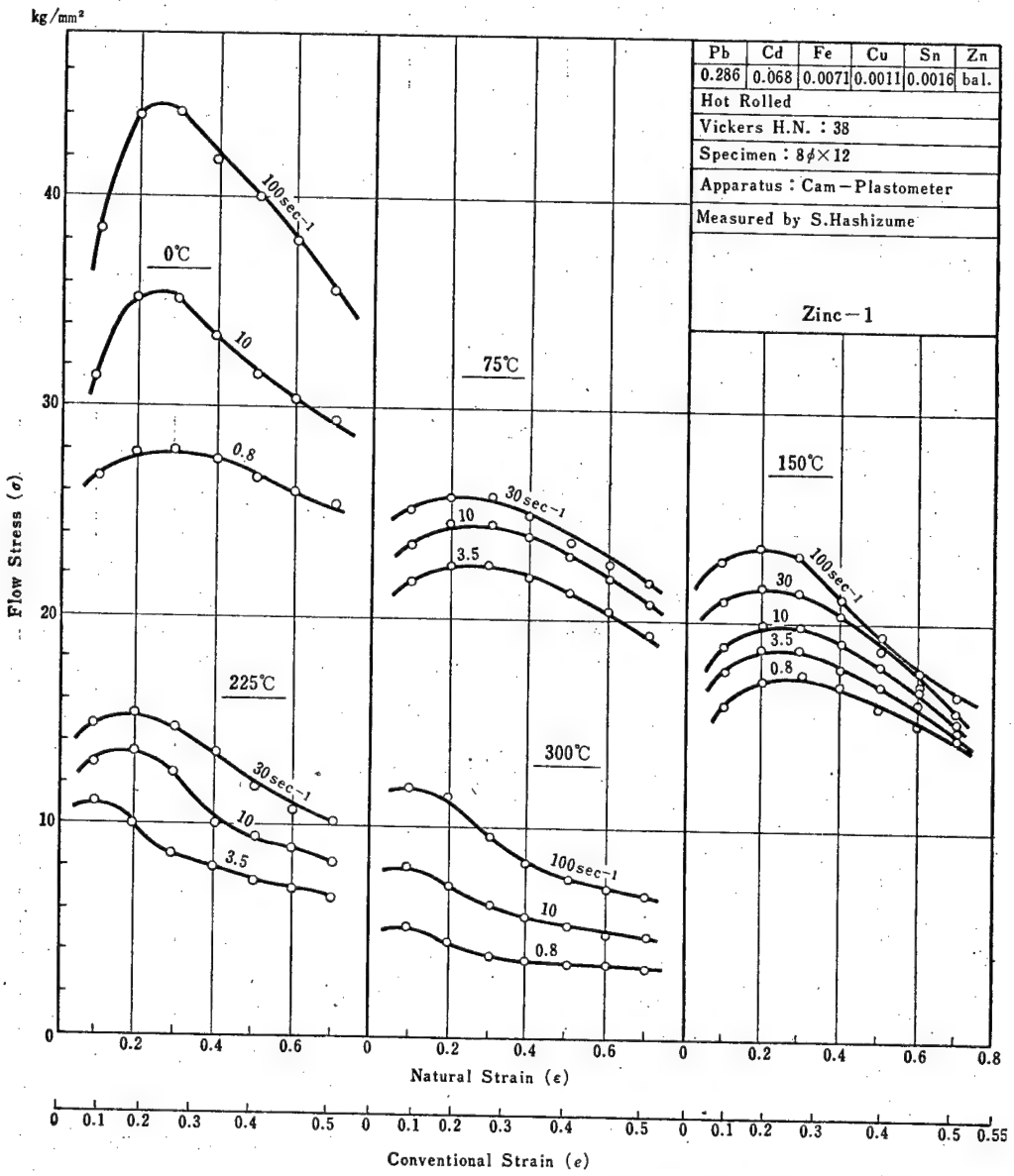

Fig. 4·17 Flow Stress-Strain Curves of Zinc-1. Temperature Range: 0～300°C, Strain Rate Range: 0.8～100 sec^{-1}.

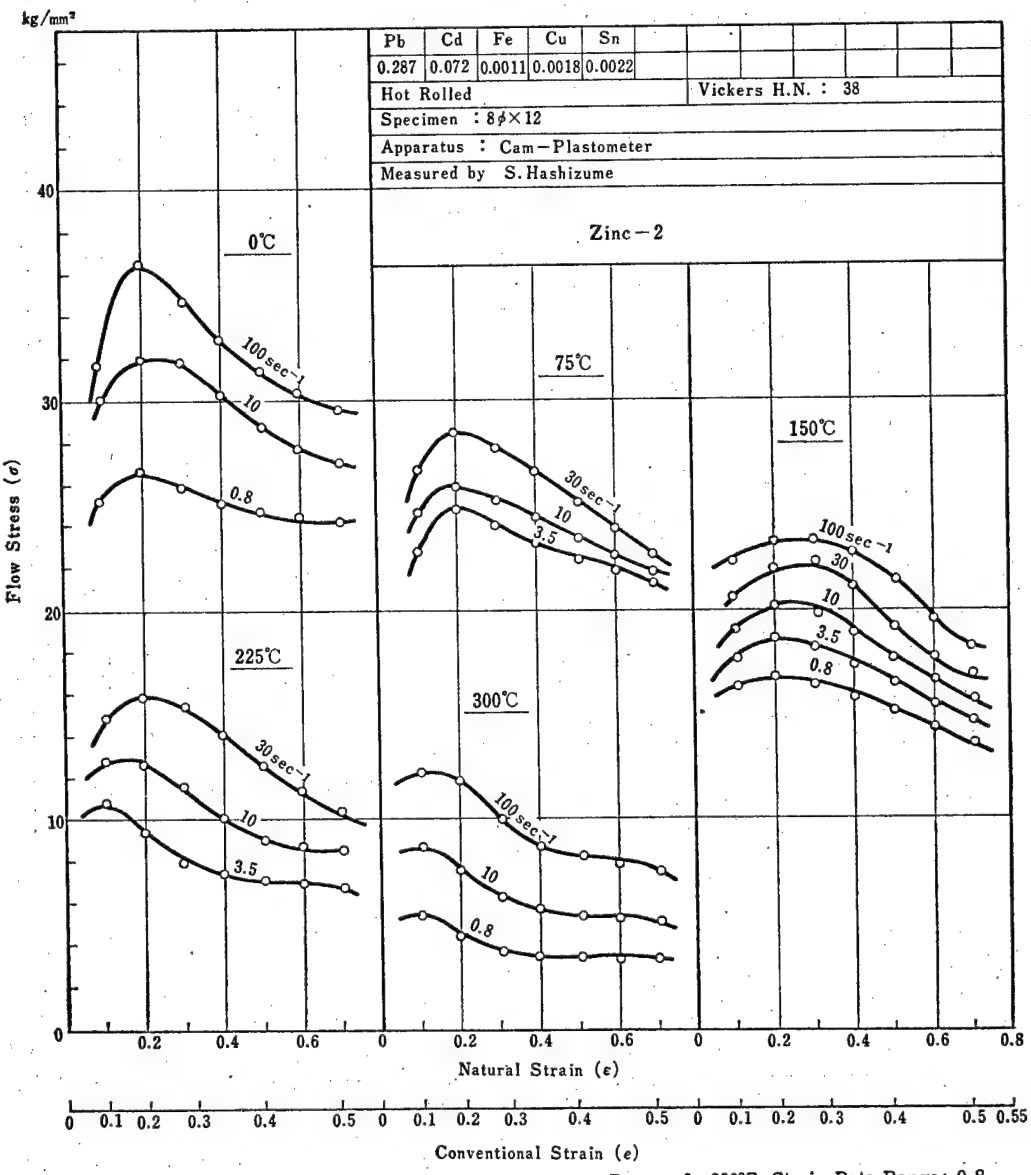

Fig. 4·18 Flow Stress-Strain Curves of Zinc-2. Temperature Range: 0~300°C, Strain Rate Range: 0.8~100 sec^{-1}.

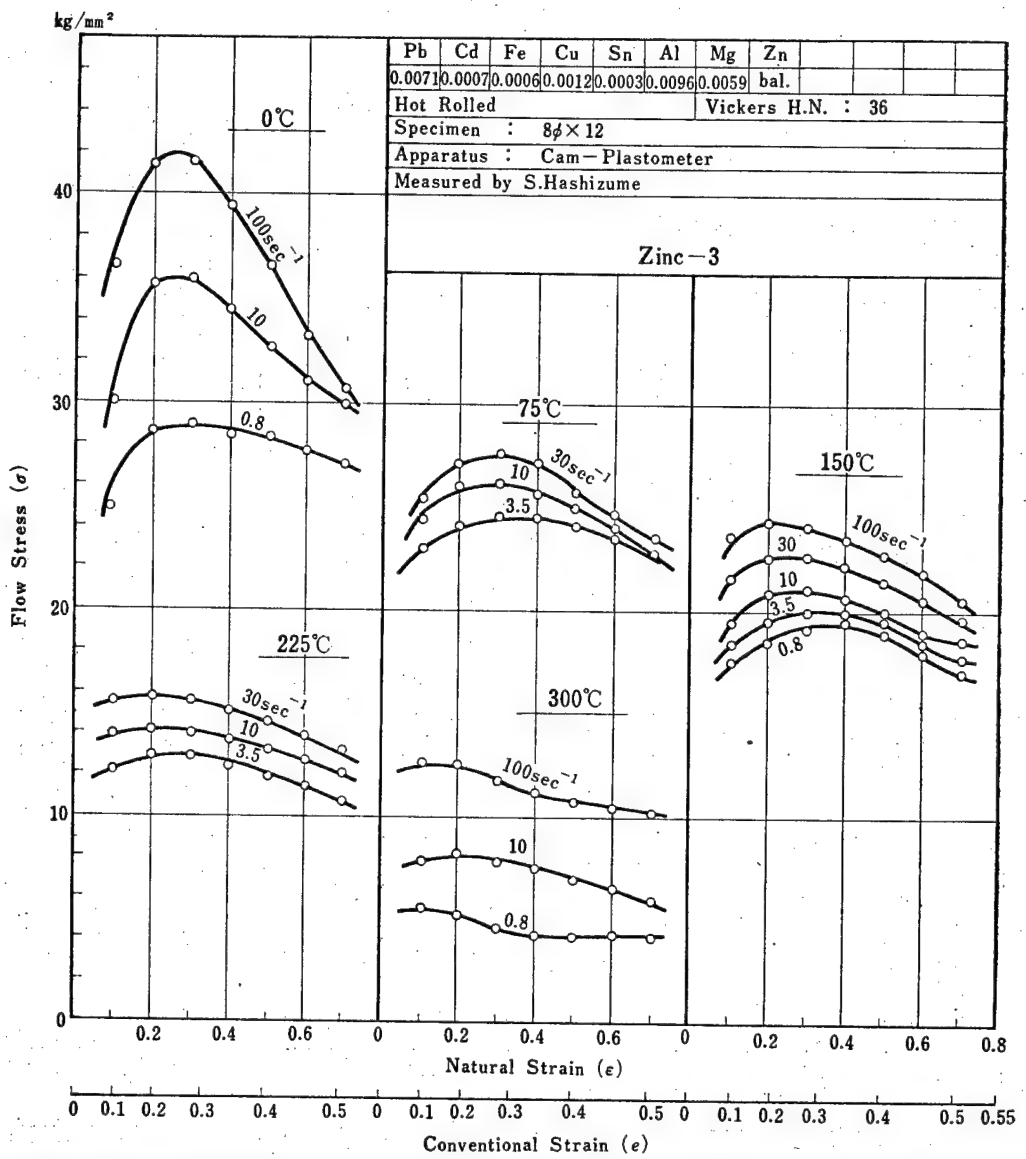

Fig. 4·19 Flow Stress-Strain Curves of Zinc-3. Temperature Range: 0~300°C, Strain Rate Range: 0.8~100 sec^{-1}.

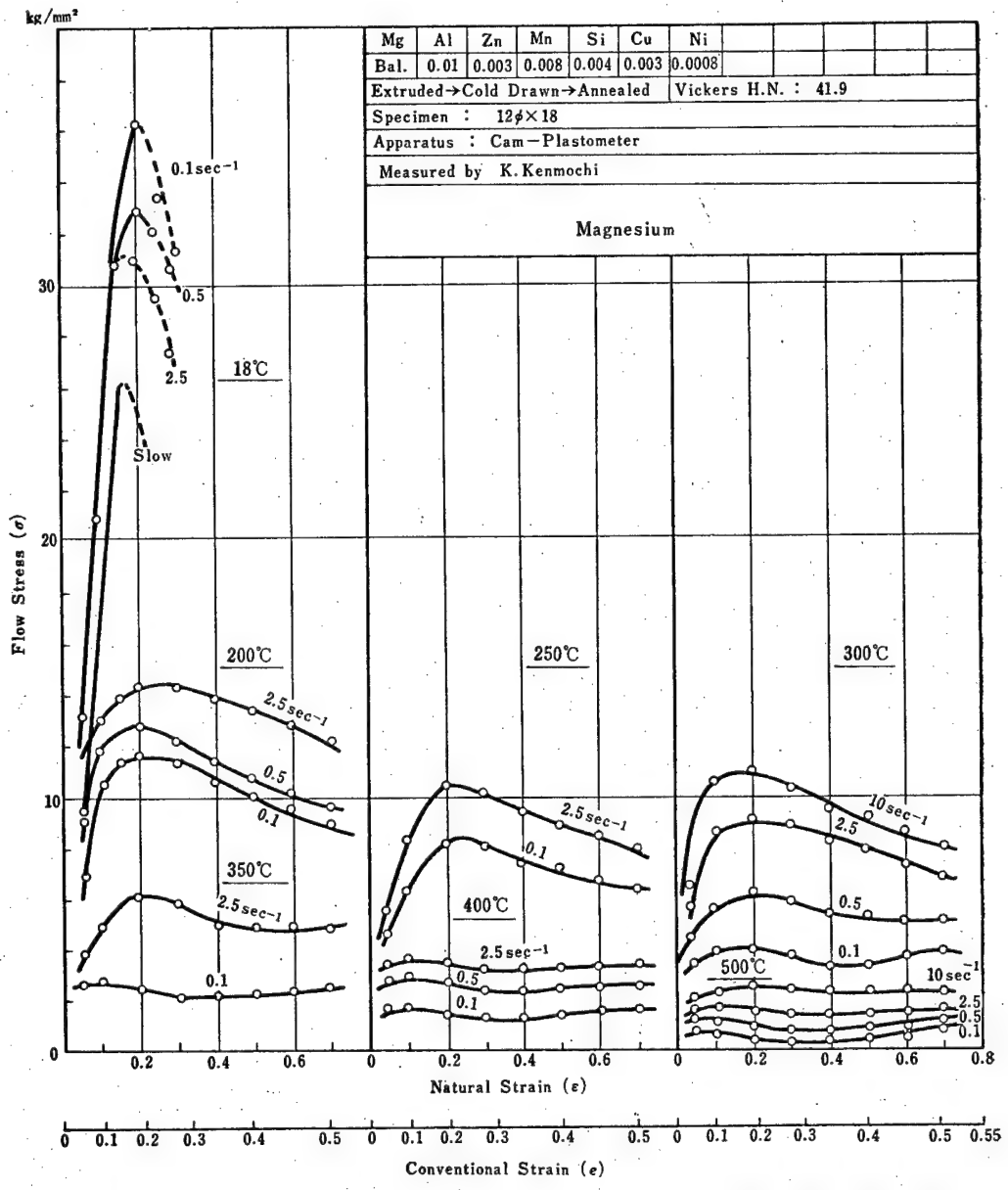

Fig. 4·20 Flow Stress-Strain Curves of Magnesium. Temperature Range: 18～500°C, Strain Rate Range: 0.1 ～10 sec^{-1}.

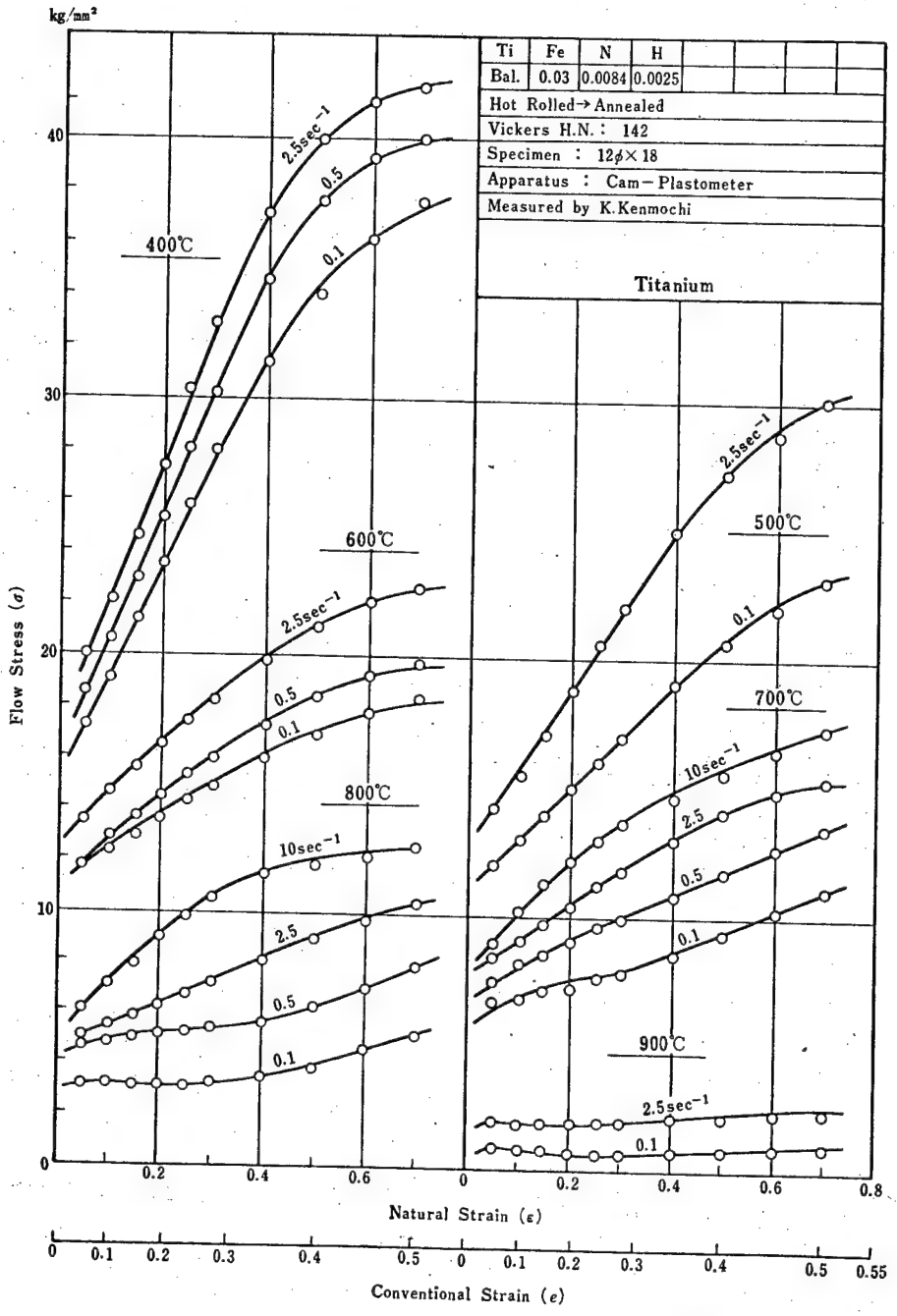

Fig. 4·21 Flow Stress-Strain Curves of Titanium. Temperature Range: 400~900°C, Strain Rate Range: 0.1~10 sec⁻¹.

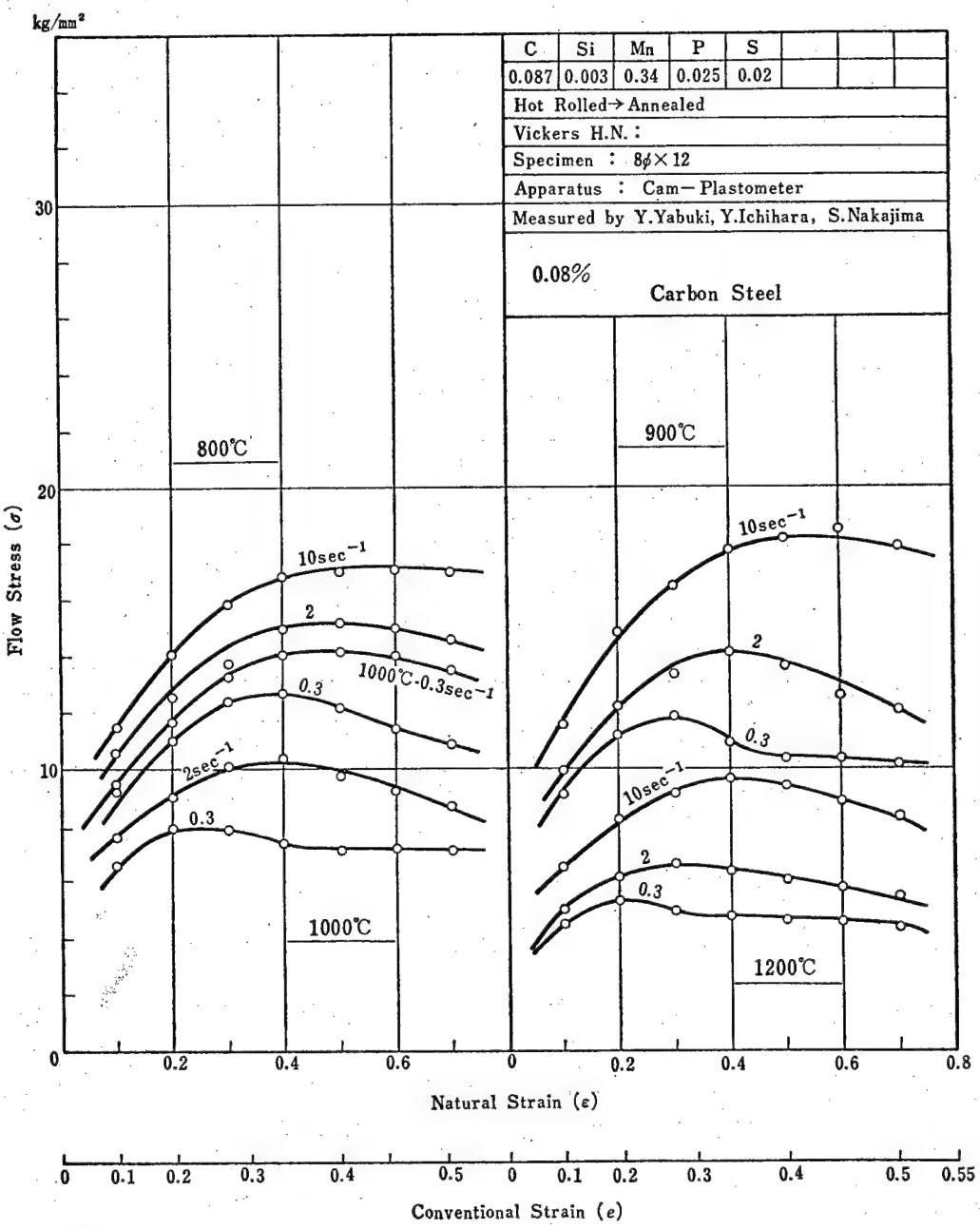

Fig. 4-22 Flow Stress-Strain Curves of 0.08% C Steel. Temperature Range: 800~1200°C, Strain Rate Range: 0.3~10 sec^{-1}.

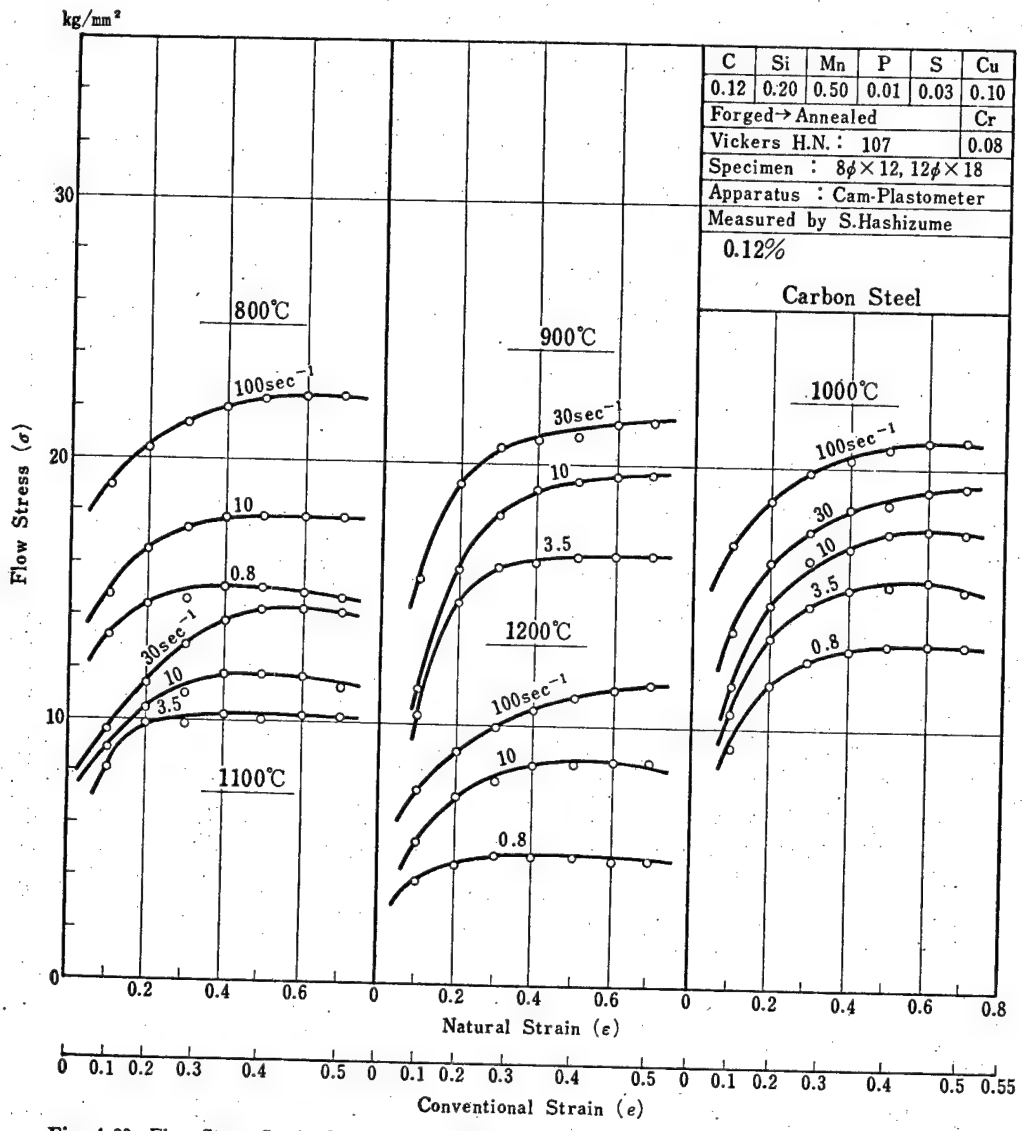

Fig. 4·23 Flow Stress-Strain Curves of 0.12% C Steel. Temperature Range: 800~1200°C, Strain Rate Range: 0.8~100 sec^{-1}.

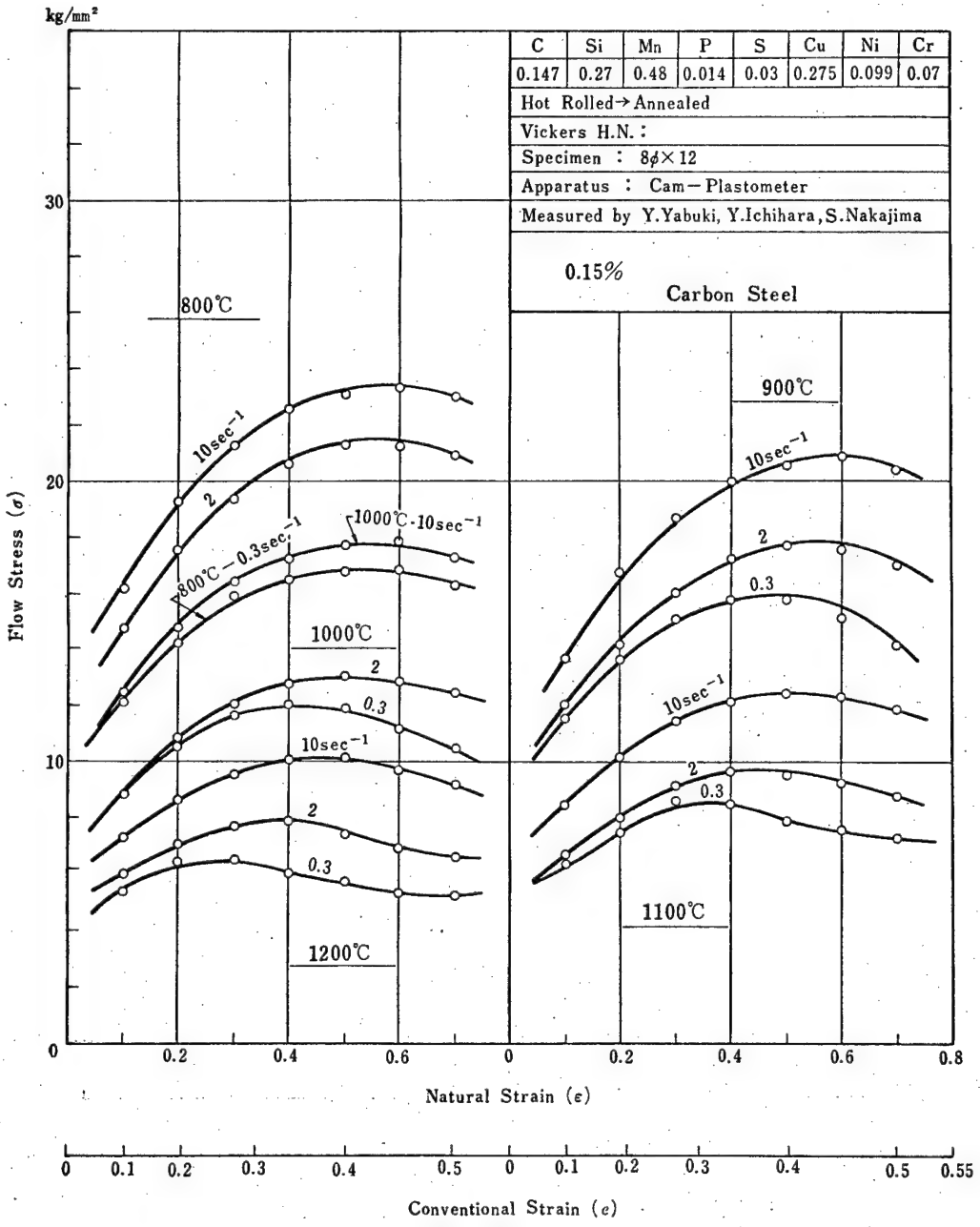

Fig. 4·24 Flow Stress-Strain Curves of 0.15% C Steel. Temperature Range: 800~1200°C, Strain Rate Range: 0.3~10 sec^{-1}.

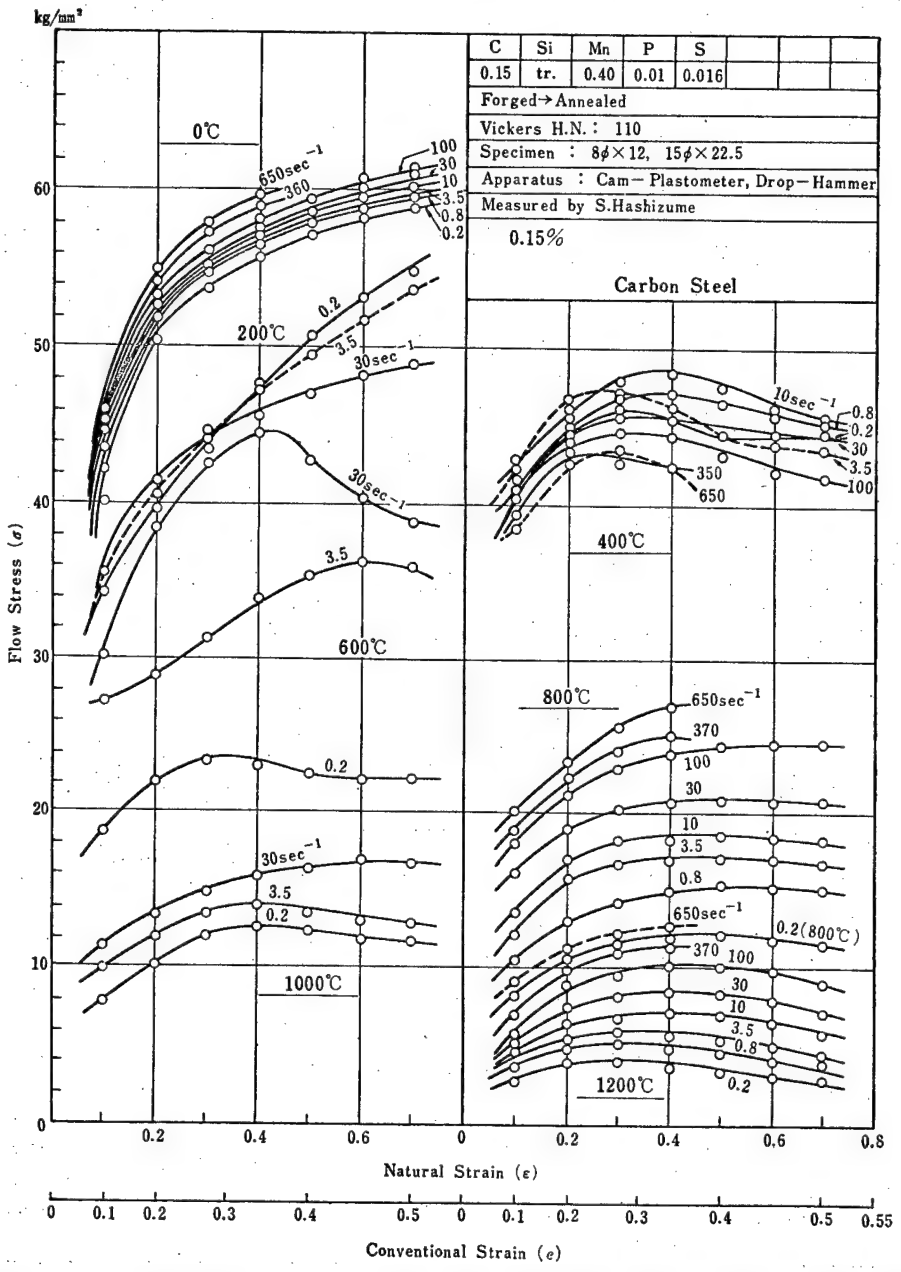

Fig. 4·25 Flow Stress-Strain Curves of 0.15% C Steel. Temperature Range: 0~1200°C, Strain Rate Range: 0.2~650 sec⁻¹.

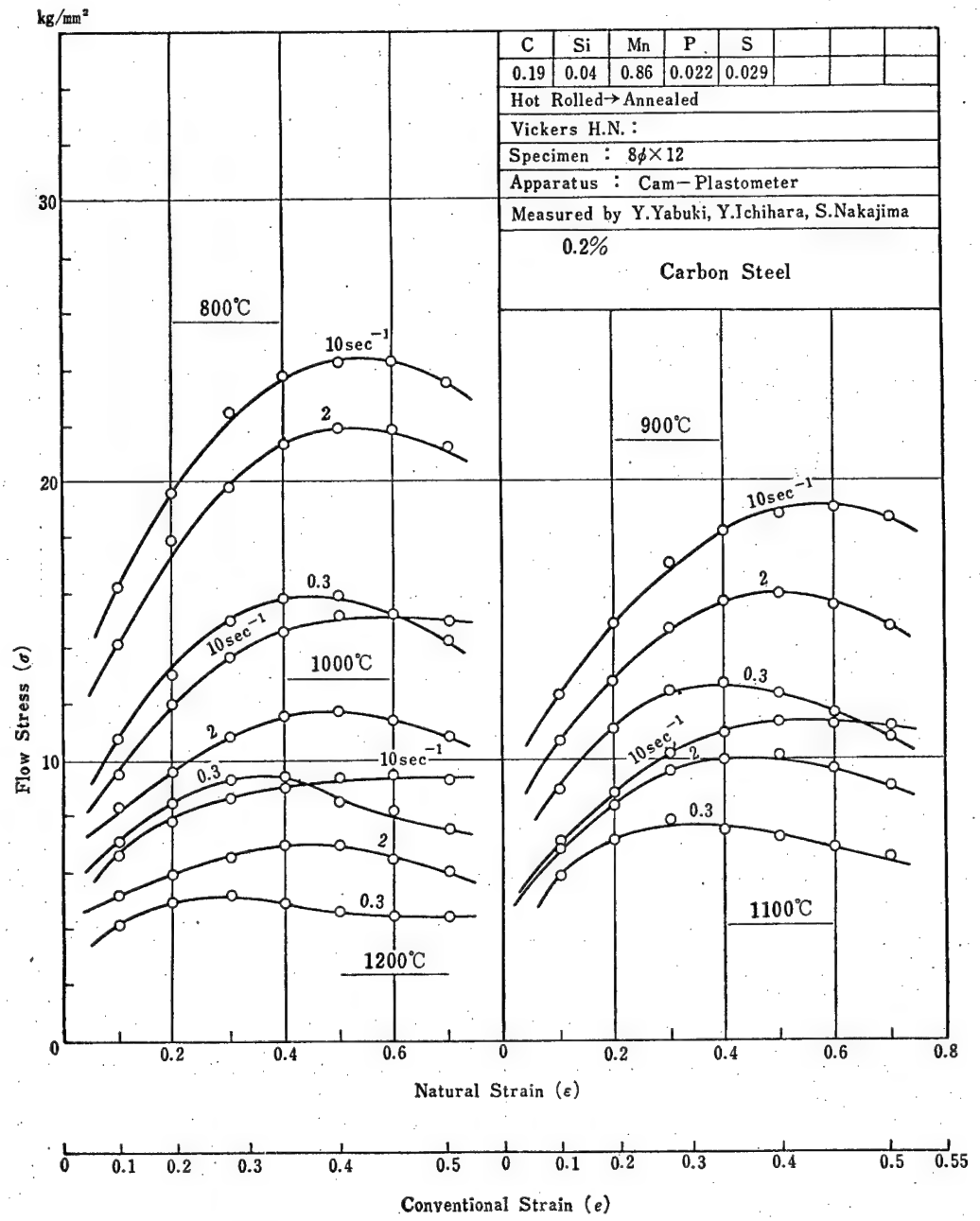

Fig. 4·26 Flow Stress-Strain Curves of 0.2% C-Steel. Temperature Range: 800~1200°C, Strain Rate Range: 0.3~10 sec^{-1}.

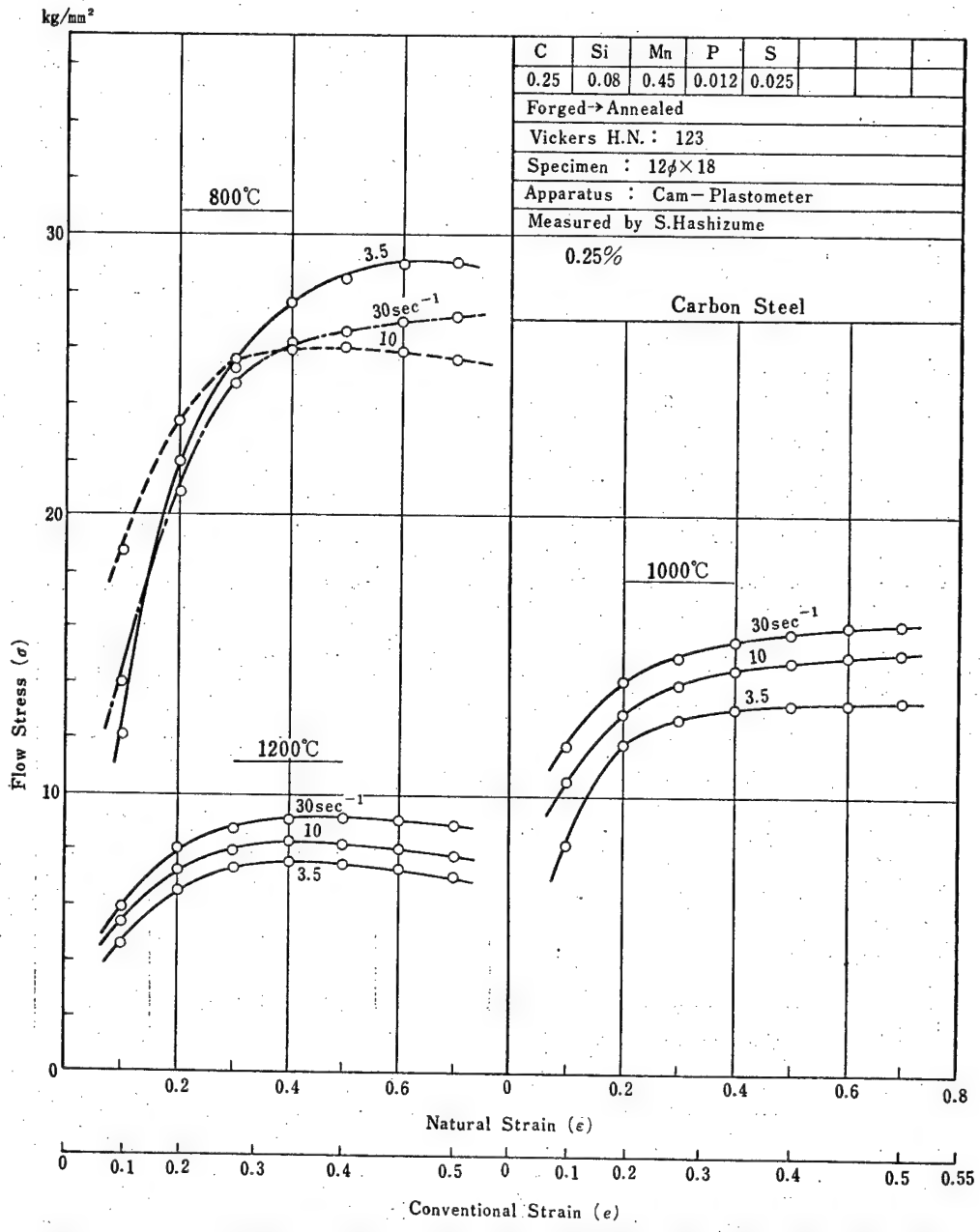

Fig. 4·27 Flow Stress-Strain Curves of 0.25% C Steel. Temperature Range: 800~1200°C, Strain Rate Range: 3.5~30 sec⁻¹.

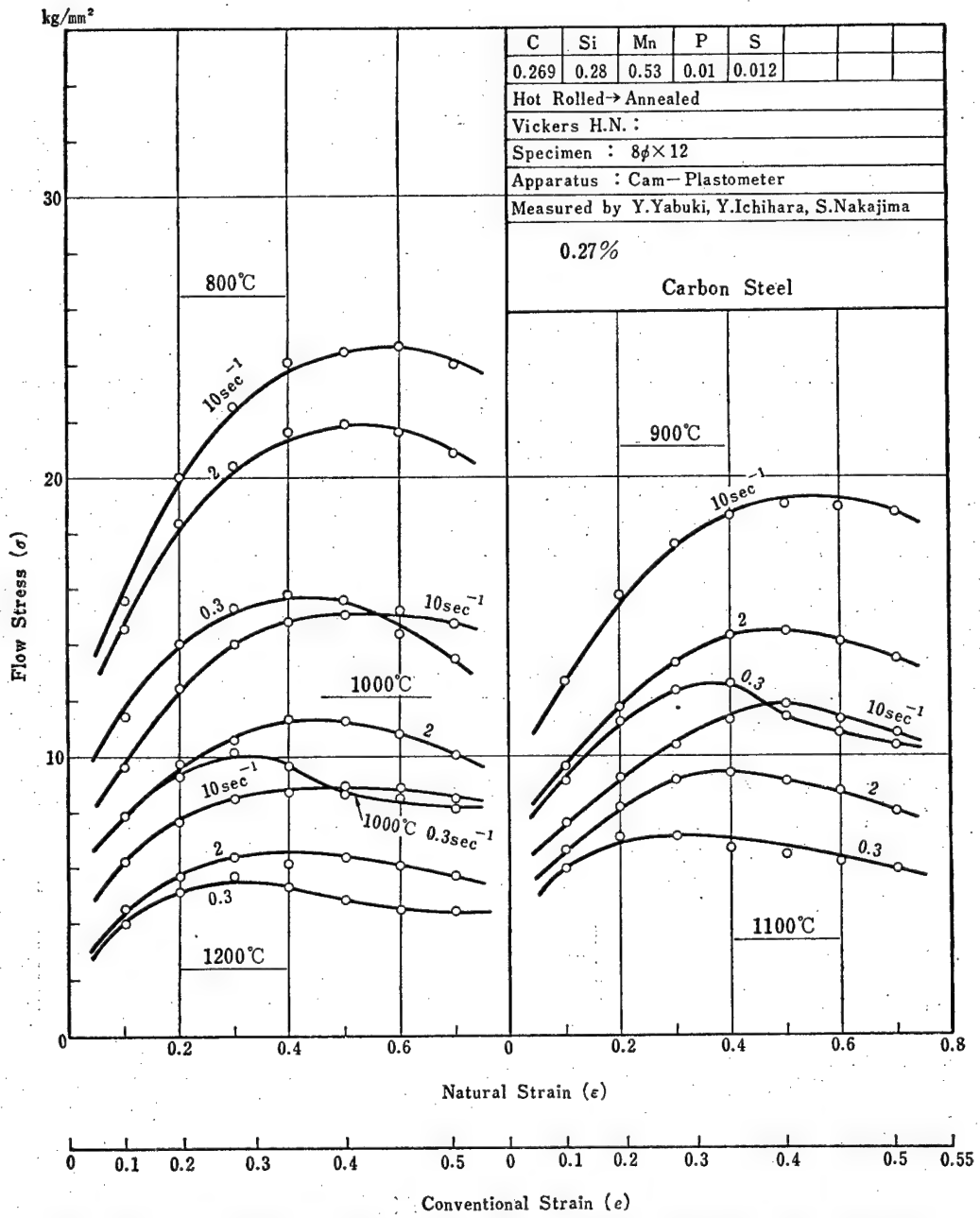

Fig. 4·28 Flow Stress-Strain Curves of 0.27% C-Steel. Temperature Range: 800~1200°C, Strain Rate Range: 0.3~10 sec⁻¹.

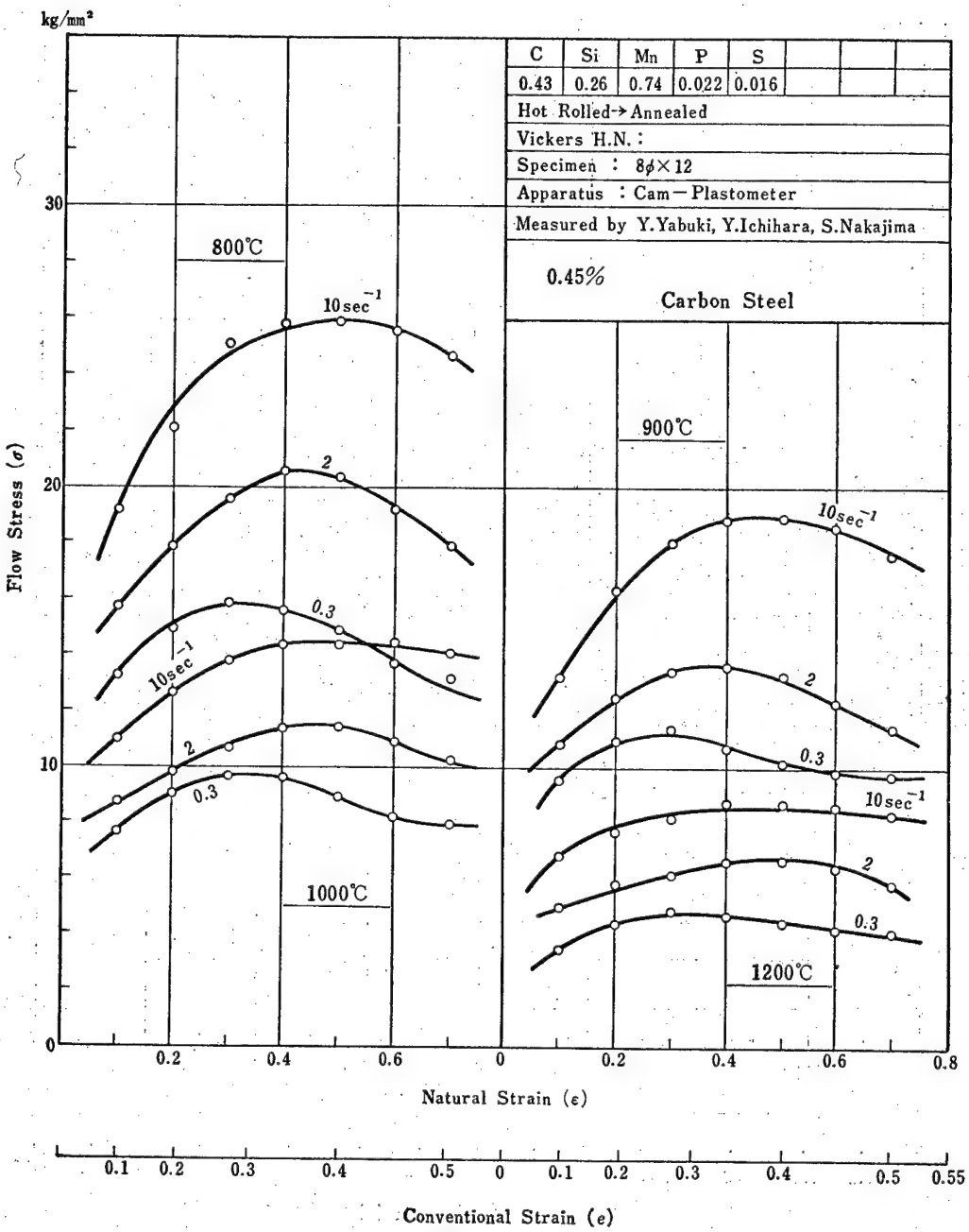

Fig. 4·29 Flow Stress-Strain Curves of 0.45% C-Steel. Temperature Range: 800~1200°C, Strain Rate Range: 0.3~10 sec⁻¹.

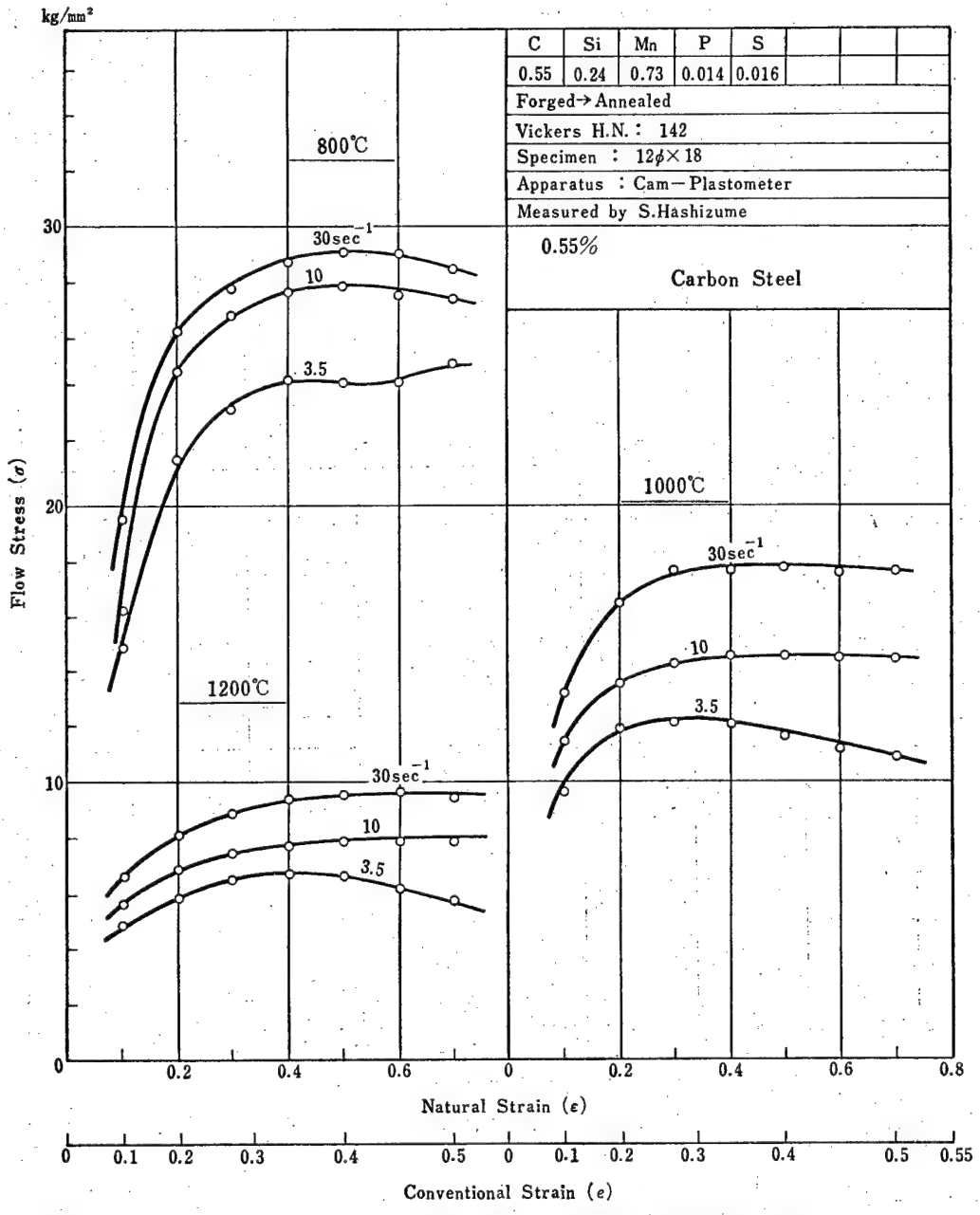

Fig. 4·30 Flow Stress-Strain Curves of 0.55% C Steel. Temperature Range: 800~1200°C, Strain Rate Range: 3.5~30 sec^{-1}.

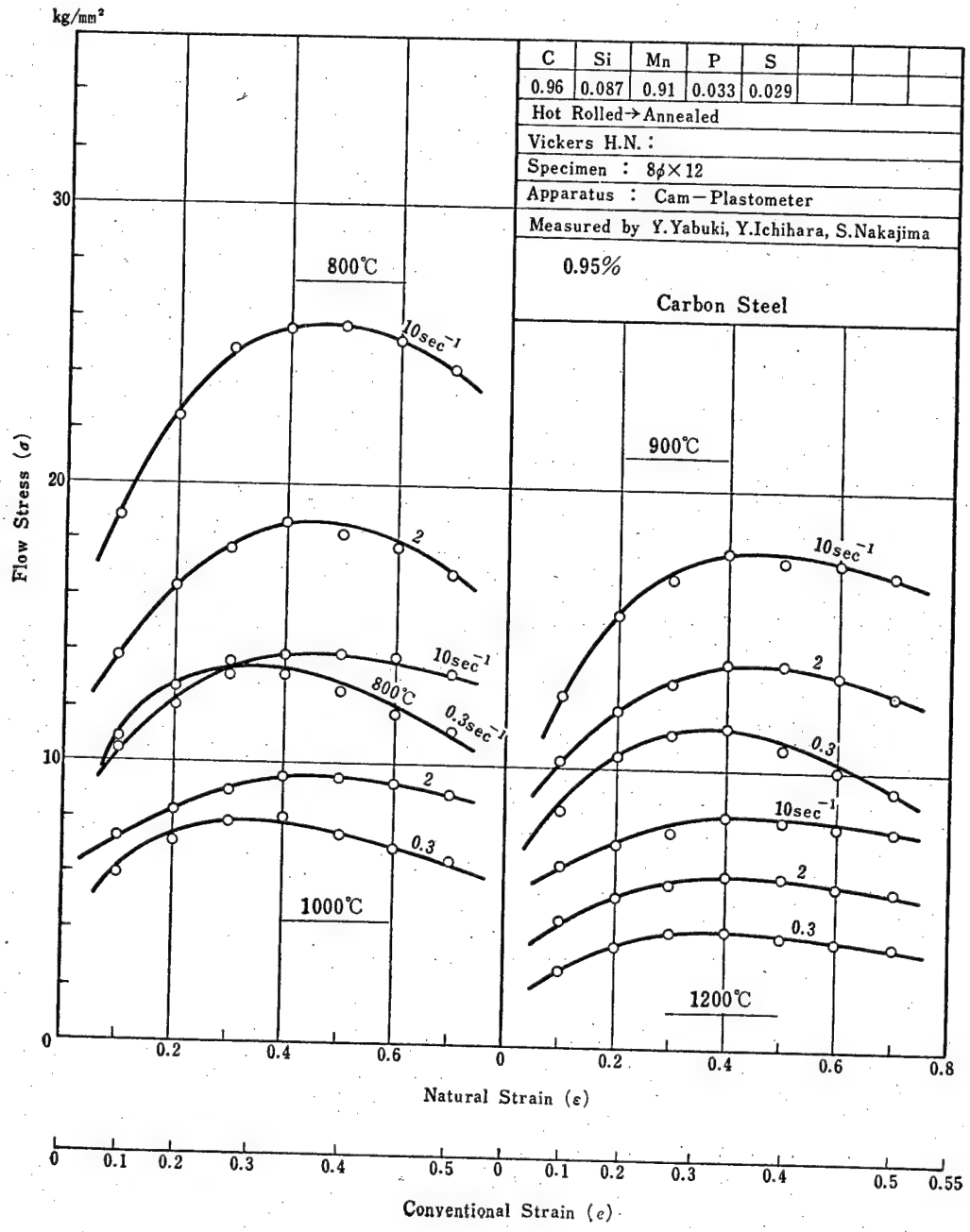

Fig. 4·31 Flow Stress-Strain Curves of 0.95% C-Steel. Temperature Range: 800~1200°C, Strain Rate Range: 0.3~10 sec⁻¹.

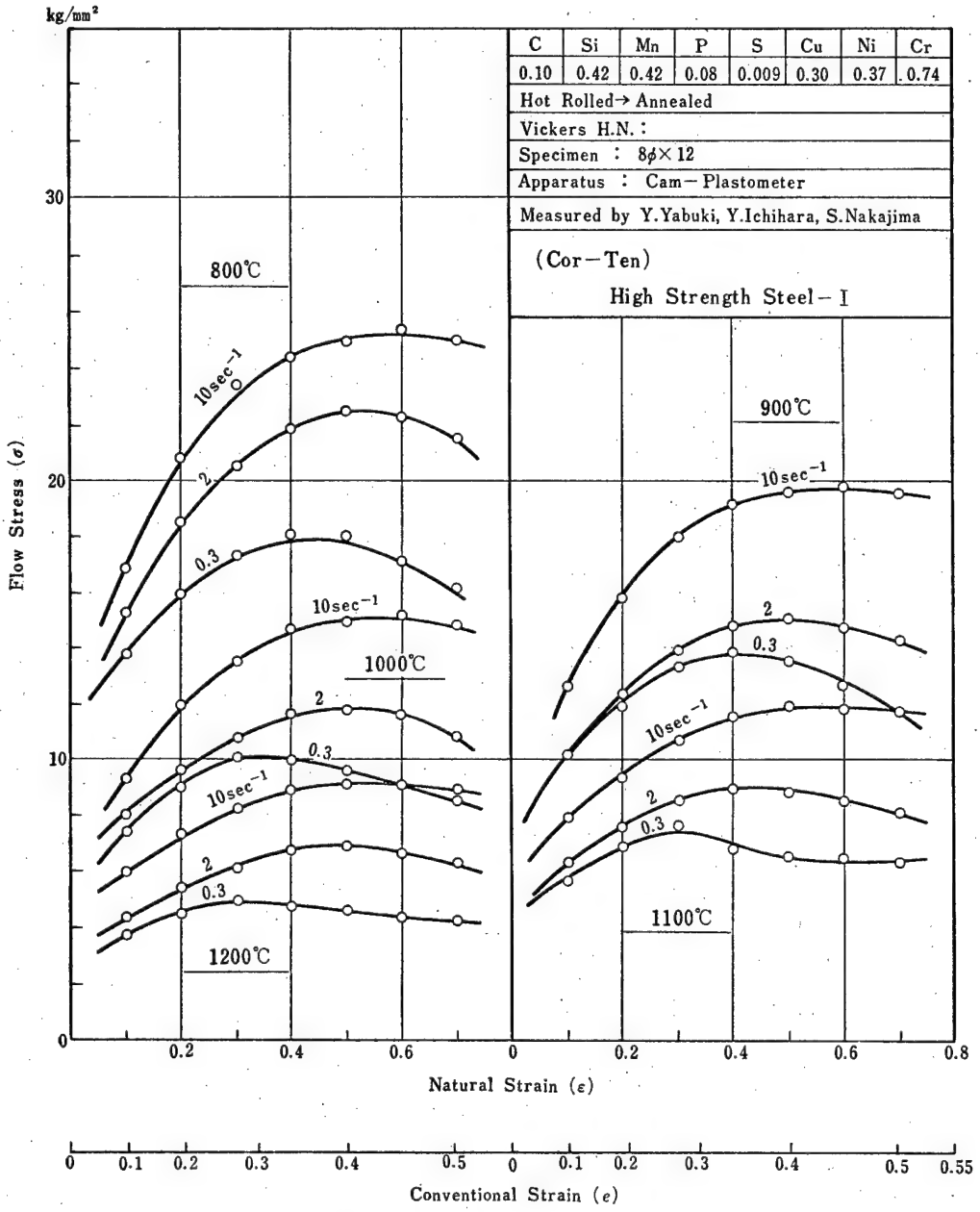

Fig. 4·32 Flow Stress-Strain Curves of High Strength Steel-I. Temperature Range: 800~1200°C, Strain Rate Range: 0.3~10 sec^{-1}.

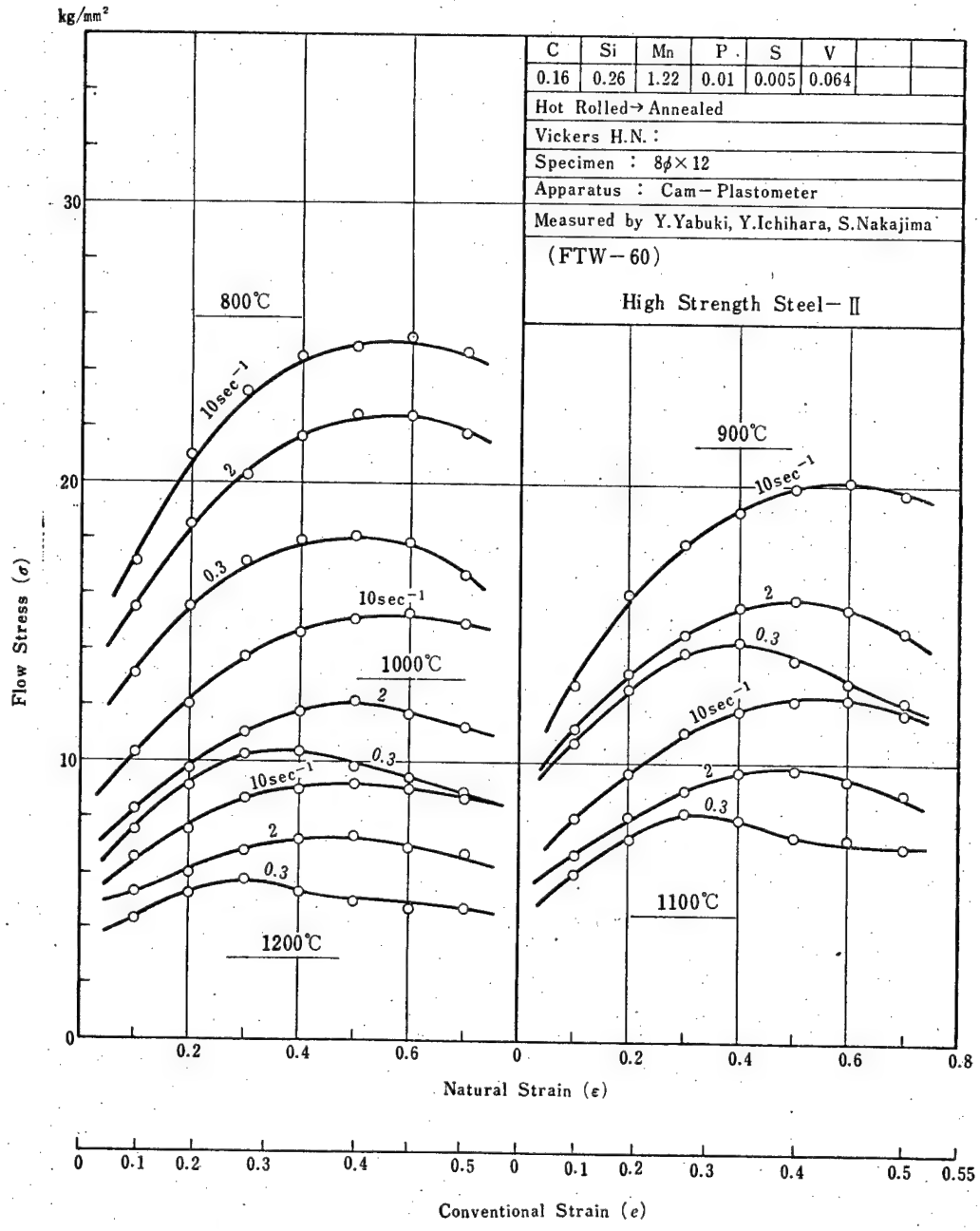

Fig. 4·33 Flow Stress-Strain Curves of High Strength Steel-II. Temperature Range: 800~1200°C, Strain Rate Range: 0.3~10 sec⁻¹.

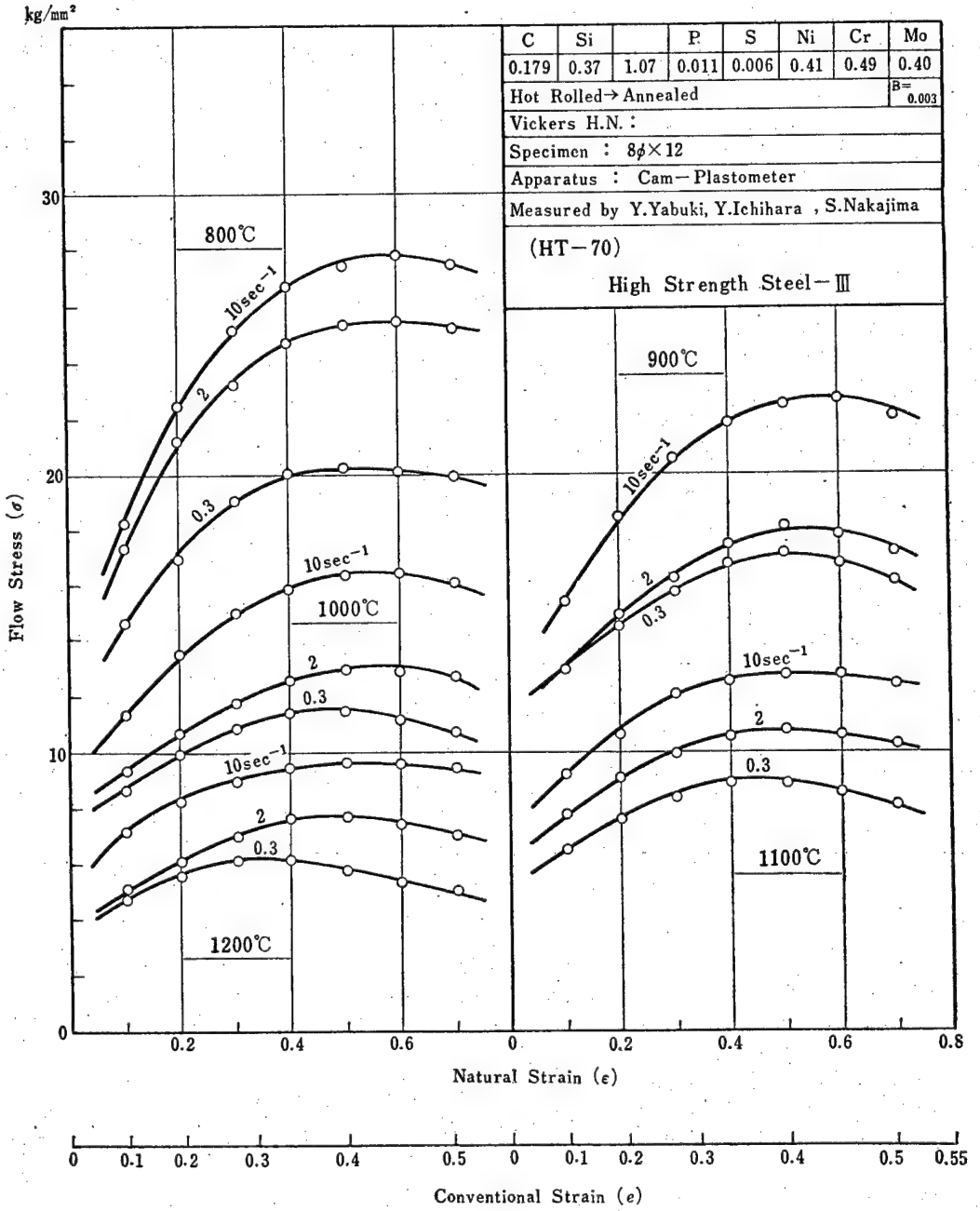

Fig. 4·34 Flow Stress-Strain Curves of High Strength Steel-III Temperature Range: 800~1200°C, Strain Rate Range: 0.3~10 sec⁻¹.

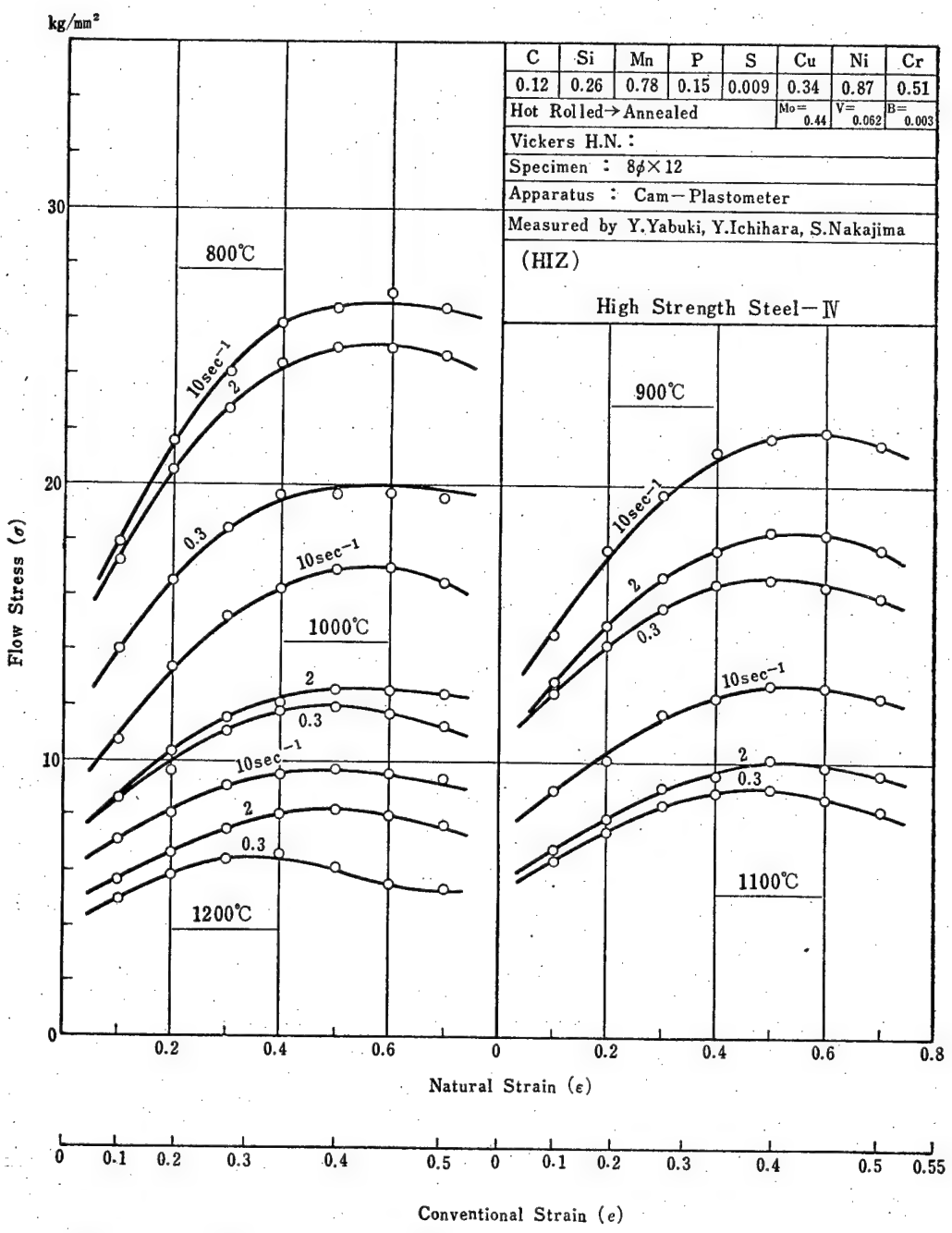

Fig. 4·35 Flow Stress-Strain Curves of High Strength Steel-IV. Temperature Range: 800~1200°C, Strain Rate Range: 0.3~10 sec^{-1}.

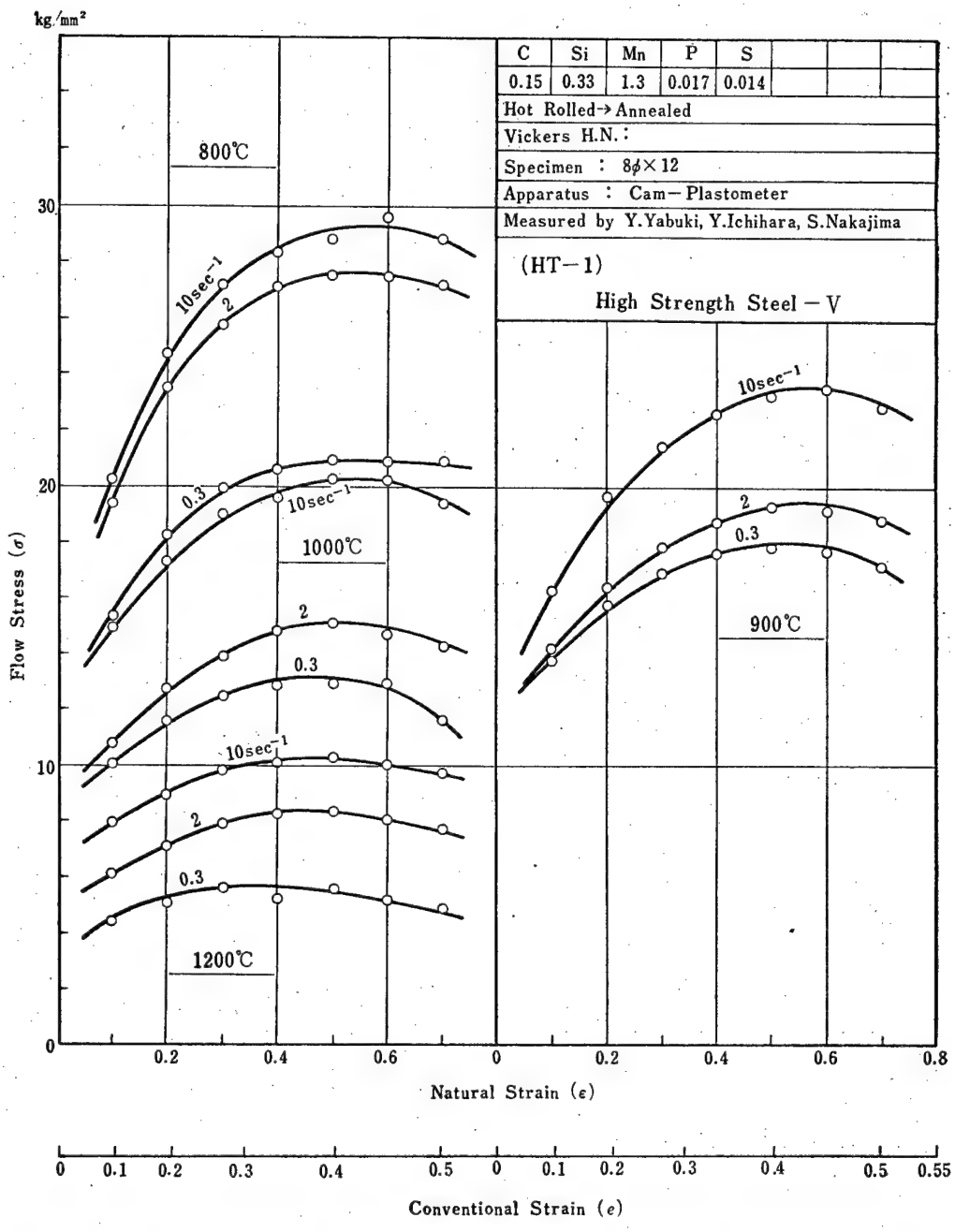

Fig. 4·36 Flow Stress-Strain Curves of High Strength Steel-V. Temperature Range: 800~1200°C, Strain Rate Range: 0.3~10 sec⁻¹.

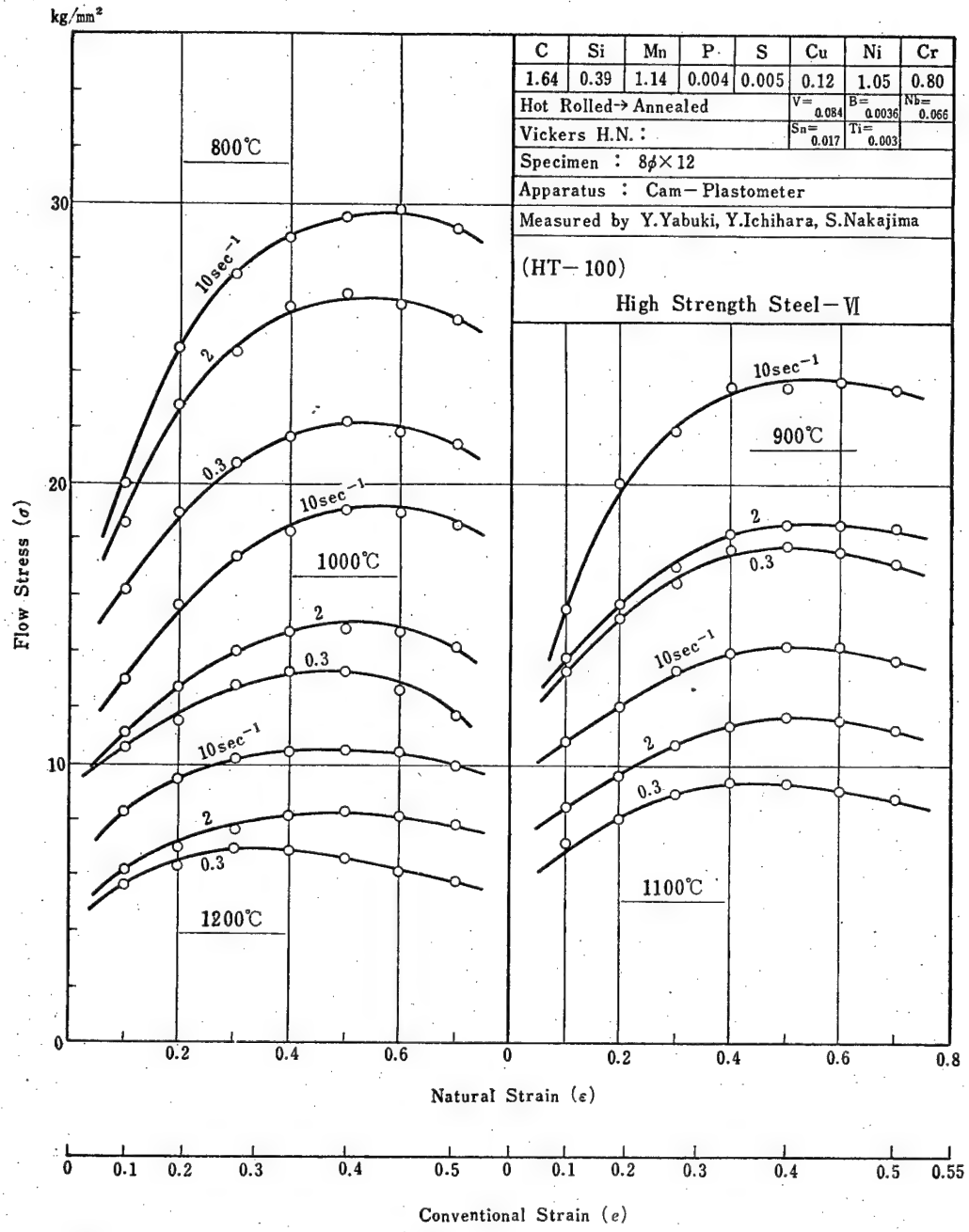

Fig. 4·37 Flow Stress-Strain Curves of High Strength Steel-VI. Temperature Range: 800~1200°C, Strain Rate Range: 0.3~10 sec^{-1}.

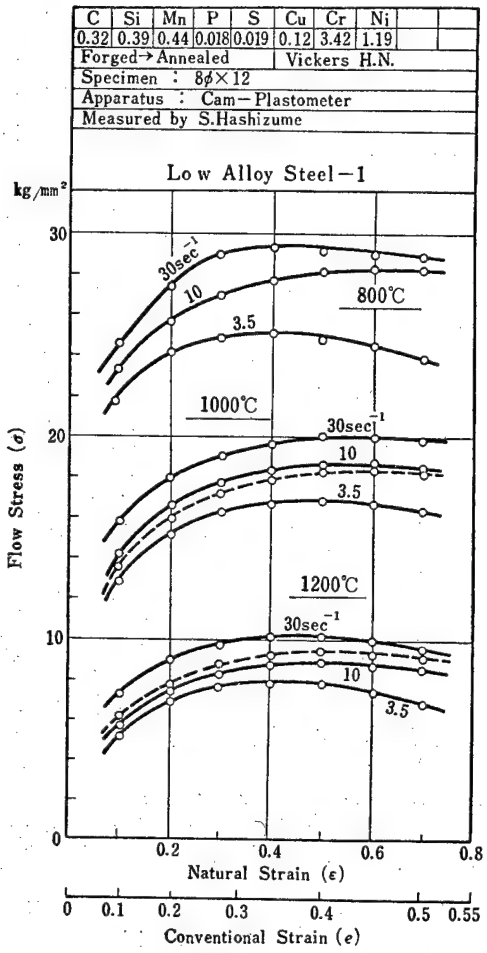

Fig. 4·38 Flow Stress-Strain Curves of Low Alloy Steel-1. Temperature Range: 800~1200°C, Strain Rate Range: 3.5~30 sec^{-1}.

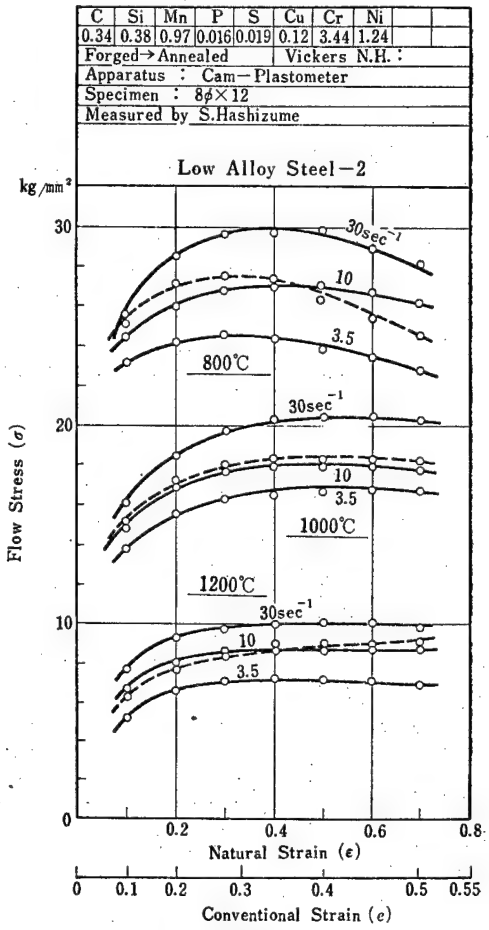

Fig. 4·39 Flow Stress-Strain Curves of Low Alloy Steel-2. Temperature Range: 800~1200°C, Strain Rate Range: 3.5~30 sec^{-1}.

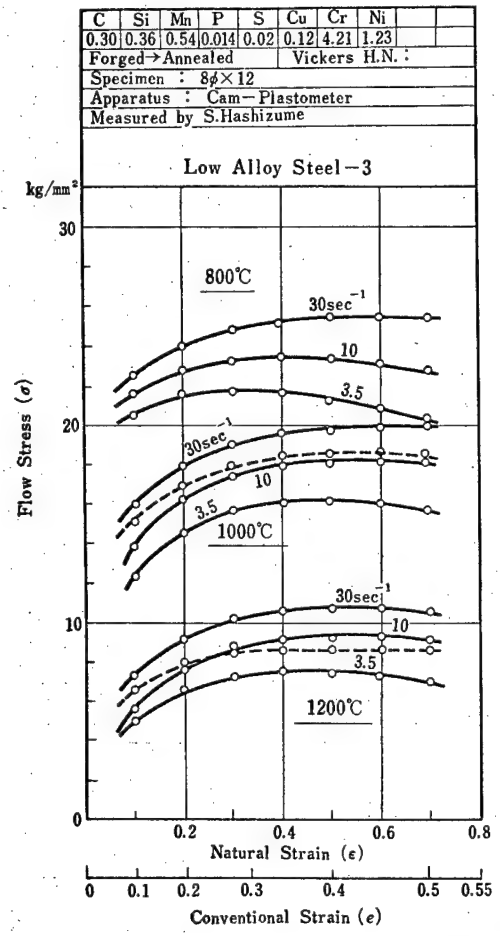

Fig. 4·40 Flow Stress-Strain Curves of Low Alloy Steel-3. Temperature Range: 800～1200°C, Strain Rate Range: 3.5～30 sec⁻¹.

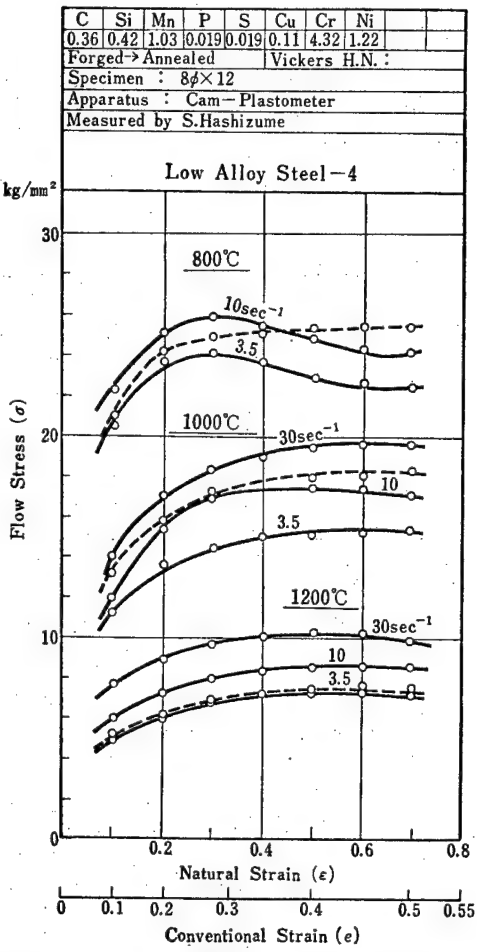

Fig. 4·41 Flow Stress-Strain Curves of Low Alloy Steel-4. Temperature Range: 800～1200°C, Strain Rate Range: 3.5～10 sec⁻¹.

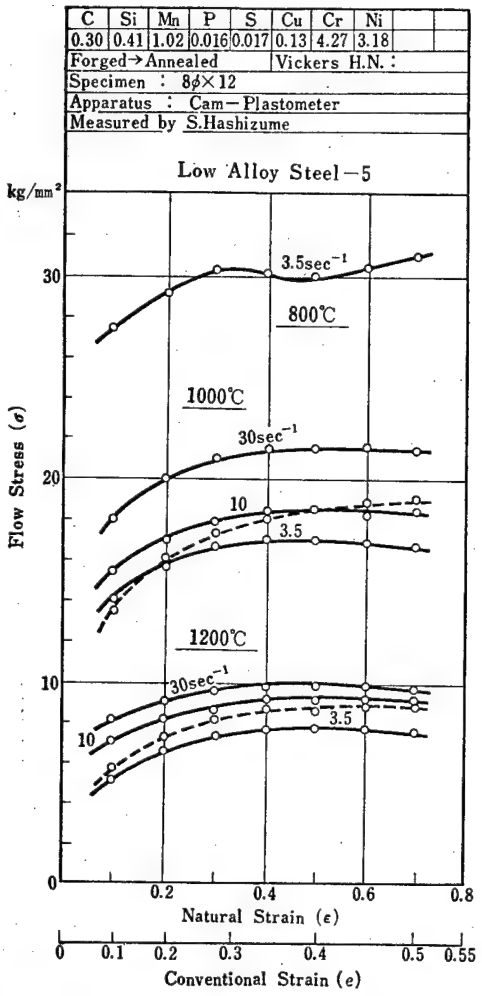

Fig. 4·42 Flow Stress-Strain Curves of Low Alloy Steel-5. Temperature Range: 800~1200°C, Strain Rate Range: 3.5~30 sec^{-1}.

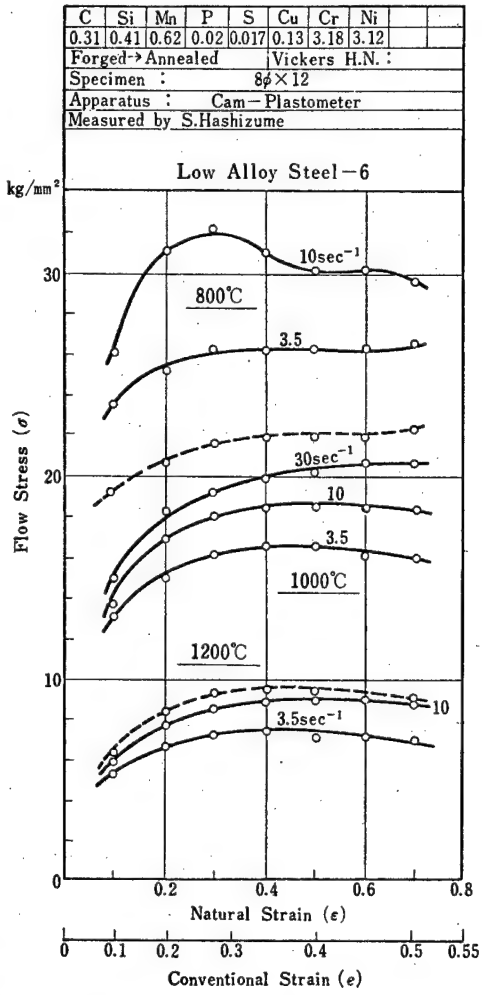

Fig. 4·43 Flow Stress-Strain Curves of Low Alloy Steel-6. Temperature Range: 800~1200°C, Strain Rate Range: 3.5~30 sec^{-1}.

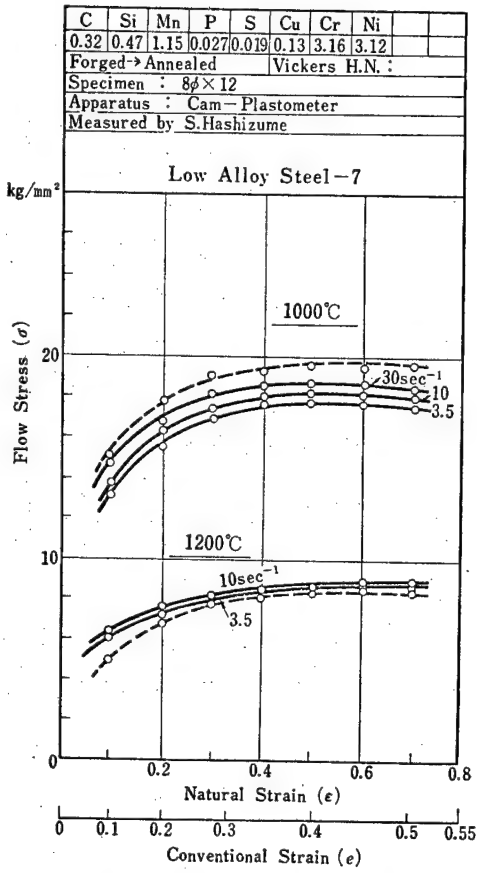

Fig. 4·44 Flow Stress-Strain Curves of Low Alloy Steel-8. Temperature 1000 and 1200°C, Strain Rate Range: 3.5～30 sec^{-1}.

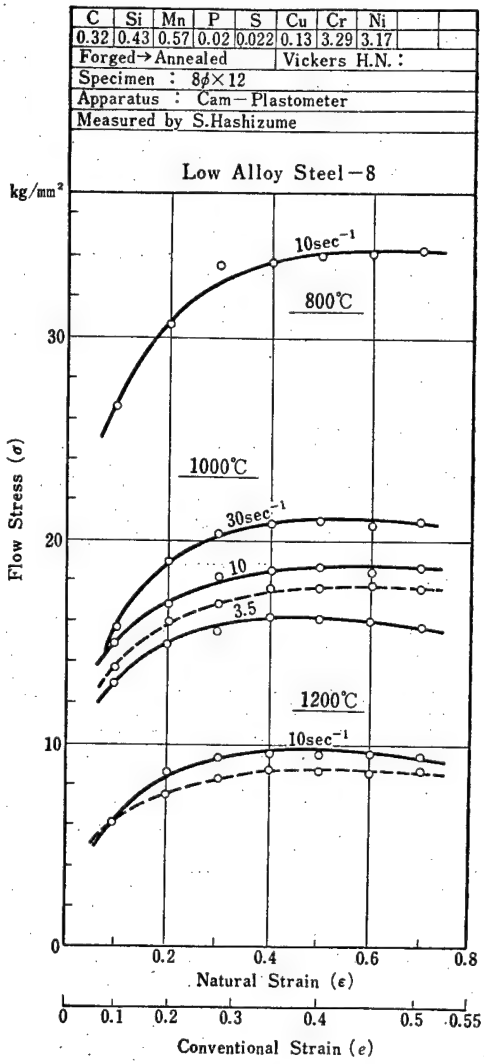

Fig. 4·45 Flow Stress-Strain Curves of Low Alloy Steel-8. Temperature Range: 800～1200°C, Strain Rate Range: 3.5～30 sec^{-1}.

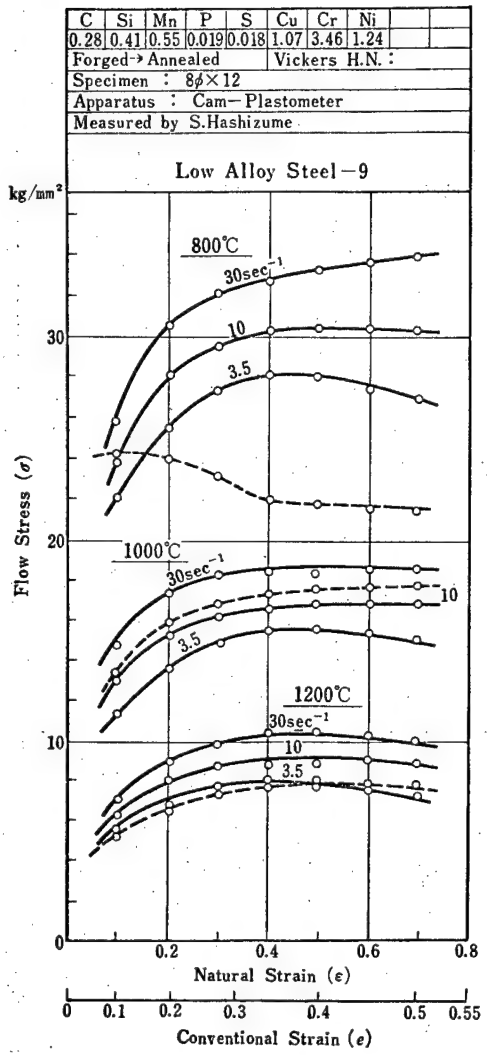

Fig. 4·46 Flow Stress-Strain Curves of Low Alloy Steel-9. Temperature Range: 800~1200°C, Strain Rate Range: 3.5~30 sec^{-1}.

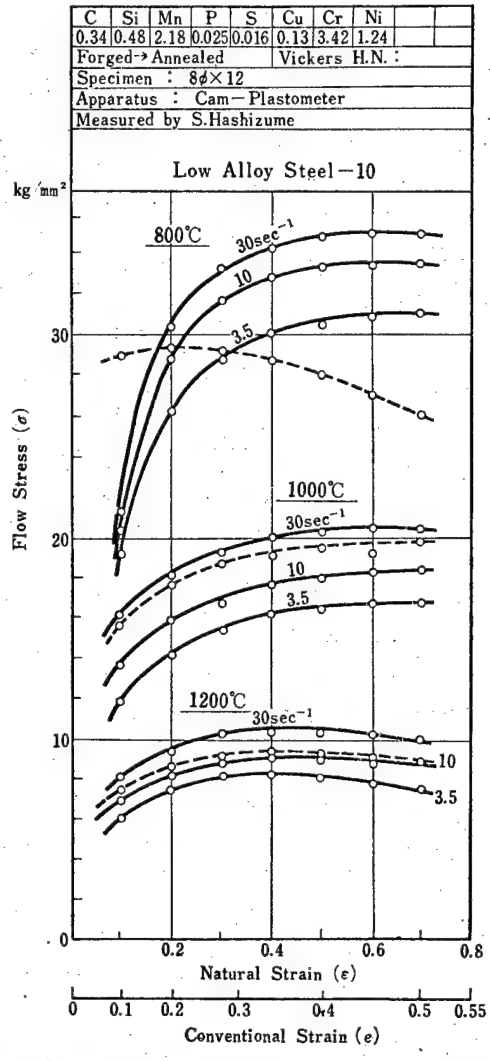

Fig. 4·47 Flow Stress-Strain Curves of Low Alloy Steel-10. Temperature Range: 800~1200°C sec^{-1}, Strain Rate Range: 3.5~30 sec^{-1}.

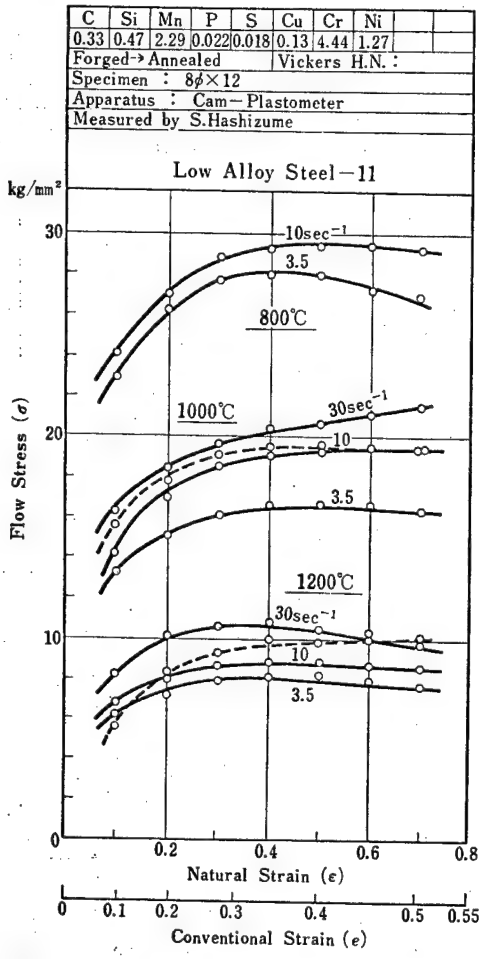

Fig. 4·48 Flow Stress-Strain Curves of Low Alloy Steel-11. Temperature Range: 800～1200°C, Strain Rate Range: 3.5～30 sec⁻¹.

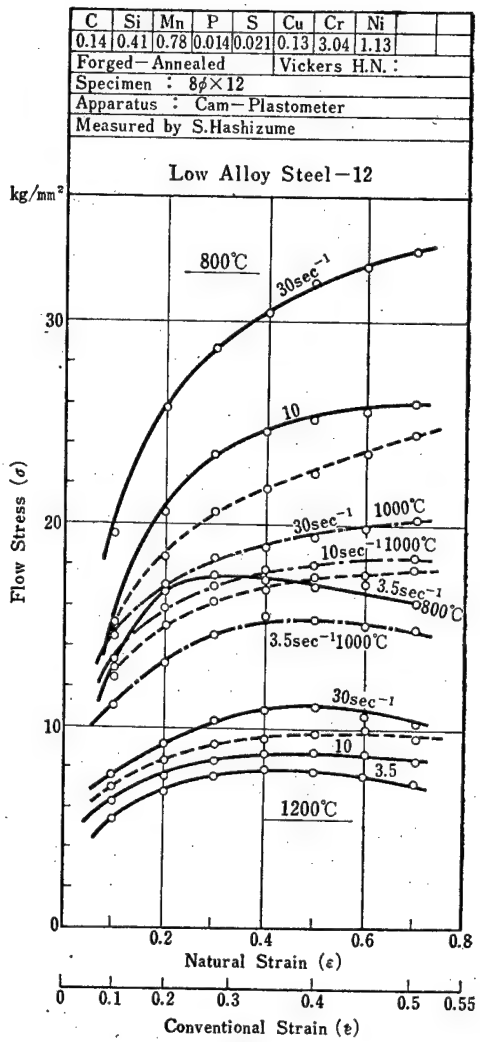

Fig. 4·49 Flow Stress-Strain Curves of Low Alloy Steel-12. Temperature Range: 800～1200°C, Strain Rate Range: 3.5～30 sec⁻¹.

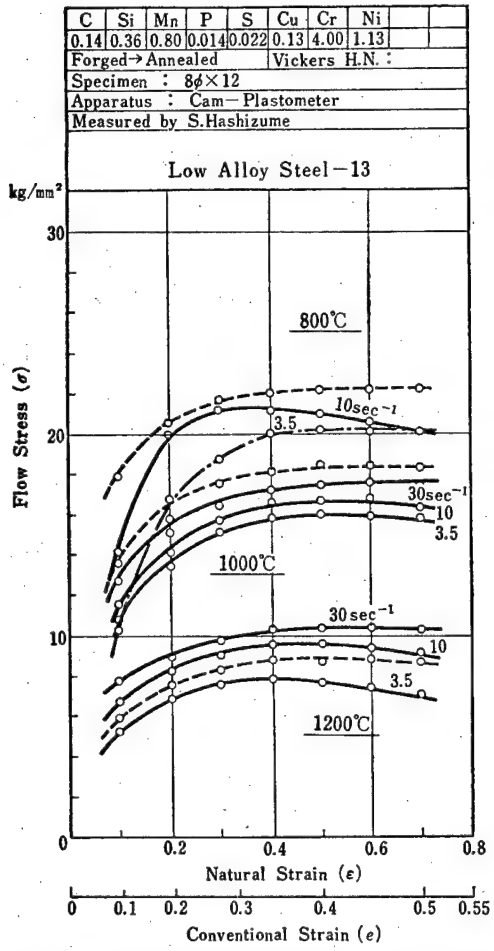

Fig. 4·50 Flow Stress-Strain Curves of Low Alloy Steel-13. Temperature Range: 800～1200℃, Strain Rate Range: 3.5～30 sec⁻¹.

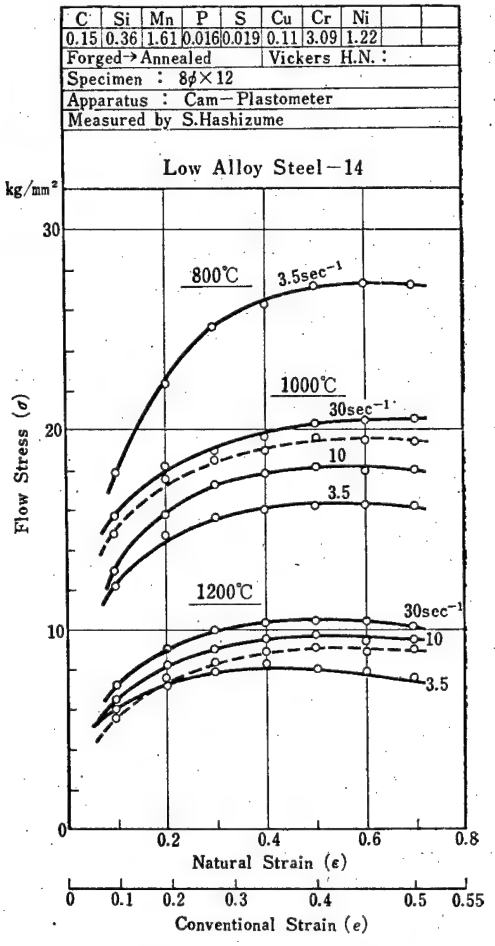

Fig. 4·51 Flow Stress-Strain Curves of Low Alloy Steel-14. Temperature Range: 800～1200℃, Strain Rate Range: 3.5～30 sec⁻¹.

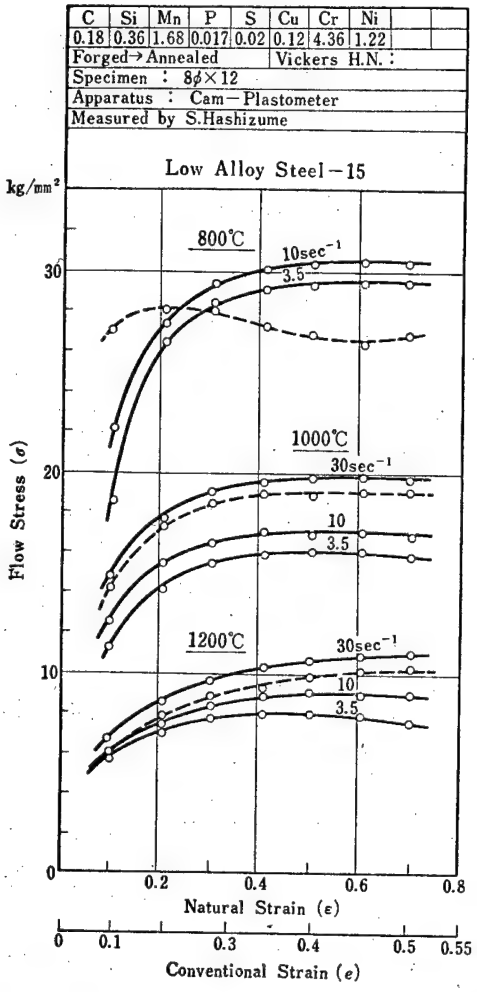

Fig. 4·52 Flow Stress-Strain Curves of Low Alloy Steel-15. Temperature Range: 800～1200°C, Strain Rate Range: 3.5～30 sec⁻¹.

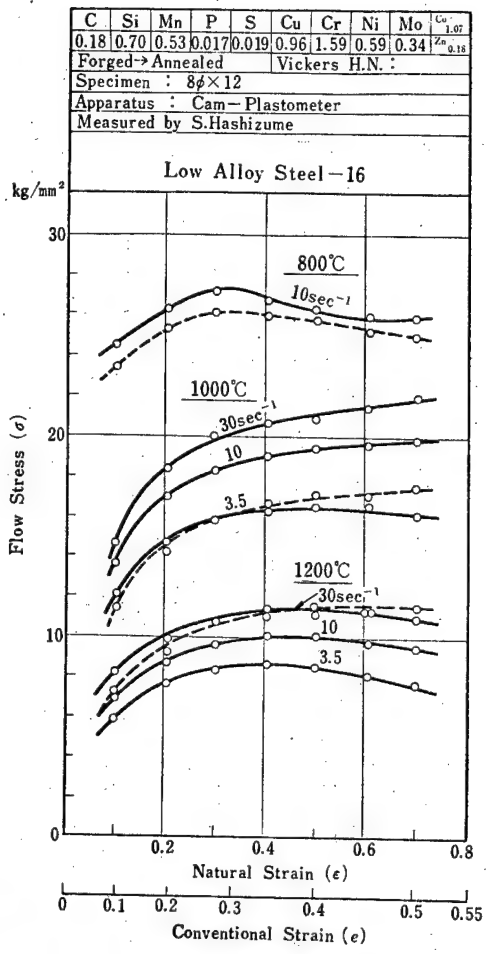

Fig. 4·53 Flow Stress-Strain Curves of Low Alloy Steel-16. Temperature Range: 800～1200°C, Strain Rate Range: 3.5～30 sec⁻¹.

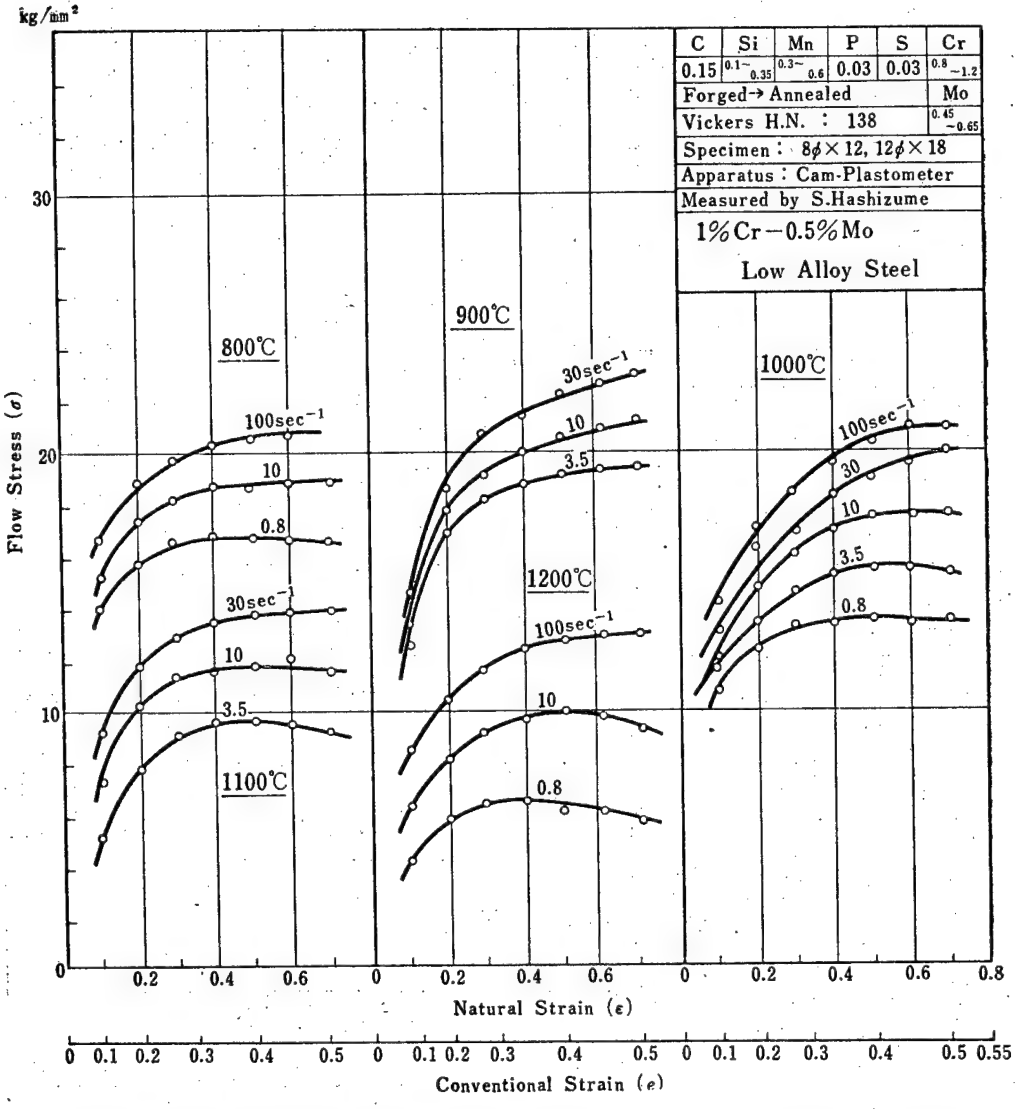

Fig. 4·54 Flow Stress-Strain Curves of 1% Cr-0.5% Mo Low Alloy Steel. Temperature Range: 800~1200°C, Strain Rate Range: 0.8~100 sec^{-1}.

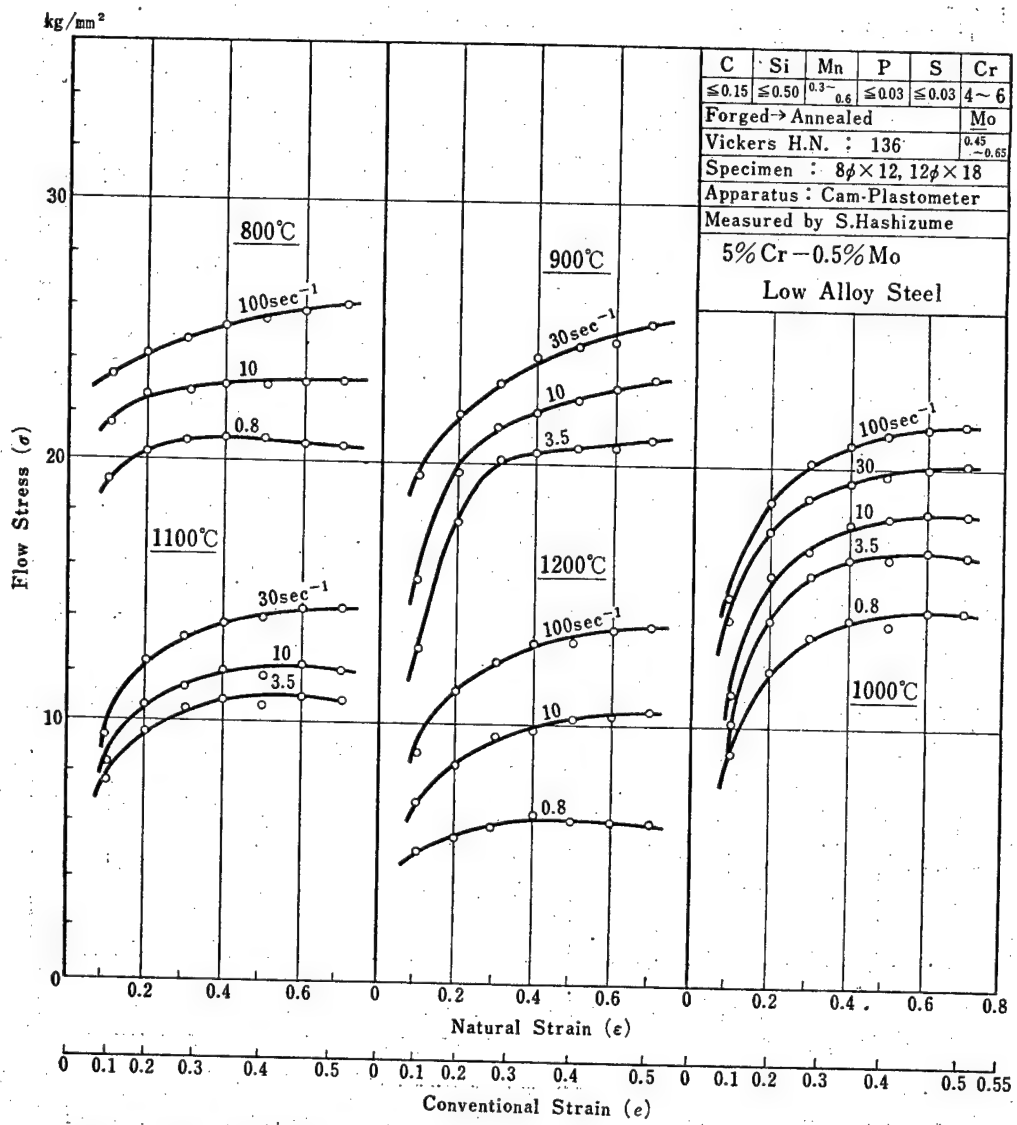

Fig. 4·55 Flow Stress-Strain Curves of 5% Cr-0.5% Mo Low Alloy Steel. Temperature Range: 800～1200°C, Strain Rate Range: 0.8～100 sec^{-1}.

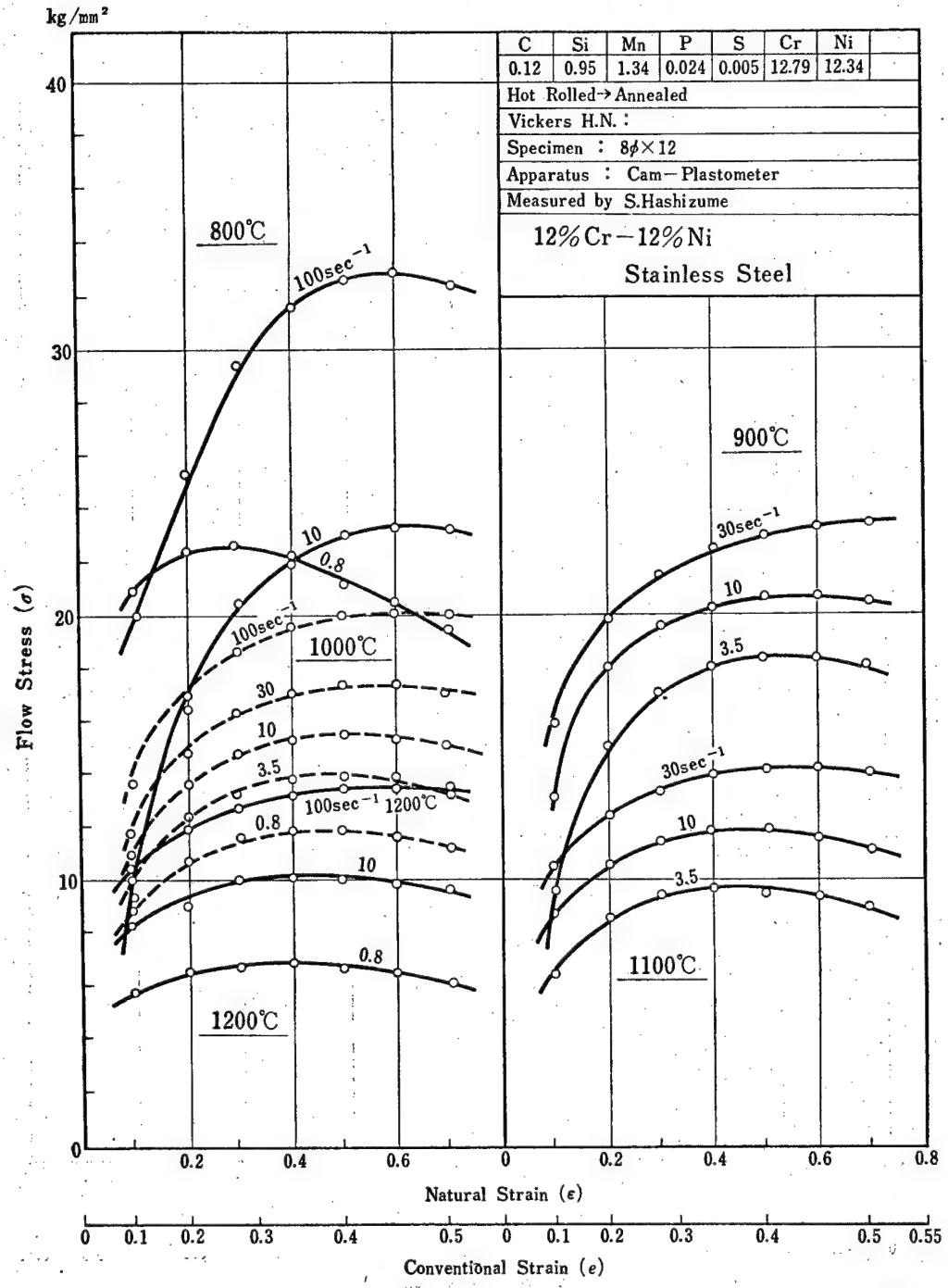

Fig. 4-56 Flow Stress-Strain Curves of 12% Cr-12% Ni Stainless Steel. Temperature Range: 800~1200°C, Strain Rate Range: 0.8~100 sec⁻¹.

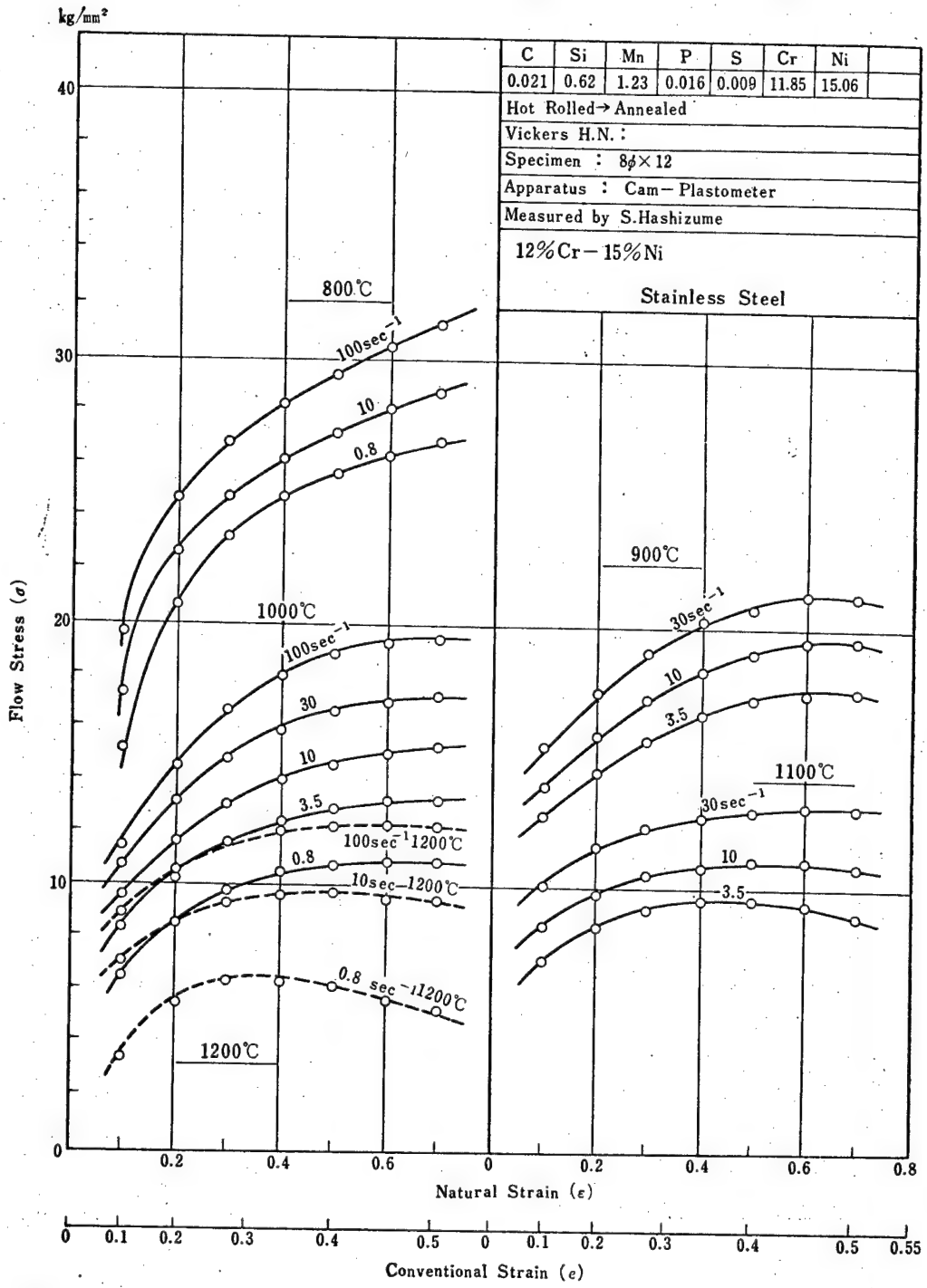

Fig. 4·57 Flow Stress-Strain Curves of 12% Cr-15% Ni Stainless Steel. Temperature Range: 800~1200°C, Strain Rate Range: 0.8~100 sec^{-1}.

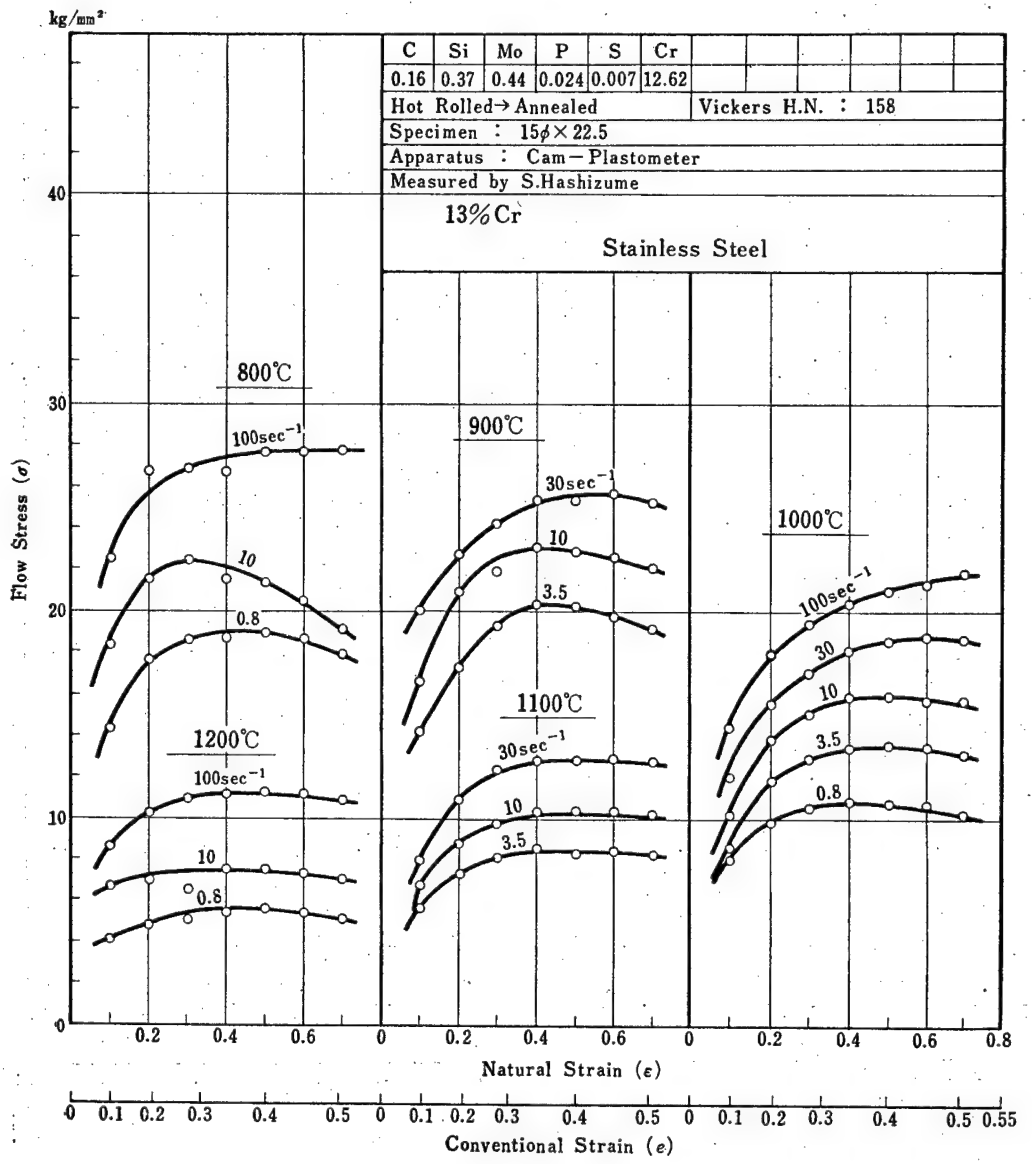

Fig. 4·58 Flow Stress-Strain Curves of 13% Cr Stainless Steel. Temperature Range: 800~1200°C, Strain Rate Range: 0.8~100 sec⁻¹.

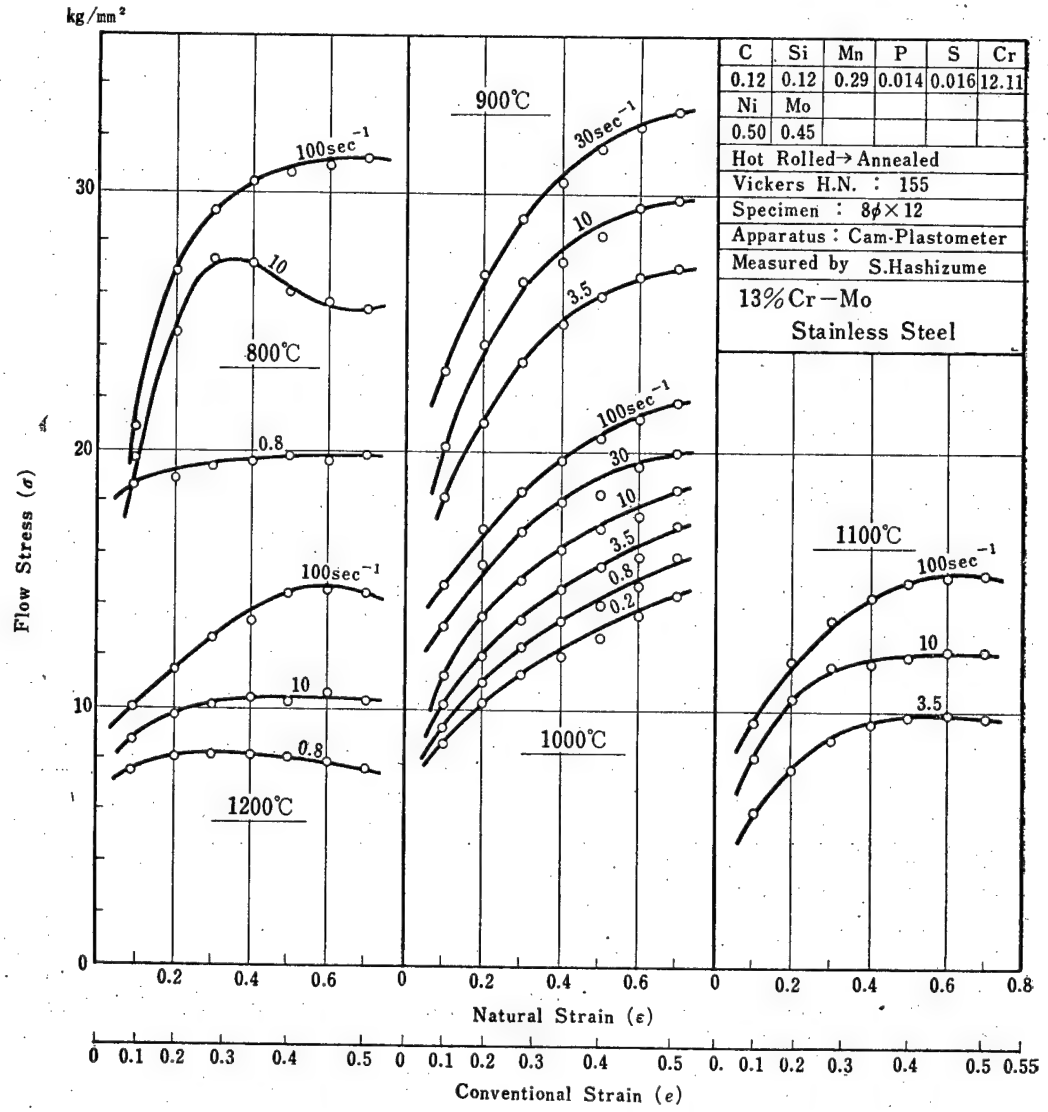

Fig. 4·59 Flow Stress-Strain Curves of 13% Cr-Mo Stainless Steel. Temperature Range: 800~1200°C, Strain Rate Range: 0.2~100 sec^{-1}.

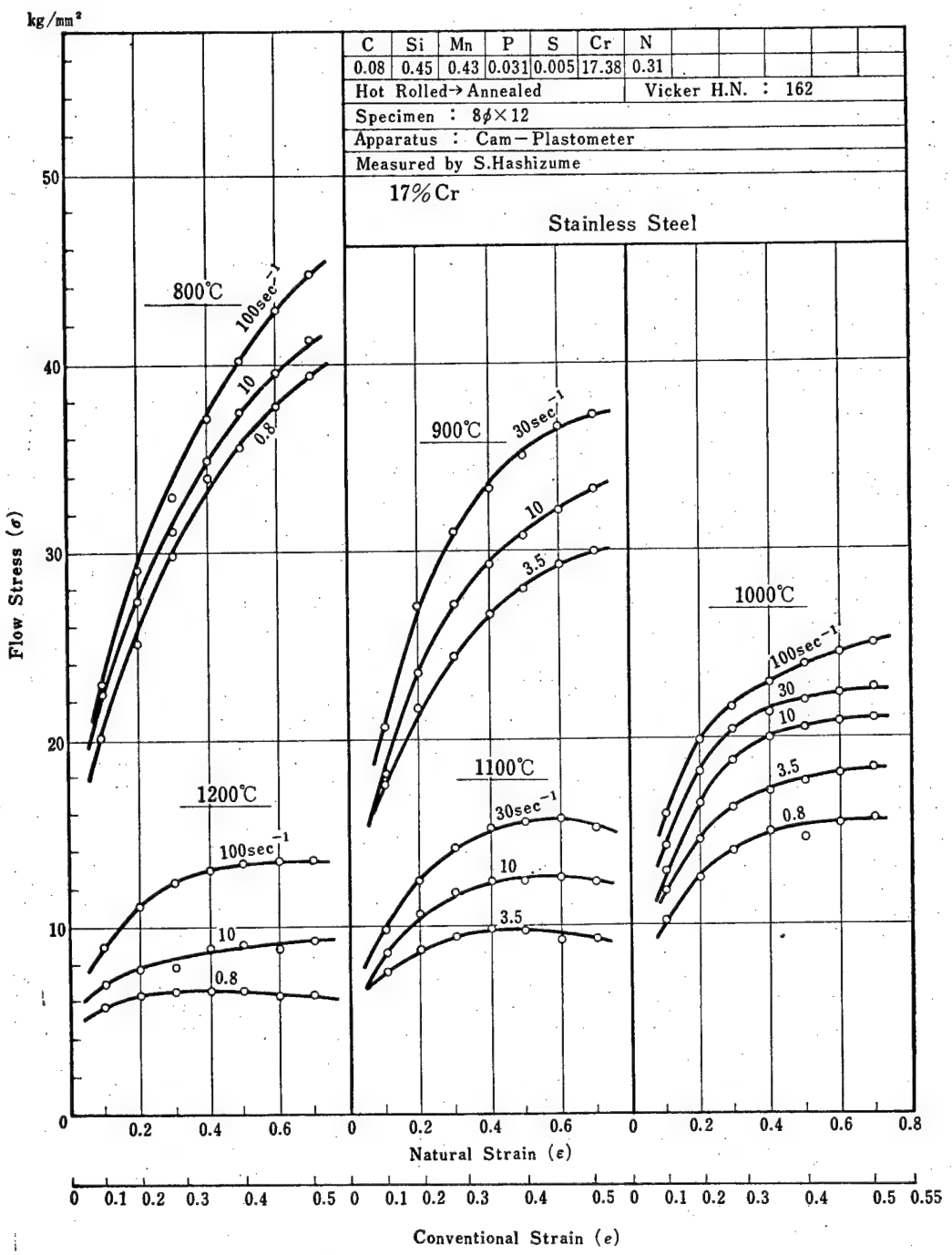

Fig. 4·60 Flow Stress-Strain Curves of 17% Cr Stainless Steel. Temperature Range: 800~1200°C, Strain Rate Range: 0.8~100 sec^{-1}.

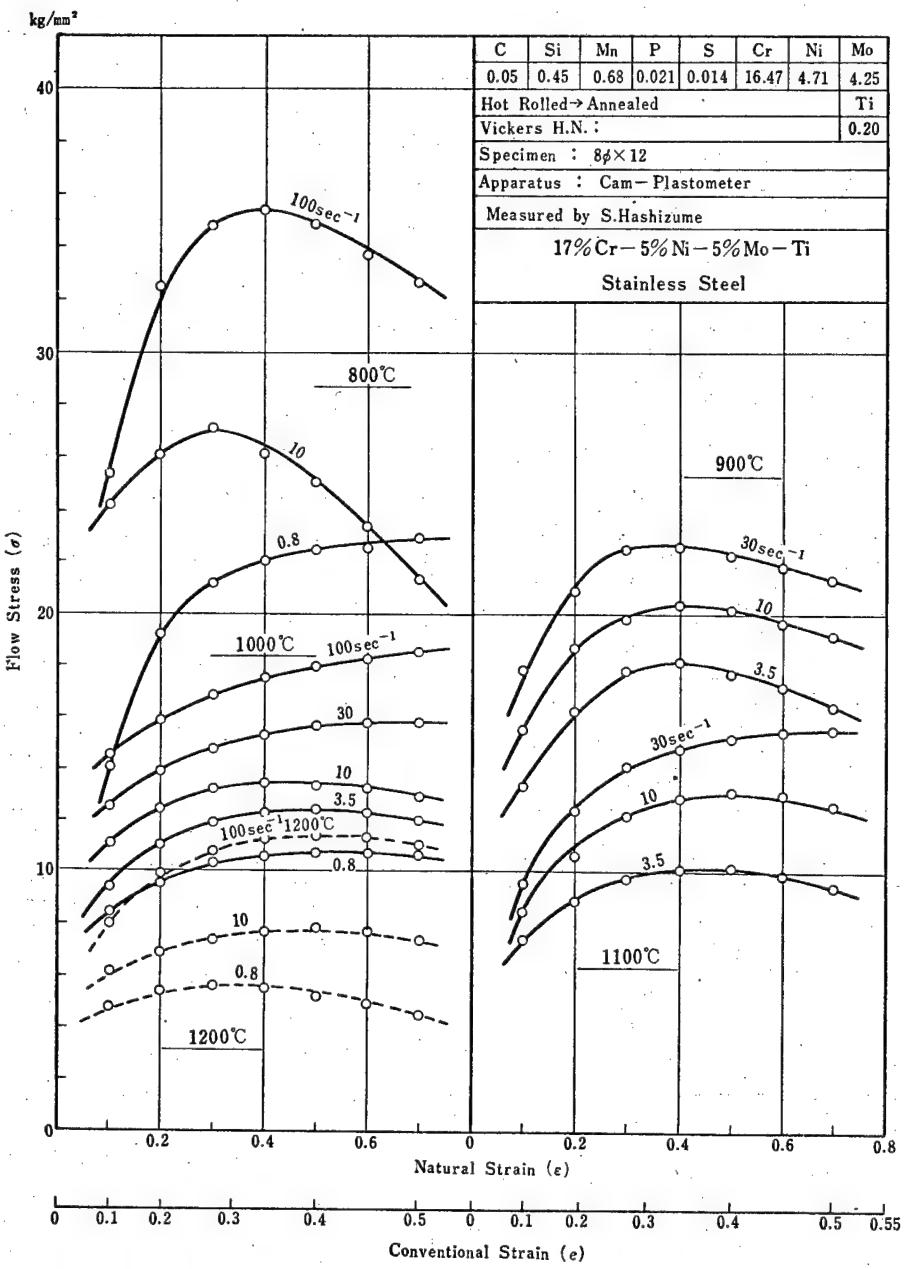

Fig. 4·61 Flow Stress-Strain Curves of 17% Cr-5% Ni-5% Mo-Ti Stainless Steel. Temperature Range: 800~1200°C, Strain Rate Range: 0.8~100 sec^{-1}.

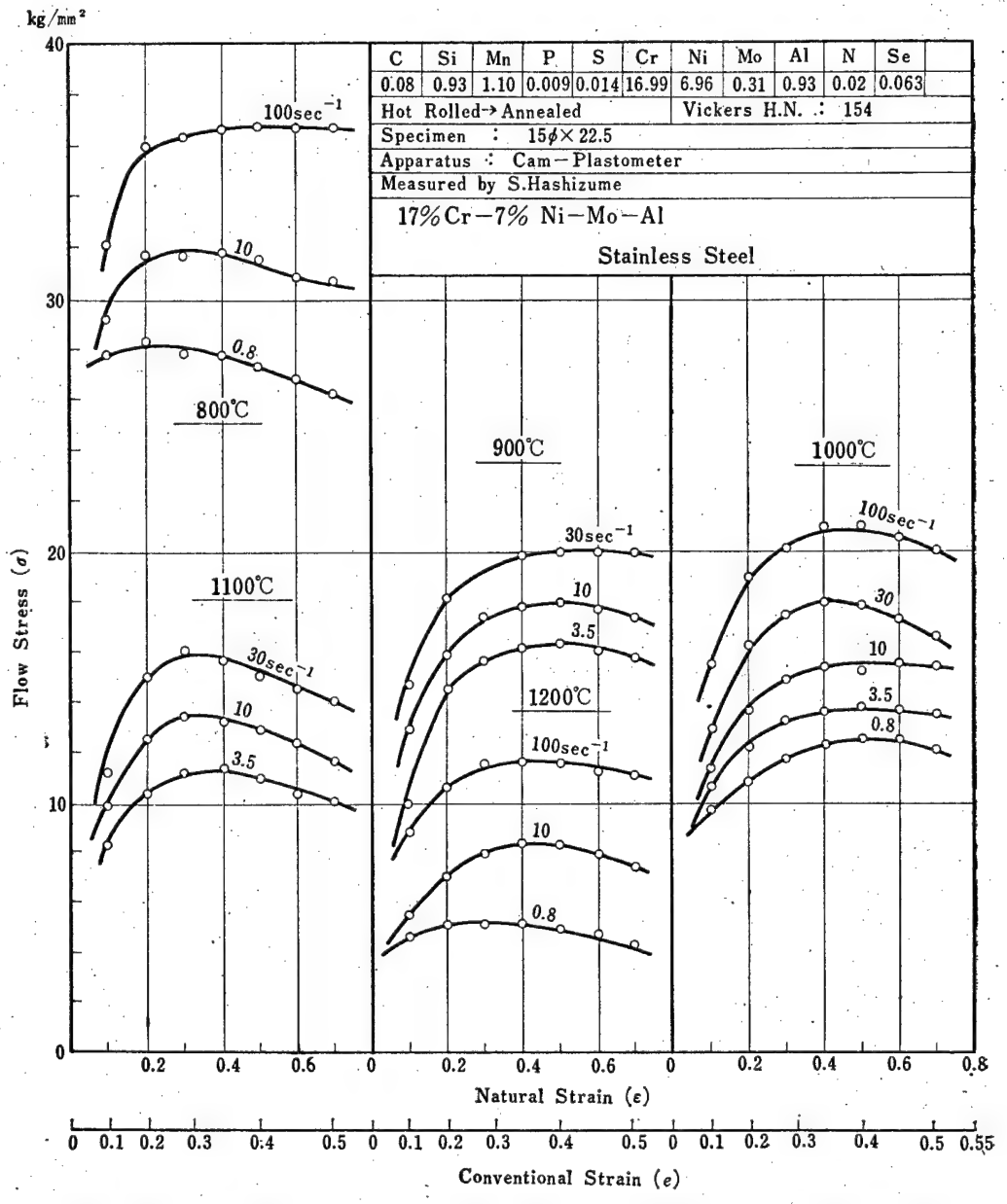

Fig. 4·62 Flow Stress-Strain Curves of 17% Cr-7% Ni-Mo-Al Stainless Steel. Temperature Range: 800~1200°C, Strain Rate Range: 0.8~100 sec^{-1}.

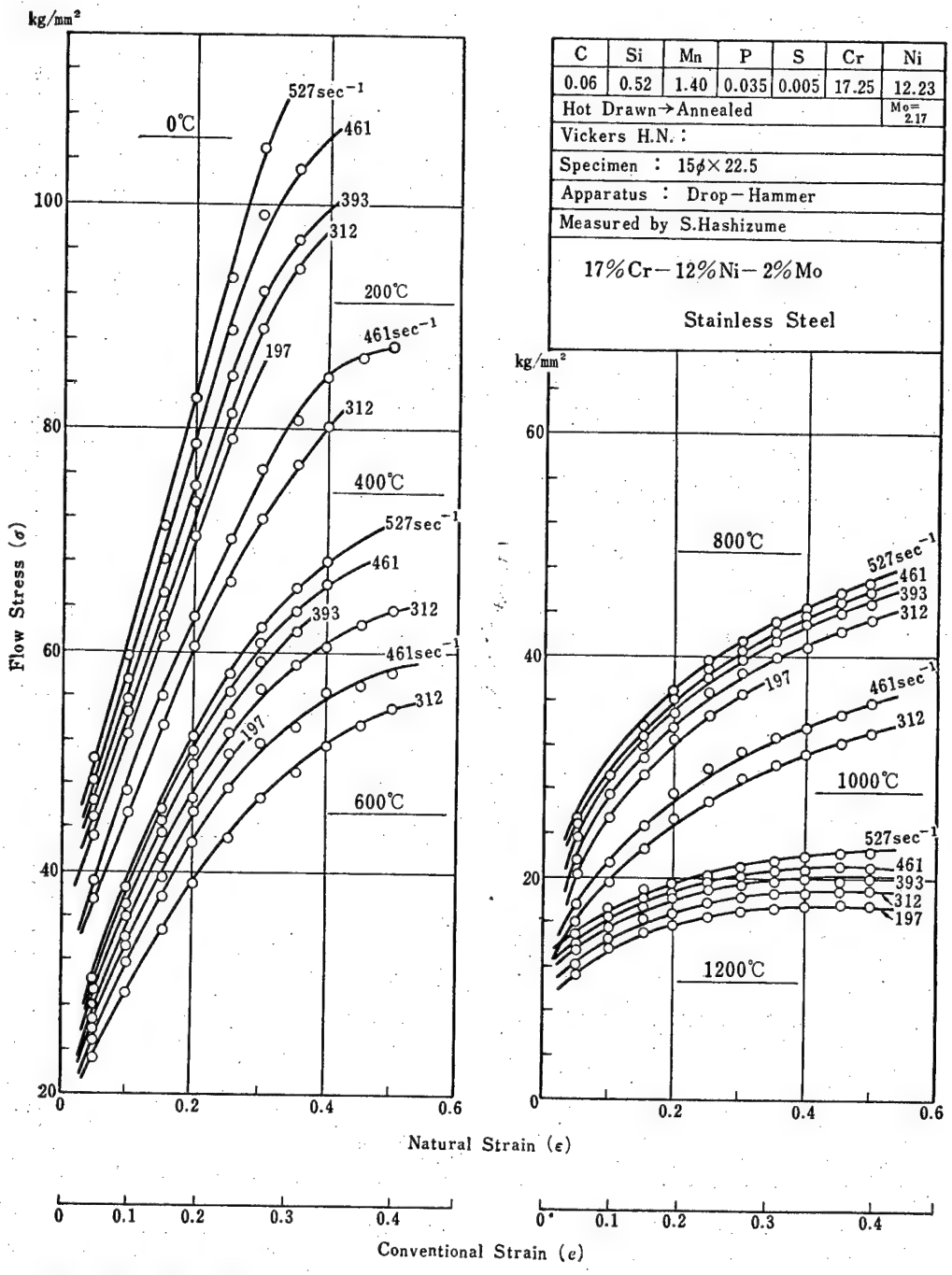

Fig. 4·63 Flow Stress-Strain Curves of 17% Cr-12% Ni-2% Mo Stainless Steel. Temerature Range: 0~1200°C, Strain Rate Range: 197~527 sec^{-1}.

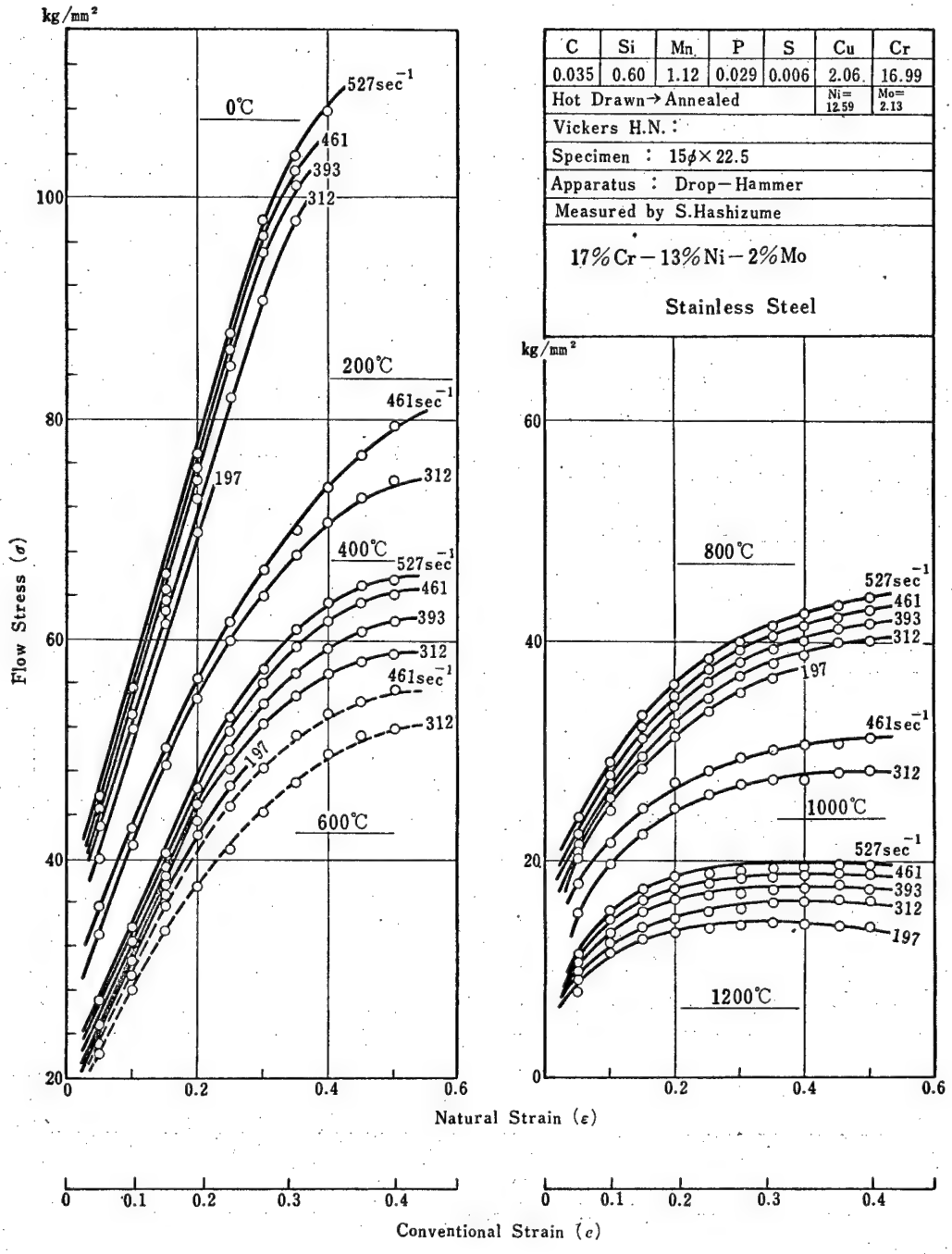

Fig. 4·64 Flow Stress-Strain Curves of 17% Cr-13% Ni-2% Mo Stainless Steel. Temperature Range: 0~1200°C, Strain Rate Range: 197~527 sec^{-1}.

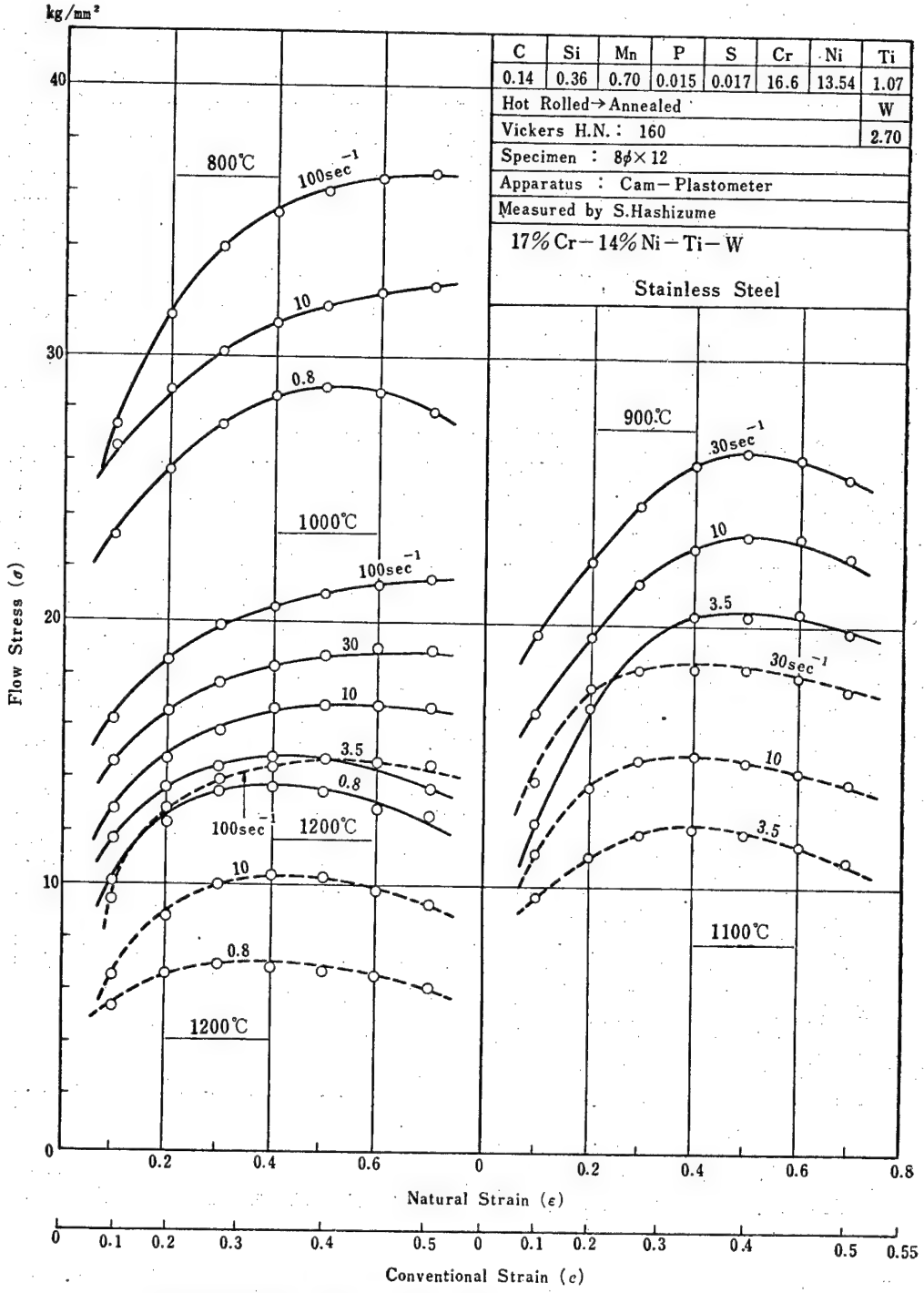

Fig. 4·65 Flow Stress-Strain Curves of 17% Cr-14% Ni-Ti-W Stainless Steel. Temperature Range: 800～1200°C, Strain Rate Range: 0.8～100 sec^{-1}.

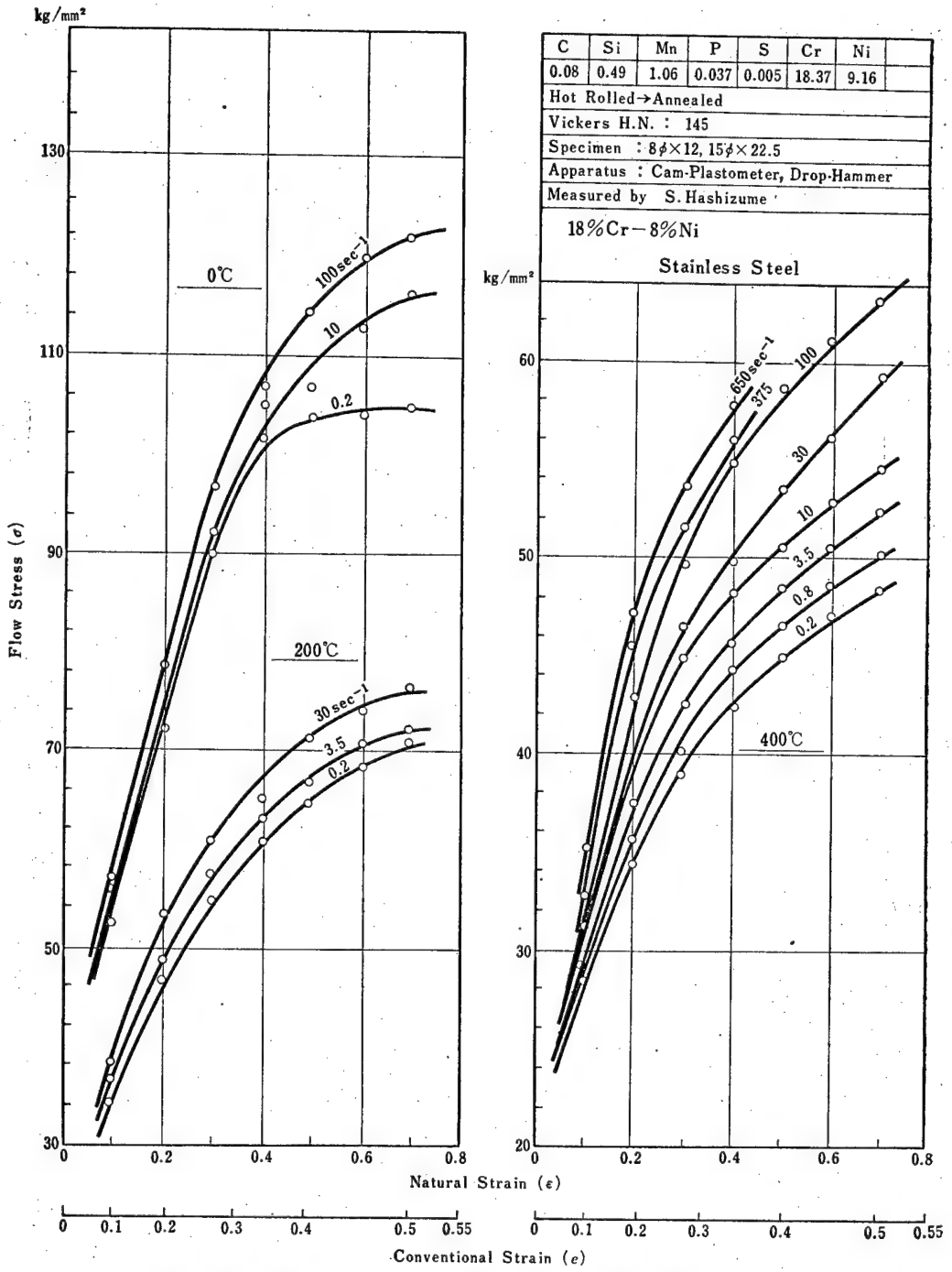

Fig. 4·66 (a) Flow Stress-Strain Curves of 18% Cr-8% Ni Stainless Steel. Temperature Range: 0～400°C, Strain Rate Range: 0.2～650 sec^{-1}.

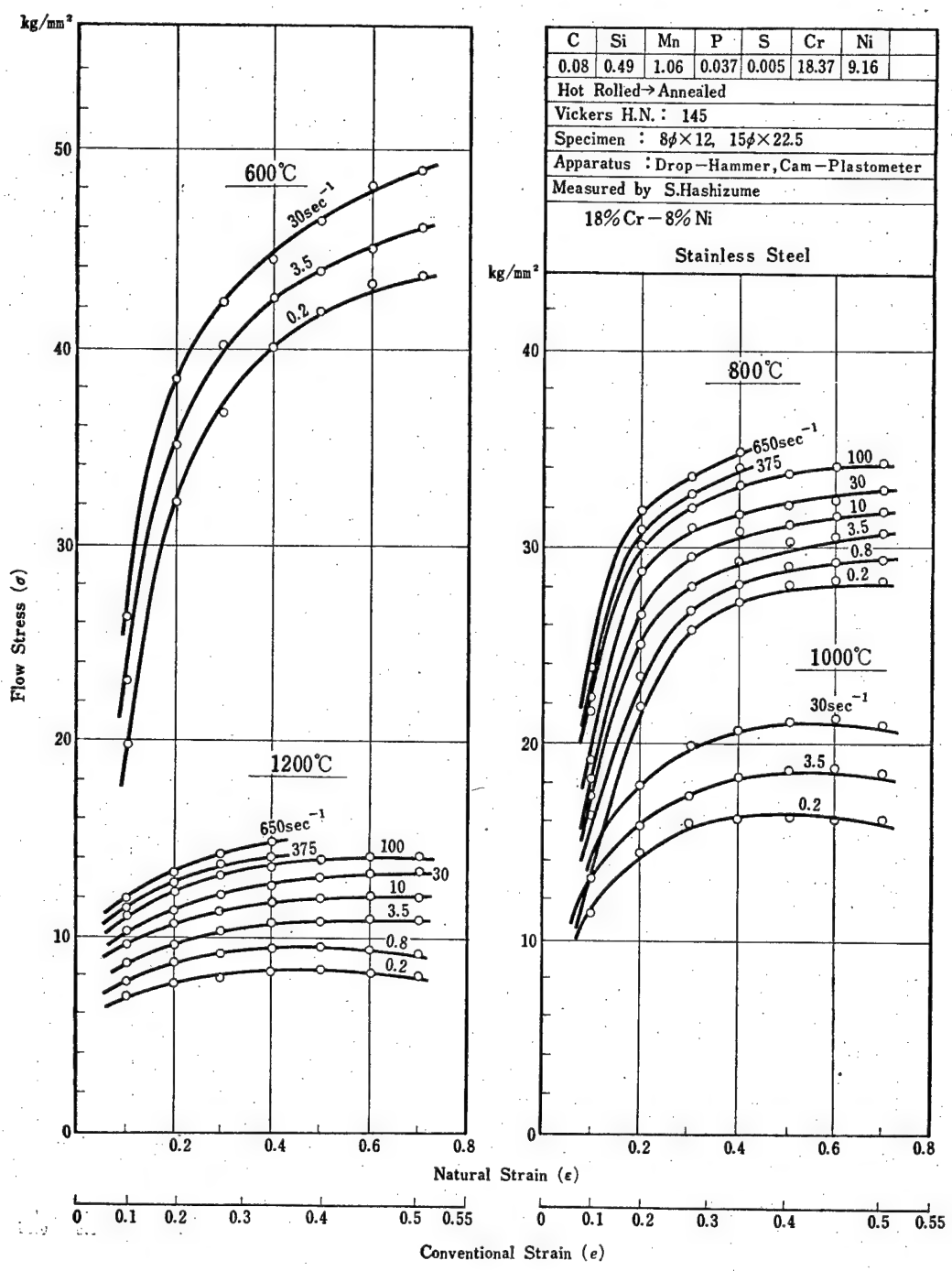

Fig. 4·66 (b) Flow Stress-Strain Curves of 18% Cr-8% Ni Stainless Steel. Temperature Range: 600～1200°C, Strain Rate Range: 0.2～650 sec^{-1}.

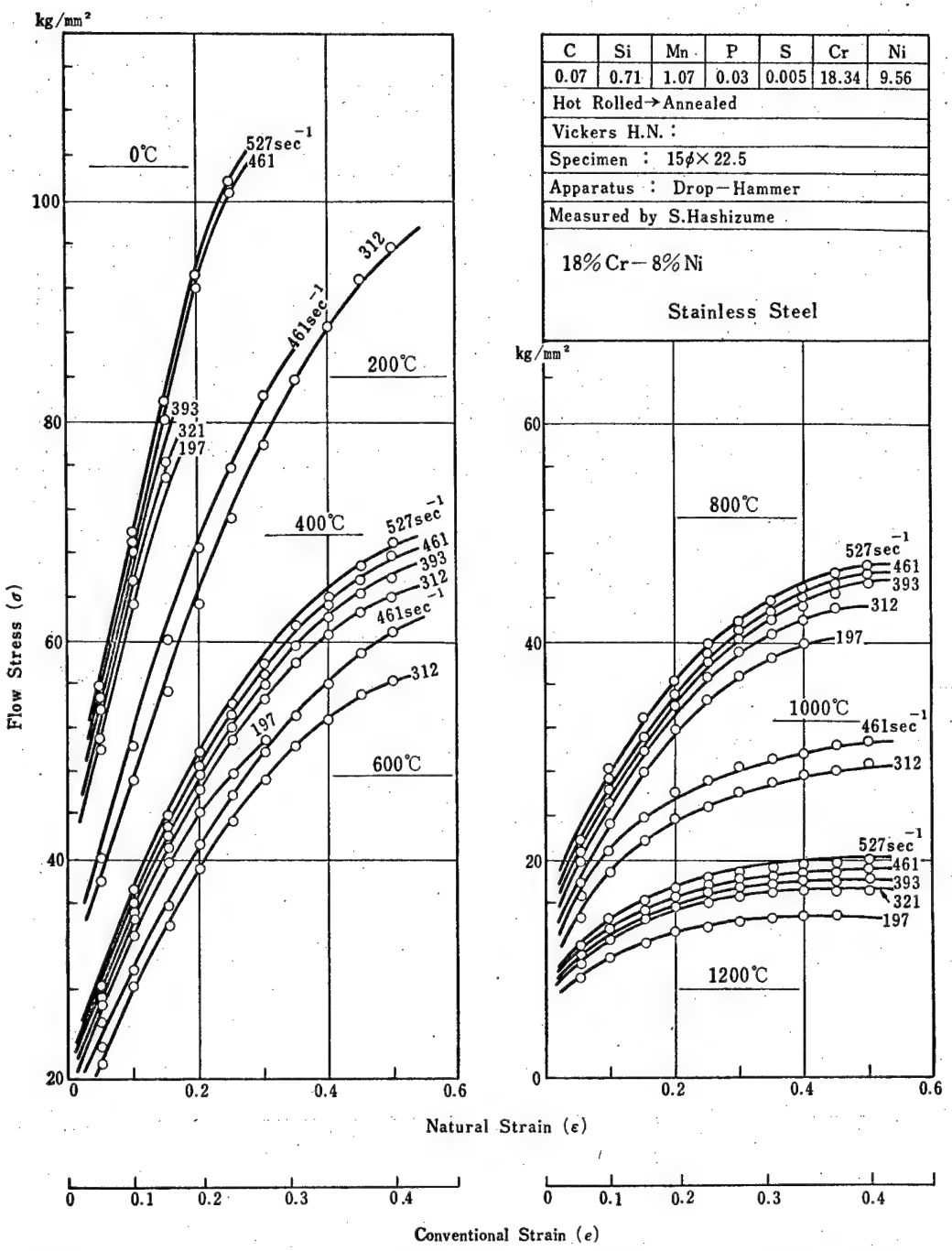

Fig. 4·67 Flow Stress-Strain Curves of 18% Cr-8% Ni Stainless Steel. Temperature Range: 0~1200°C, Strain Rate Range: 197~527 sec^{-1}.

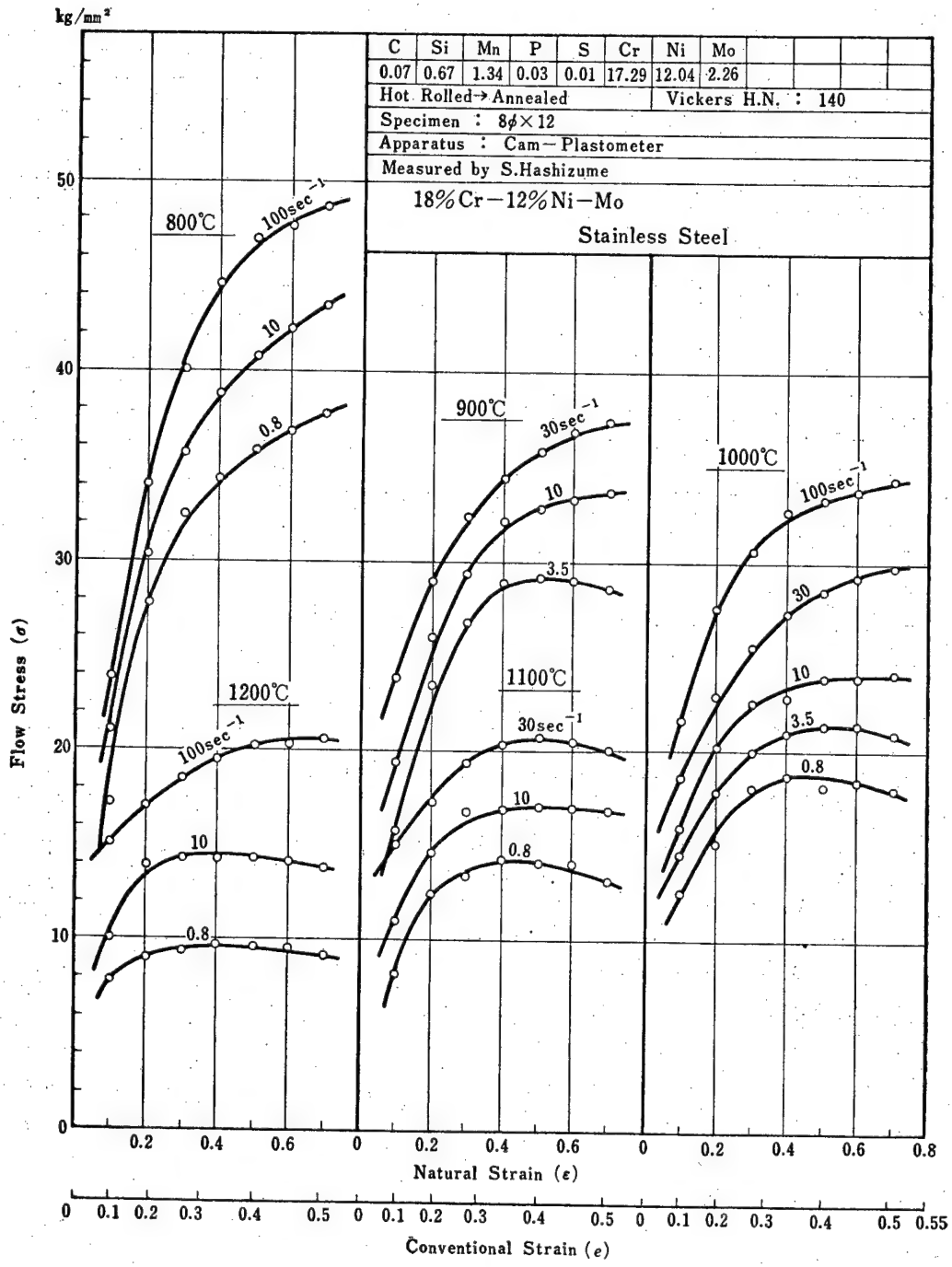

Fig. 4·68 Flow Stress-Strain Curves of 18% Cr-12% Ni-Mo Stainless Steel. Temperature Range: 800~1200°C, Strain Rate Range: 0.8~100 sec^{-1}.

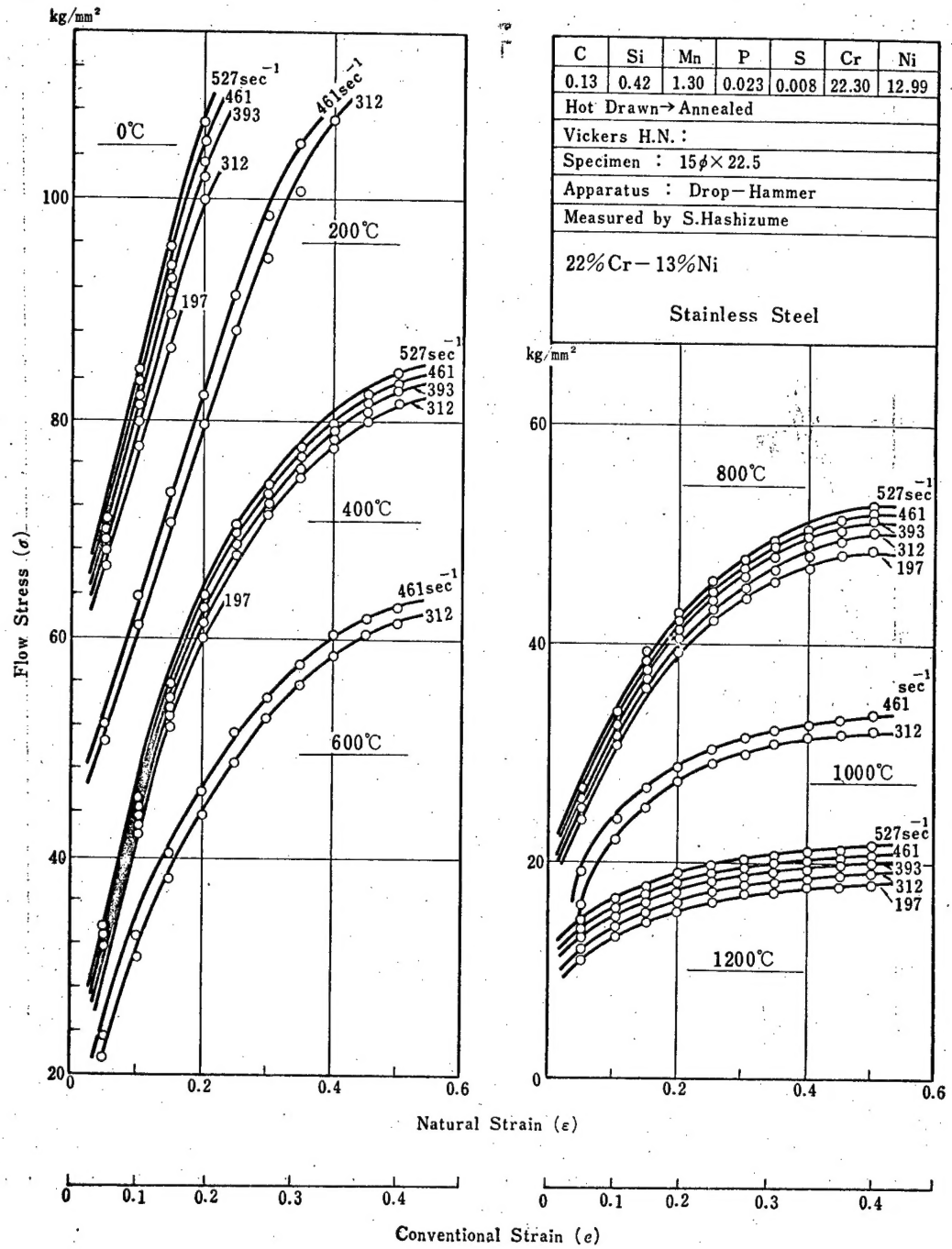

Fig. 4·69 Flow Stress-Strain Curves of 22% Cr-13% Ni Stainless Steel. Temperature Range: 0~1200°C, Strain Rate Range: 197~527 sec^{-1}.

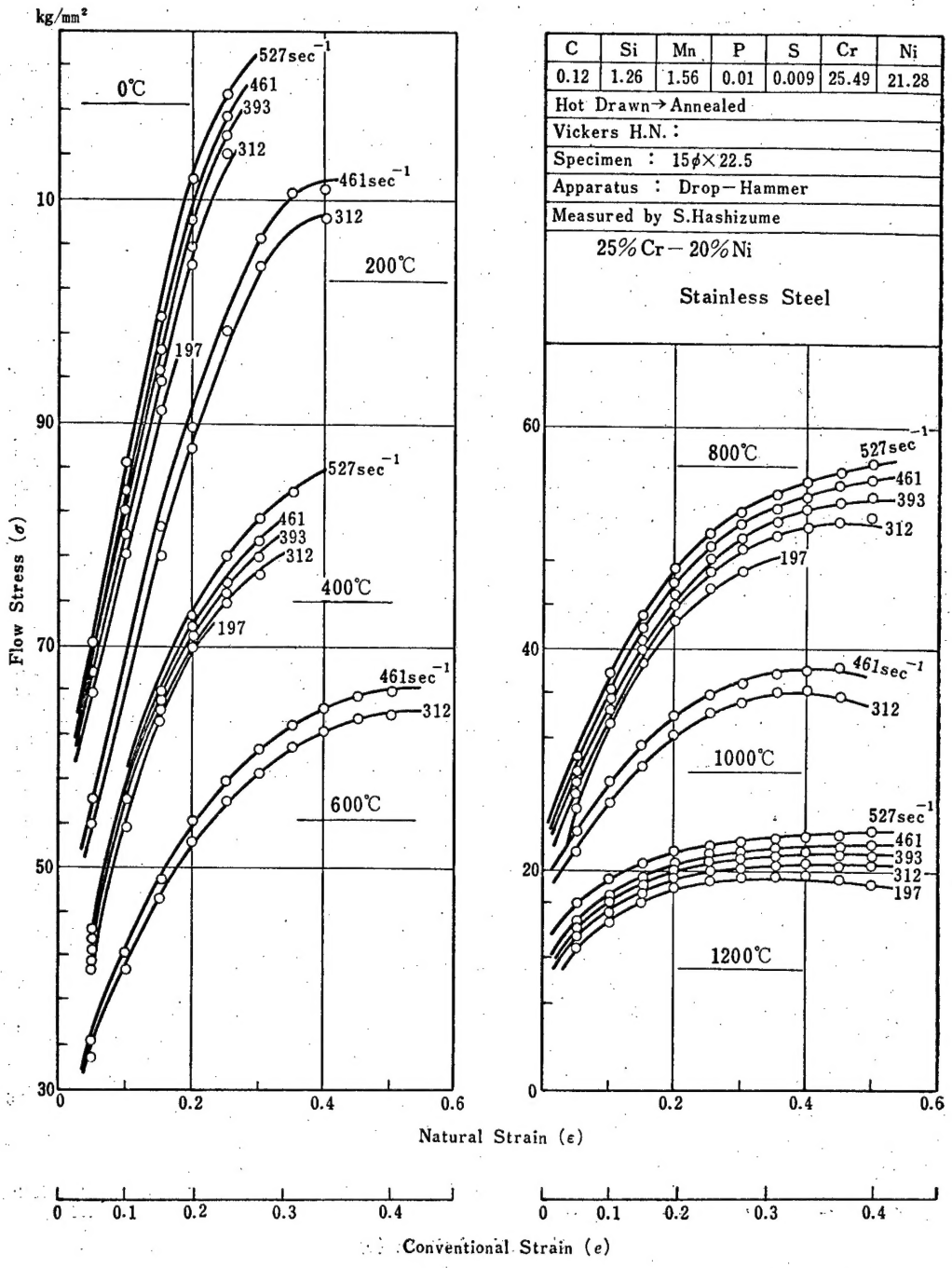

C	Si	Mn	P	S	Cr	Ni
0.12	1.26	1.56	0.01	0.009	25.49	21.28

Hot Drawn→Annealed
Vickers H.N. :
Specimen : 15φ×22.5
Apparatus : Drop−Hammer
Measured by S.Hashizume

25% Cr − 20% Ni
Stainless Steel

Fig. 4·70 Flow Stress-Strain Curves of 25% Cr-20% Ni Stainless Steel. Temperature Range: 0~1200°C, Strain Rate Range: 197~527 sec⁻¹.

東京大学生産技術研究所報告　第18巻　第3号
通巻 第117号

昭和 43 年 2 月 24 日 印 刷
昭和 43 年 3 月 2 日 発 行

発行所　東京大学生産技術研究所
東京都港区六本木 7-22-1

印刷所　三美印刷株式会社
東京都荒川区西日暮里 5-9-8

この報告は不定期に発行し 累計およそ 300 頁で巻を改める.

PUBLISHED AT IRREGULAR INTERVALS BY THE INSTITUTE OF INDUSTRIAL SCIENCE,
THE UNIVERSITY OF TOKYO, 7-22-1, ROPPONGI, MINATO-KU, TOKYO JAPAN

REPORTS ALREADY PUBLISHED

Vol. 14

No. 1	Yoshikatsu TSUBOI: *Theory and Applications of Shallow Spherical Shells.*	March, 1964
No. 2	Shunzo OKAMOTO, Noboru YOSHIDA, Katsuyuki KATO and Motohiko HAKUNO: *Dynamic Behavior of an Arch Dam during Earthquakes* (In English).	December, 1964
No. 3	Atsushi WATARI: *Research on the Motion of Automobiles.*	July, 1965
No. 4	Yoichi FUJII: *Studies on Electron Beam Noise* (In English).	August, 1965
No. 5	Shôhei INOKUTI: *Considerations Hydrauliques sur la Formation des Bancs Obliques dans le Lit de Cours d Eau Alluvionnaire.*	October, 1965

Vol. 15

No. 1	Hisayoshi SATO: *A Study on Aseismic Design of Machine Structure.*	November, 1965
No. 2	Yoshikatsu TSUBOI and Mamoru KAWAGUCHI: *Design Problems of a Suspenion Roof Structure*-Tokyo Olympic Swimming Pools (In English).	November, 1965
No. 3	Teiich HOMMA: *The Influence of the Microscopic and Macroscopic Structures of Oxides upon the Oxidation Mechanism of Metals.*	December, 1965
No. 4	Takakazu MARUYASU, Kazusuke KODAYASHI and Yoshifumi SAKAMOTO: *Studies on Portland Blast Furnace Slag Cement concrete.*	February, 1966

Vol. 16

No. 1	Yoshio NAGAI: *Studies on Syntheses of Aromatic Polycyclic Compounds.*	March, 1966
No. 2	Masahisa MATSUNAGA: *Fundamental Studies on Lapping* (In English).	June, 1966
No. 3	Takakazu MARUYASU and D. G. T. REES: *Movements of Bed-Sediment in Mountain Rivers* (In English).	August, 1966
No. 4	Shunzo OKAMOTO, Choshiro TAMURA, Katsuyuki KATO and Michiko OTAWA: *Dynamic Behavior of Earth Dam during Earthquakes* (In English).	October, 1966

Vol. 17

No. 1	Tadashi YAMASHITA and Masahiro MORI: *Fundamental Approaches to Control of Powder Flows.*	November, 1966
No. 2	Toshimitsu ASAKURA: *Effect of Amplitude Filters on the Diffraction Image and the Maréchal's Aberration Tolerance Conditions* (In English).	December, 1966
No. 3	Shinichi KIKUCHI: *Study on the Photographic Fog Inhibitors especially by means of Silver Potentiometric Titration.*	January, 1967
No. 4	Masahisa MATSUNAGA and Yoshiaki HAGIUDA: *Researches on Barrel Finishing* (In English).	February, 1967
No. 5	Shuhei AIDA: *Theory and Applications of IMICTRON: A Control Element having Mechanisms of a Living Neuron* (In English).	March, 1967
No. 6	Shin TAMIYA: *On Ship Experiment Tank with Wind Tunnel.*	March, 1967
No. 7	Osamu HIRAO, Eiichi KIKUCHI and Naoyuki YAMADA: *Improvement of Handling Characteristics of the Vehicle as a Man-Machine System* (In English).	May, 1967

Vol. 18

No. 1	Tomo-o ISHIHARA, Richard I. EMORI and Haruhiko SAITO: *Non-Steady Characteristics of Hydroaynamic Transmission* (In English)	October, 1967
No. 2	Tadaaki TANI and Sin-ichi KIKUCHI: *Spectral Sensitization in Photography and Electrophotography*	February, 1968

—Complete list is inserted in the last number of each volume—